TATOOINE'S FUTURE: DYNAMICAL EVOLUTION OF PLANETS ORBITING TWO STARS

Keavin Moore

A THESIS SUBMITTED TO
THE FACULTY OF GRADUATE STUDIES
IN PARTIAL FULFILLMENT OF THE REQUIREMENTS
FOR THE DEGREE OF

MASTER OF SCIENCE

Graduate Program in Physics and Astronomy
York University
Toronto, Ontario

September 2017

Abstract

Science fiction has long teased our imaginations with tales of planets with two suns. How these planets form and evolve, and their survival prospects, are active fields of research. Expanding on previous work, four new *Kepler* candidate circumbinary planet systems were evolved through the complex common-envelope phase. The dynamical response of the planets to this dramatic evolutionary phase was simulated using open-source binary star evolution and numerical integrator codes. All four systems undergo at least one common-envelope phase; one experience two and another, three. Their planets tend to survive the common-envelope phase, regardless of relative inclination, and migrate to wider, more eccentric orbits; orbital expansion can occur well within a single planetary orbit. During the secondary common-envelope phases, the planets can gain sufficient eccentricity to be ejected from the system. Depending on the mass-loss rate, the planets either migrate adiabatically outward within a few orbits, or non-adiabatically to much more eccentric orbits. Their final orbital configurations are consistent with those of post-common-envelope circumbinary planet candidates, suggesting a possible origin for the latter. The results from this work provide a basis for future observations of post-common-envelope circumbinary systems.

Acknowledgements

Space has fascinated me since I was a kid; I remember watching the first *Star Wars* and realizing just how much more the night sky was than just a black sheet with tiny dots of light. When I realized I could get a degree in studying space, I couldn't say no, and I appreciate everything I learned during my undergraduate space science degree. The professors at York were a great help, and the Physics & Astronomy department was extremely welcoming, helping shape the research-oriented person I am today. I look back fondly on those four and a half years (although finishing in four would have been nice...), and all the experiences during that time.

The opportunity to spend a couple years studying exoplanets was an amazing one, and the granditude of it is not lost on me (Fun fact: The first confirmed exoplanet detection was in the year I was born, 1992). Not many people have the time to look at one of their greatest interests in their free time, let alone get paid to do it. I never planned to stay at York, but given the opportunity to work with Ray Jayawardhana studying survival prospects of planets around binary stars (another *Star Wars* connection, which made the offer all the more enticing), I couldn't say no. My independent work ethic stems from his busy schedule, and if it wasn't for the guidance of his former postdoc, Veselin Kostov, I don't know if I would have had the motivation to get through all the hard parts of research. Veselin was like a second advisor to me, and I ran a lot of work by him before showing Ray to make sure it was up to standards. He also helped push the research along when I got busy with coursework, and I'm forever grateful for the second-author paper we worked on, which I've presented posters and talks on in the months since. Without the combination of these two exoplanet experts, I may have written a much more somber acknowledgement section, but it was a pleasant experience all around.

I can't finish this master's thesis without thanking my family, as clichéd as it may be. My mom stayed home with me and my sister when we were young, helping out with school work and taking care of us when we weren't at school (she claims that I got my intelligence from her – I won't argue with her about that, though). Whether it be going to the park or watching the finale of *Lost*, she was always willing to spend time with me. My dad worked especially hard to provide for us, and he's the reason I went to university in the first place, having saved money in the 18 years leading up to it. I'm grateful for never having to rely on OSAP, as it seems to be quite the nightmare. Without

that funding, I'm not sure I would have gone to grad school, since I would have been worried about paying student loans. In the past couple years, I've realized we're more alike than I thought through hanging out in the garage, and it's awesome that he's supportive of my choice to be a "professional student". My sister's been my support since she was born, and I relished the weekends and holidays when I could go home to hang out with her, since we share many of the same interests (it's probably my fault that she's so interested in reality TV and comics – sorry, Shayl). I'll always look forward to visiting my family back home, and discussions with all three of them really pushed me to finish writing, even when I felt like there was no end in sight.

There are many other people that I should thank, but I don't want this to drag on. Marlene Caplan helped get through the financial and enrolment issues, and stopping by her office became less of a chore the more I talked to her. Paul Delaney gave me the opportunity to give my first public lecture regarding my research (at the Ontario Science Centre, no less), and without that, I may have still had intense presentation anxiety. Norbert Bartel provided me with my first exposure to actual scientific research during my undergraduate program, and from then on, I was hooked; learning at my own pace for a satisfying end-goal was probably the catalyst to finally apply to grad school.

Finally, I appreciate the email correspondence with Jarrod Hurley, who helped me figure out the binary star evolution code that he wrote when I first downloaded it two years ago. Marten van Kerkwijk, an expert on binary evolution at UofT, solidified our use of this code, providing useful information about the feasibility of the project as well. Dan Tamayo was also a great help in debugging the numerical integrator code we used to simulate the planets, letting us know when crucial updates were published online and adding features which we would find useful for our particular project. I gratefully acknowledge the support of the Ontario Graduate Scholarship for my 2 years of study.

It's been a long road to get here, but I'm not done just yet. These past two years have really helped me grow academically, and taught me great time-management through working independently. In a few more years, when I've completed my Ph.D. studies, I'll hopefully look back and be proud of all my achievements, including this thesis. In the words of Blink-182,

Well I guess this is growing up.

Keavin Moore

July 7, 2017

Table of Contents

Abstract **ii**

Acknowledgements **iii**

Table of Contents **v**

List of Tables **vii**

List of Figures **viii**

1 Introduction **1**
1.1 Background & History . . . 1
1.2 Single Star Evolution . . . 2
1.3 Binary Star Evolution . . . 8
1.4 Post-Common-Envelope Circumbinary Planets . . . 16
1.5 Previous Work . . . 16

2 Methods & Materials **19**
2.1 Relevant Equations . . . 19
2.2 Binary Star Evolution Code . . . 21
2.3 Dynamical Simulations . . . 27

3 Simulations & Results **30**
3.1 Select Highlights of Previous Results . . . 30
3.2 New Results . . . 33
3.2.1 Kepler-64 . . . 33
3.2.2 KIC7821010 . . . 36
3.2.3 KIC3938073 . . . 48
3.2.4 KIC8610483 . . . 56
3.2.5 KIC5095259 . . . 59
3.3 Summary of the Results . . . 67

4 Discussions & Conclusions **70**
4.1 Discussion & Contribution . . . 70
4.2 Future Directions . . . 75
4.3 Conclusion . . . 76

Bibliography **78**

A Appendix **82**
A.1 Abbreviations & Parameters 82
A.2 Additional Tables 83

List of Tables

2.1 *Kepler* Binary-CBP Candidate Default Initial Parameters 23
2.2 BSE Stellar Types 23
2.3 BSE Parameter Space 24
2.4 BSE Output Evolution Stages 25
2.5 Example BSE Outputs 26

3.1 PCE CBP a_{CBP} & e_{CBP}, $\alpha_M = 1.0 M_\odot\ yr^{-1}$ 68
3.2 PCE CBP a_{CBP} & e_{CBP}, $\alpha_M = 0.1 M_\odot\ yr^{-1}$ 69

A.1 BSE Binary Evolution Results. 84

List of Figures

1.1 HR Diagram with Solar Evolutionary Track 4
1.2 Common-Envelope Evolution 12
1.3 CE Evolutionary Channels 13

3.1 Kepler-47 Primary CE Merger 32
3.2 Kepler-64 Merger 35
3.3 Kepler-64 Non-merger 36
3.4 KIC782 Orbital Reconfiguration 39
3.5 KIC782 Primary CE Merger 40
3.6 KIC782 Primary CE Non-merger 41
3.7 KIC782 Merger Phase Dependence 42
3.8 KIC782 Non-Merger Phase Dependence 43
3.9 KIC782 Primary CE Merger Histograms 44
3.10 KIC782 Primary CE Non-merger Histograms 45
3.11 KIC782 Secondary CE 46
3.12 KIC782 Secondary CE Histograms 47
3.13 KIC393 Primary CE Merger, $i_{CBP} = 0°$ 50
3.14 KIC393 Primary CE Non-Merger, $i_{CBP} = 0°$ 51
3.15 KIC393 Merger Phase Dependence 52
3.16 KIC393 Non-Merger Phase Dependence 53
3.17 KIC393 Primary CE Merger and Non-Merger, $i_{CBP} = 90°$ 54
3.18 KIC393 Primary CE Merger and Non-Merger, $i_{CBP} = 180°$ 55
3.19 KIC861 Orbital Reconfiguration 57
3.20 KIC861 Primary CE Non-merger 58
3.21 KIC861 Non-Merger Phase Dependence 59
3.22 KIC509, Z=0.01 Primary CE Merger 62
3.23 KIC509, Z=0.01 Primary CE Non-merger 63
3.24 KIC509 Merger Phase Dependence 64

3.25 KIC509 Non-Merger Phase Dependence 65
3.26 KIC509, Z=0.02 Primary CE Merger 66
3.27 KIC509, Z=0.02 Primary CE Non-merger 67

4.1 Pre-CE *Kepler* vs. PCE CBPs 72
4.2 *Kepler* vs. PCE CBPs 74

Chapter 1

Introduction

1.1 Background & History

Since their discovery in the 1990s, extra-solar planets (or simply exoplanets) have been a focus of great interest in the astronomical community, as their very existence seems to amplify our expectations for the presence of life elsewhere in the Universe. Films such as *Star Wars*, which included Luke Skywalker's home planet of Tatooine around a binary star, have long teased our imagination, and it is only with recent advances in technology that an abundance of not only planets orbiting single stars, but also Tatooine-like circumbinary planets, have been discovered. A Tatooine-like planet orbits both stars in a close binary system, as opposed to a circumprimary or circumsecondary planet orbiting only one of the stars (the primary or secondary, respectively) in a wide binary system. Circumbinary planets orbiting main sequence stars are a very recent discovery (Doyle et al., 2011), and scientists still have a myriad of questions about planets in multiple systems, such as how they form and evolve, and whether they survive the changes in their parent stars.

As one of the pillars of modern astrophysics, stellar evolution has been studied extensively over the years, and we know that once they leave the main sequence, single stars expand and evolve on timescales of millions to billions of years (Veras, 2016; Kippenhahn & Weigert, 1990, and references therein), depending on their mass. Whether a planet orbiting an evolving star survives depends not only on its orbital distance, but also on the mass of its host star; with this in mind, our own planet may not survive the Sun's long-term evolution (e.g. Silvotti et al., 2007; Schröder & Connon Smith, 2008). When the Sun evolves off the main sequence (MS), closer-in planets, such as Mercury, Venus, and our home, the Earth, will likely be engulfed as the solar envelope expands past Earth's orbit.

Recent studies have shown that at least half of all solar-type stars in the Universe are members of binary or higher-order multiple systems (Raghavan et al., 2010), and 1 in 4 binary systems are close enough that the two stars will affect each other's evolution (Willems & Kolb, 2004), underlining the importance of studying the complex evolution of these systems. The existence of

planets orbiting close binary stars in particular, known as circumbinary planets (or CBPs), allows interesting comparisons to be made with our own single-star home system, and offers a glimpse into their survivability throughout the dramatic evolution of their host stars.

While there has been a strong emphasis on testing the long-term stability of the progenitors of CBPs in post-common envelope (PCE) systems (e.g. Mustill et al., 2013; Portegies Zwart, 2013), and on circumprimary planets in wide binary systems (Kratter & Perets, 2012), the details and impact of common-envelope (CE) evolution must be taken into account. The CE phase of a close binary star is a complex, turbulent, and uncertain process, in which the stars share an atmosphere for timescales of years, experience dramatic mass loss and orbital shrinkage, and eventually eject their shared atmosphere (Paczynski, 1976; Hilditch, 2001). The evolving binary strongly influences the CBP during this phase, and CE evolution is likely to determine whether the planet is able to survive from its formation until much later in the system's lifetime, or whether the observed PCE CBPs (i.e., planets orbiting binaries which have already evolved through the CE phase) form late in the stars' lifetime from a PCE disk.

Inspired by discoveries made by the *Kepler* telescope of planets orbiting nine close binary systems, we recently conducted a study on the response of these CBPs as their host stars evolve through a CE phase, assuming coplanar, circular orbits (Kostov et al., 2016). Planetary orbits are not always coplanar and circular, and here we add a more realistic orbital representation through the inclusion of four new *Kepler* CBP candidates on inclined, eccentric orbits. Previously simulated systems with non-zero eccentricities are updated and compared to the previous results. This allows us to quantify the effects that CBP inclination and eccentricity have on the evolution and survivability prospects of CBPs in close binary systems.

This thesis is divided as follows. The remainder of Chapter 1 will outline the evolution of single and binary star systems, as well as the presence of post-common envelope circumbinary planets, before discussing some previous studies within the field. Chapter 2 will focus on the method used in our simulations, with an explanation of both codes, including some important equations. Chapter 3 will briefly touch on the results of our first study before exploring the results of the new systems with the addition of CBP eccentricity and inclination. In Chapter 4, the results of our simulations will be discussed and justified through comparisons with the literature, followed by conclusions of the study.

1.2 Single Star Evolution

Solar-mass stars will follow an evolutionary track similar to that of our own Sun, while low-mass stars will evolve much slower, and high-mass stars may eventually end their lifetimes as neutron stars or black holes. An overview of single star evolution can be found in multiple sources (see Hurley et al., 2000; Carroll & Ostlie, 1996; Boehm-Vitense, 1989, and references therein). For completeness,

I briefly review the standard treatment below.

A star's lifetime, which depends critically on its mass, can be measured from what is known as the zero-age main sequence (ZAMS), as the time from collapse of the protostellar cloud until hydrogen-fusion in the core creates sufficient pressure to support the overlying envelope (i.e. when the star reaches the end of the Hayashi track (Hayashi, 1961), a nearly vertical line in the Hertzsprung-Russell diagram which the star follows during its brief pre-main sequence evolution) is very short. While a star is on the main sequence (MS), like our own Sun, it fuses hydrogen to helium within its core. Fusion produces enough energy for the luminosity, L, to increase, and effective temperature, T_{eff} (determined in the stellar atmosphere), to either increase or decrease (depending on stellar mass) (e.g. Hurley et al., 2000) with the evolution. It is in this stage that a star spends the majority of its lifetime. These two observable properties can be plotted on a Hertzsprung-Russell (H-R) diagram, which can be seen in Fig. 1.1, after Hurley et al. (2000), including a track of the Sun's evolution. As the hydrogen fuel within the stellar core is depleted, the star evolves away from the MS.

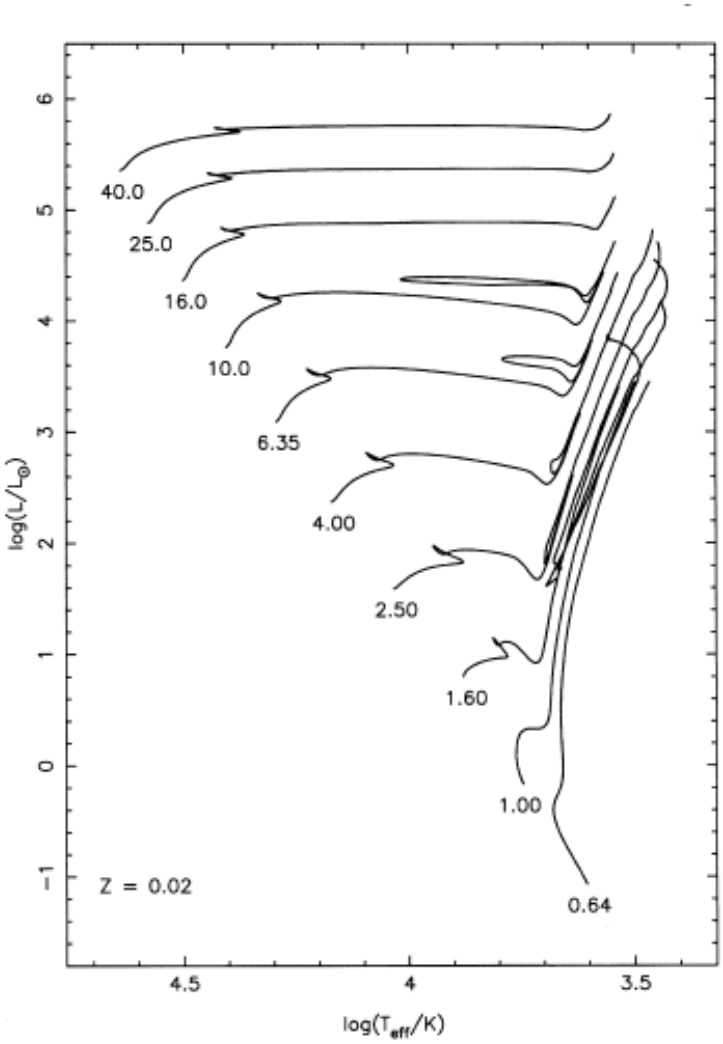

Figure 1.1: An HR diagram, showing tracks for various stellar masses, all for a metallicity of $Z = 0.02$ after Hurley et al. (2000). Since the Sun reached the ZAMS roughly 4.57 Gyr ago, its L and T_{eff} have steadily increased, and its radius has expanded. The Sun will evolve off the main sequence (MS) into a red giant branch star (RGB) when it exhausts the hydrogen fuel in its core. From there, it will evolve onto the asymptotic giant branch (AGB), burning helium in its core; once that has been exhausted, it will produce a planetary nebula (PN) by ejecting its outer layers in a helium flash, and will leave behind a remnant core of $M < M_{Ch} = 1.4M_{\odot}$, which will continue to cool as a dim white dwarf (WD) for the remainder of its lifetime. Note that the MS has a finite width; this is to account for the aforementioned composition differences, as well as observational uncertainties.

There are two types of cores that form, depending on the mass of the star: lower mass stars ($M \lesssim 1.2M_{\odot}$) have radiative cores, while higher mass stars have convective cores, a result of the steep temperature gradient in their interior. Very low-mass stars ($M \lesssim 0.3M_{\odot}$) also have convective

cores, a result of their high surface opacities allowing convection to occur deep within the stellar interior. The MS evolutionary track of a star also strongly depends on its mass – a low-mass star will increase in both L and T_{eff}, moving up and left (blueward) in the HR diagram; higher-mass stars, with $M \gtrsim 1.5M_{\odot}$, will also experience an increase in L, but a decrease in T_{eff}, instead moving up and right (redward) (Boehm-Vitense, 1989).

The radius of low-mass stars continues expanding, and the star moves right in the HR diagram, at constant surface L. This region is known as the Hertzsprung Gap (HG), or the subgiant branch, a stage in which very few stars are observed due to its short timescale (e.g. Hurley et al., 2000). As high-mass stars have convective cores, they will proceed through an additional stage first: once the core-hydrogen is exhausted, mixing in the core leads to the inner region rapidly contracting, leading to the hydrogen-exhausted phase gap, otherwise known as the MS hook (Hayashi & Cameron, 1962; Hurley et al., 2000).

As a star evolves through the HG phase, its radius increases greatly, thus decreasing T_{eff}, leading to the star developing a convective envelope. This expansion leads the star onto the Giant Branch (GB), a nearly vertical line on the HR diagram similar to the Hayashi track. Since a high enough core temperature has been reached, fusion is now only occurring in a thick outward-moving hydrogen-burning shell, which is adding helium to the already helium-rich core, and causing it to contract but increase in mass. The core contraction leads to an increase in both hydrogen-shell and helium-core temperatures, and the luminosity is much higher than the previous phase. The star is now fully convective, and its surface luminosity is increasing, but its T_{eff} is relatively constant as it moves up the GB. The convective envelope may reach deep into the stellar interior, mixing already-processed fusion materials to the surface in a process known as the first dredge-up (e.g. Carroll & Ostlie, 1996; Hurley et al., 2000).

Eventually, the central temperature is high enough for core-helium fusion to begin, surrounded by the hydrogen-burning envelope. This ignition happens gently for massive stars with $M \gtrsim 2.0M_{\odot}$, causing the star to move back down the GB; after some time, contraction causes the star to move back towards the MS in a blue loop, the size of which depends on the mass. Core-helium burning (CHeB) leads to both carbon and oxygen production, but as with the hydrogen-burning stage, the helium supply is limited. Lower-mass stars react more violently at the onset of helium-burning, instead abruptly igniting in a core-helium flash due to their degenerate helium core, suddenly releasing up to 10^{11} $L_{\odot}$ of energy for a few seconds (Carroll & Ostlie, 1996), then quickly migrating to the zero-age horizontal branch (ZAHB). These lower-mass stars will appear bluer at this point than their higher-mass counterparts, as there is less material above the hydrogen-burning shell to shield its luminosity. High-mass stars, with $M \gtrsim 6M_{\odot}$, experience blue-loop excursions in the H-R diagram (i.e. the stars move blueward before returning redward) shortly after reaching the GB (Boehm-Vitense, 1989). Once core-helium is exhausted, fusion begins in both overlying shells (helium and hydrogen), moving the star back to the GB. Carbon fusion, along with other fusion reactions, can

lead to more very short blue loop excursions, lasting only tens of thousands of years. Very high-mass stars, with $M \gtrsim 12.0 M_{\odot}$, can potentially skip the GB altogether (e.g. Hurley et al., 2000): as their central temperature is extremely high, it is possible that CHeB begins as early as the HG instead.

Once core-helium is exhausted, the star again moves redwards toward the Hayashi track as its convective envelope deepens and its inert carbon-oxygen (C-O) core contracts, beginning the next phase of its evolution: the asymptotic giant branch (AGB). The star now consists of a dense C-O core, and its increase in temperature leads to the ignition of the surrounding helium-burning shell, which itself is surrounded by an initially extinguished hydrogen-burning shell during the early AGB (EAGB) phase. At this point, a massive star's convective envelope will once again reach into the deep interior and mix processed material to the surface in a second dredge-up (Carroll & Ostlie, 1996). The helium-burning shell is constantly adding material to the contracting C-O core, and will eventually meet the hydrogen-burning shell, re-igniting it as the predominant source of energy, and thus luminosity. The helium-burning shell is degenerately unstable during the AGB, a result of helium from the overlying hydrogen-burning shell being constantly added to it. The additional helium increases the temperature of the helium-burning shell, sometimes leading to sudden releases of luminosity known as helium shell flashes, analogous to, but much weaker than, the core-helium flashes seen in low-mass stars. To balance this abrupt energy release, the star expands, and briefly extinguishes the hydrogen-burning shell through its rapid cooling (Carroll & Ostlie, 1996); at the same time, the convection zone reaches deep into the stellar interior, mixing both processed helium and carbon to the surface. The star then contracts, causing the convection zone to recede, the helium-burning slows, and allows re-ignition of the hydrogen-burning shell, thus ending the third dredge-up (Hurley et al., 2000). This process can be repeated periodically with each helium flash, and is visible as variations in the surface luminosity of the star. Nonetheless, the star evolves up the AGB with the hydrogen-burning shell as the predominant source of energy output. Due to the repeating nature of these helium flashes, this phase is known as the thermally-pulsing asymptotic giant branch (TPAGB), during which the star has constant T_{eff} but an overall increasing L.

These pulses, along with the overall expansion of the star, lead to an increase in luminosity and a decrease in mass, lowering the surface gravity and causing surface material to be less tightly bound. Mass loss becomes significant on the AGB, and actually accelerates with evolution up the AGB; however, the mechanism behind it is widely debated – some attribute the high mass-loss rates later in the evolution to superwinds (of up to $10^{-4}\ M_{\odot}\ yr^{-1}$), or to the helium flashes themselves (Carroll & Ostlie, 1996, and references therein). This mass loss eventually removes enough of the envelope that the hydrogen-burning shell is exposed, and the star evolves blueward toward higher T_{eff} at constant L. The expelled material accumulates as dust grains in the interstellar medium (ISM) around the relatively cool AGB star. The energy released by the star, as ultraviolet photons, is absorbed by the ejected material, which excites electrons to a higher energy level (but also ionizes some material, if the photonic energy is high enough) (Carroll & Ostlie, 1996). When these electrons

settle back to lower energy levels, visible photons are emitted, and it may be possible to observe this illuminated material as a planetary nebula (PN). Mass loss eventually removes the remainder of the envelope, and the remnant core is extremely hot but much dimmer than when the star existed on the MS; it has now reached the end of its nuclear-burning lifetime, having exhausted all of its nuclear fuel and leaving a degenerate C-O core, and is known as a white dwarf (WD), which will slowly cool over billions to trillions of years. Stars up to about 7 $M_{\odot}$ will become WDs, as their degenerate C-O core will be less than $M_{Ch} = 1.4M_{\odot}$, the Chandrasekhar mass (e.g. Boehm-Vitense, 1989; Carroll & Ostlie, 1996).

More massive stars, with $M \gtrsim 7M_{\odot}$, do not have a degenerate C-O core, and core contraction will lead to the ignition of carbon, with fusion processes quickly leading to the formation of an iron core (Hurley et al., 2000). The luminosity of the star remains constant, but photodisintegration of iron, along with electron capture, removes the electron degeneracy pressure supporting the core, sending the core into free-fall (Boehm-Vitense, 1989); thus, instead of becoming an isothermal WD, the core, with $M > M_{Ch}$, rebounds, ejecting a massive amount of energy outwards through the overlying layers. These massive stars die in a supernova (SN) explosion during the AGB phase and do not experience the thermally-pulsing AGB phase. The core will become either a neutron star (NS) supported by neutron degeneracy pressure or, in the even more massive case, a mass-consuming black hole (BH). [1]

Stars with $M \gtrsim 15M_{\odot}$ can evolve very differently throughout their lifetimes, which can be attributed to the significant effect of mass loss. Analogous to smaller stars on the AGB, these massive stars can lose their entire envelope much earlier (either during CHeB or, sometimes, during the HG), exposing the nuclear-processed material and resulting in a naked helium star. This may also lead to the formation of Wolf-Rayet stars, massive stars found near the MS, which are losing mass at very high rates, and have spectra characterized by weak, or no, hydrogen lines (Hurley et al., 2000). Objects that may evolve into Wolf-Rayet stars, luminous blue variables (LBVs), also display very high mass-loss rates after evolving off the MS (Vink, 2013, and references therein).

Naked helium stars can also be formed in a binary (e.g. Hurley et al., 2000). Tidal influence can cause mass transfer between the primary and secondary star, slowing stripping away the (usually less massive) star's atmosphere. A common-envelope stage resulting in a non-merger may result in one evolved star and another which has had its original envelope ejected along with the shared atmosphere at the end of this stage (Hurley et al., 2002). Binary evolution will be explored more thoroughly in the next section.

While single star evolution is critically dependent on the initial mass of the star on the ZAMS, the composition (for example, a star's metallicity) can lead to different evolutionary tracks through the HR diagram (e.g. Carroll & Ostlie, 1996; Hurley et al., 2000), and will likely play a factor in determining the final fate of the star.

[1] Supermassive black holes, which can be as massive as millions to billions of $M_{\odot}$, can be seen at the centre of galaxies throughout the Universe, including Sagittarius A* at the centre of the Milky Way (e.g. Melia & Falcke, 2001).

Single star evolution is important to understand as stars in detached binaries, which do not interact with each other through effects such as tides or wind accretion, will evolve independently. We still see the stages detailed in this section in binary evolution, but the paths and timescales at which these different stages occur are strongly affected by the influence of both stars on one another within an evolving binary.

1.3 Binary Star Evolution

Stars far enough separated evolve in isolation as single stars; thus, wide binaries, in which the stars are separated by many solar radii ($R_\odot$), do not influence each other's evolution, and the stellar evolution theory previously outlined is sufficient to describe their evolution. It is only when the binary is close enough that the stars begin to interact through mass transfer that the evolution changes. Hence, we can categorize two distinct types of binary systems: wide binaries, which are gravitationally bound but evolve mainly as single stars, and close binaries, in which at least one component has the potential to fill its Roche lobe – a gravitational potential region around the stars (in a frame rotating with the binary) in which all mass within is gravitationally bound to the star at its centre – strongly affecting each other's evolution and potentially entering the common-envelope (CE) phase (also known as interacting binaries (Hilditch, 2001)). To determine if a CE phase will occur depends critically on the mass ratio of the stars and their evolutionary stage at the onset of mass transfer (Iben & Livio, 1993).

Stars can still interact in a wide system, and orbital angular momentum will be conserved; although the stars are detached, tidal friction can synchronize the spin of the stars with the orbit, and circularize an eccentric orbit, as the binary tends towards a minimum energy equilibrium state (Hurley et al., 2002; Ivanova et al., 2013). Tidal interactions cannot be neglected in close binary evolution, and become significant when the orbital separation is roughly two to three times larger than the radius of the giant (e.g. Portegies Zwart & Meinen, 1993). Since the stars are not in contact, tides must be causing the observed stellar spin-orbit synchronization. The tides between the stars cause a torque, and it is this torque that is responsible for transferring angular momentum from stellar spin to the orbit. The total energy of the system will decrease due to tides, changing the orbital parameters. Thus, tides will either cause the system to approach its minimum energy equilibrium state, or accelerate the spiral-in of the stars. It is interesting to note that, after tidally-induced synchronization has been achieved, the system can avoid a CE if it remains resistant to the Darwin instability (Darwin, 1879), in which the removal of angular momentum causes spin-up of the binary orbit.

When the more massive star in a close binary, the primary, begins expanding and evolves off the MS, it slowly fills its Roche lobe. During this expansion stage, it is possible the binary could lose

mass at the same rate as AGB superwinds, $\dot{M} = 10^{-4}\ M_{\odot}\ yr^{-1}$, enlarging the orbit and potentially allowing the binary to avoid a CE. Otherwise, the primary will eventually fill its Roche lobe, and matter will flow from the outer layers of the star through the inner Lagrange point towards the secondary on a dynamical timescale – this is the beginning of Roche lobe overflow (RLOF), known as the onset of mass transfer. This leads to dramatically different evolution of the binary than if the stars were isolated. Some of this mass may accrete onto the secondary through this mass transfer, but if the mass-loss rate is high enough (for example, if the primary is a giant with a convective envelope, or mass ratio $q = M_2/M_1 \ll 1$), the transferred matter will start to accumulate in the secondary's Roche lobe as well, gradually filling it. A giant primary transferring mass to an MS secondary is the most commonly observed scenario in close binary evolution (van den Heuvel, 1976), and thus this evolution can be expected in over 70% of all unevolved close binaries (van den Heuvel, 1969). RLOF can also be caused by orbital shrinkage due to orbital angular momentum losses, thus filling the Roche lobe at a much earlier stage than if contraction did not occur. These orbital momentum losses may be caused by either a magnetic stellar wind or gravitational wave radiation (Iben & Livio, 1993), but the latter is only important in binaries that have already experienced a CE stage and thus have very short orbital periods.

If the primary is a giant or much more massive than the secondary (i.e. if RLOF is dynamically unstable), the secondary cannot accept all transferred material, and it begins filling its own Roche lobe with the transferred mass. Eventually, the secondary's Roche lobe is also filled, and the expelled mass spills out of both Roche lobes and forms into a shared atmosphere, with the two stellar "cores" orbiting within. This stage is not the same as a contact binary, in which the stars and envelope rotate at the same rate. Rather, due to frictional forces from the expelled material and expansion of the envelope due to radiation pressure, the envelope rotates at a slower rate than the stellar cores, causing spiralling-in of the binary orbit and transfer of energy to the envelope. The binary has now entered the common-envelope (CE) phase of its evolution. Although CE evolution is not well understood, it is a critical stage in the evolution of some close binaries, and the proposed origin of cataclysmic variables (Paczynski, 1976), X-ray binaries (van den Heuvel, 1976), and massive binaries containing neutron stars (Ostriker, 1976).

It is worth noting that the first modern explanation of the CE phase was given by Paczynski (1976). "*When a contact binary expands so much that the stellar surface moves beyond the outer Lagrangian point, a common envelope binary is formed. The suggestion is made that while the two dense stellar nuclei spiral towards each other, the envelope expands and is eventually lost. Most of the angular momentum is lost with the envelope, and therefore the final orbital period may be orders of magnitude shorter than the initial period.*" While this definition is now more than 40 years old, the general picture of the modern CE phase is strongly reliant on this description, albeit with the inclusion of many more processes and outcomes, and this is still the standard reference on the topic. Although the CE stage of close binary evolution has been known for so long, we still do not

fully understand the processes and timescales involved, and it may be the most important unsolved problem in binary evolution (Ivanova et al., 2013).

The outcome of CE evolution depends strongly on the orbital energy, but the processes leading to the outcome are not well understood. The energy formalism outlined by Ivanova et al. (2013) defines the following equation,

$$E_{bind} = \Delta E_{orb} = E_{orb,i} - E_{orb,f} = -\frac{GM_1M_2}{2a_{bin,i}} + \frac{GM_{1,c}M_2}{2a_{bin,f}} \tag{1.1}$$

where $a_{bin,i}$ and $a_{bin,f}$ are the initial and final binary separation, M_1 and M_2 are the initial stellar masses, and $M_{1,c}$ is the mass of the remnant core of the primary after the envelope is ejected. Through comparison of the difference between the initial and final orbital energies, $E_{orb,i}$ and $E_{orb,f}$, and the envelope binding energy (i.e. the energy required to eject the envelope to infinity), E_{bind}, the resulting binary can be predicted. CE ejection is not perfectly efficient, however, but must be a dynamical process. A common-envelope parametrization factor,

$$\alpha_{CE} \equiv \frac{\Delta E_{bind}}{\Delta E_{orb}} \tag{1.2}$$

was defined by Iben & Tutukov (1984) and Livio & Soker (1988), and can be used to determine the orbital period of the post-CE binary at the end of this phase. Note here that ΔE_{bind} is gravitational energy minus thermal energy of the ejected material. The parameter α_{CE} determines how efficiently the binary will dissipate its envelope, i.e., how much orbital energy is transferred and used to remove the envelope, which will in turn determine whether the stars merge or remain as a tight binary; $\alpha_{CE} = 1$ is typically used. However, other sources of energy can either reduce or increase the value of α_{CE} (Iben & Livio, 1993): efficient energy transport and accounting for nonspherical effects (which had a significant impact on calculations involving the most common CE scenario, a giant-MS pair (Meyer & Meyer-Hofmeister, 1979)) allow $\alpha_{CE} < 1$, while including additional energy sources, such as enhanced nuclear burning in stellar shells and recombination energy in ionization zones, allow $\alpha_{CE} > 1$. It is currently accepted that, when the binary separation increases during the first mass transfer phase, the energy required to do so comes from nuclear energy input as well as thermal expansion (Ivanova et al., 2013). While α_{CE} appears simple, it is probably the most important, yet extremely uncertain, factor in determining the outcome of the CE phase.

There are many outcomes to this phase; two major outcomes, the non-merger and merger cases, are shown in Fig. 1.2, while a variety of other evolutionary channels are shown in Fig. 1.3, after Ivanova et al. (2013). While inside the envelope, the stars are spiralling-in due to the frictional drag of the envelope. If the envelope is not ejected before the stars come into contact, they can smoothly coalesce, merging and retaining their envelope; the binary is now a single red giant star with an extended envelope, and will continue evolving according to the single star prescription outlined in the previous section. This coalescence need not be so smooth, however, and thus the stars can also violently collide and release a large amount of energy in a Supernova (SN). Lower-mass stars will

explode in a SN, leaving nothing behind; higher-mass stars may form a single neutron star (NS) or, if the conditions are appropriate, a single black hole (BH).

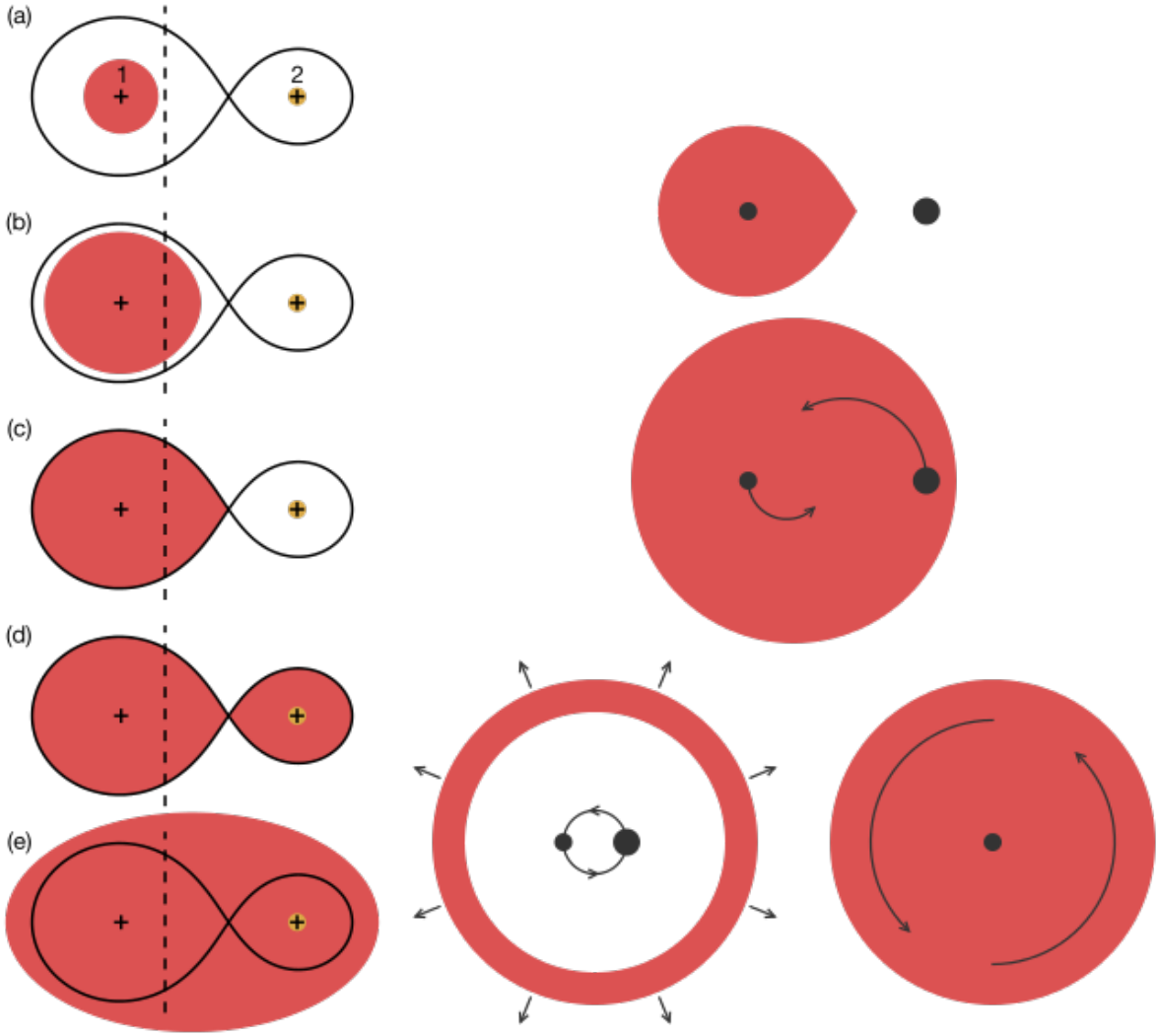

Figure 1.2: Left: (a) A close binary orbiting, with each star surrounded by its Roche lobe, and the black line the Roche equipotential surface. (b) The primary begins evolving off the MS, and its envelope expands. (c) The primary is now a giant, and has filled its Roche lobe. (d) The onset of RLOF; mass transfer begins from the primary to the secondary, and as the secondary cannot accept all transferred matter, its Roche lobe fills as well. (e) The accumulated matter in both Roche lobes spills out into a shared atmosphere, beginning the CE stage. Right: An initially detached binary enters a CE, and the core-MS pair within spirals in due to frictional drag from the envelope. If enough orbital energy is present, the envelope is ejected, and the stars remain as a tight binary; otherwise, the stars smoothly coalesce and retain their envelope, remaining as a giant star. Adapted from Izzard et al. (2012) by Philip D. Hall, Wikimedia Commons.

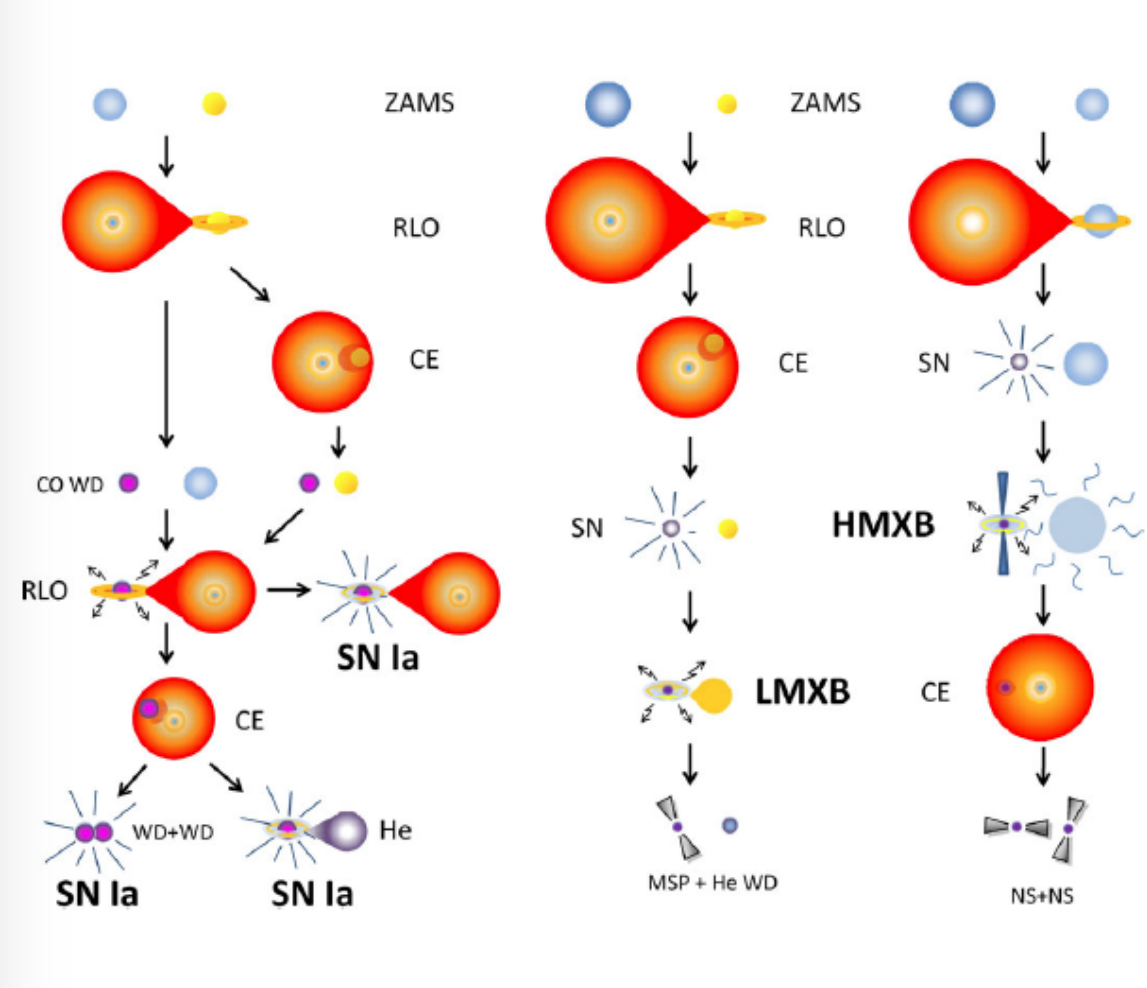

Figure 1.3: Multiple evolutionary channels of systems proceeding through the CE phase after Ivanova et al. (2013). Left: The stars begin on the ZAMS until primary RLOF, followed by either avoidance of the CE leaving a C-O WD and evolved secondary, or a CE leading to a C-O WD and MS secondary. Both of these possibilities lead to a secondary RLOF, which may cause a primary Type Ia SN, destroying the primary star. When secondary RLOF instead leads to a CE, the stars may exit the CE as a WD+WD pair leading to a SN Ia (which destroys both stars), or a WD + naked helium star, leading to a SN Ia which, again, destroys the primary. Middle: Primary RLOF once again leads to a CE, followed by a primary SN. This leaves a low-mass X-ray binary, which, through interaction, eventually evolves into a millisecond pulsar with a HeWD companion. Right: Primary RLOF leads to mass transfer onto a massive star, and a primary SN. The remaining high-mass X-ray binary then initiates a CE, and the binary leaves this stage as a NS+NS pair.

Regardless of mass, one star exploding in a SN leads to a velocity kick due to asymmetry in the explosion, which may disrupt the system if both stars survive (e.g. Hurley et al., 2002). If one (or

both) stars within the envelope is a WD, the stars may violently collide within the envelope as they spiral in, leading to a Type Ia SN. If the binary survives the SN, the separation and eccentricity will change drastically, depending on the configuration immediately before the SN. Significant mass and angular momentum will be lost from the binary in the explosion, and the remnant NS will gradually spin up to conserve the spin angular momentum of the star.

Returning to the CE phase, if enough energy is present (orbital or otherwise), the stars can avoid merging; although they still spiral-in for the duration of the CE, they instead dissipate the envelope before coming into contact, remaining as a tight binary. This is the proposed origin of many fascinating binary systems, such as cataclysmic variables (CVs) (Paczynski, 1976), consisting of a white dwarf primary and a mass-transferring secondary. CE evolution is extremely important for close binaries, as it determines whether the system spends the remainder of its life as a single star, or remains as an (albeit much tighter) binary. The secondary may also trigger another instance of Roche lobe overflow and lead to a secondary CE phase, evidence of which can be seen in observations of close NS-NS and WD-WD binaries. Interestingly, Hurley et al. (2002) found that the outcome of the CE phase was almost independent of eccentricity, since tides tend to force circularization of the orbit before the onset of RLOF. The configuration of the post-CE system may continue to change for a time after the envelope has been ejected, and as such, the eccentricity may change as the stars continue to interact through tides and stellar winds. A circumbinary disk may even form from the ejected material falling back into the plane of the orbit (e.g. Kashi & Soker, 2011).

Evidence supporting CE evolution is abundant. For example, CE evolution is the proposed origin of X-ray binaries (e.g. van den Heuvel, 1976), which may evolve from giant-MS pairs. After the primary fills its Roche lobe, mass transfer to the companion begins, and eventually terminates when core helium is ignited in the primary; it then moves to the helium MS. Its companion is still a normal MS star, however, and thus these systems may be observed as Wolf-Rayet binaries, in which the Wolf-Rayet star has a much smaller mass than its companion, although it is very blue and luminous. If the mass of the primary is below the Chandrasekhar limit, $M < M_{Ch}$, it will evolve into a WD; otherwise, the primary can explode in a SN, leaving either an NS or BH. If the companion of the remnant NS evolves into a giant, it begins losing significant mass in a stellar wind, causing the NS to emit X-rays within an X-ray binary (Ostriker, 1976). Observations of planetary nebulae (PNe, singular PN) containing a tight binary at the center seem to strongly support the need for the study of CE evolution as well, as mentioned by Paczynski (1976) in support of CVs. After spiral-in of the initial binary within the CE, the envelope is ejected, and forms a PN that may be quite different from PNe of single stars created in single star evolution. It is through observation of CE-originated PNe that the mass-loss during CE can be better understood (Jones & Boffin, 2017).

Double-core evolution (see Brown, 1995; Ivanova et al., 2013), originally proposed as a possible origin to NS-NS binaries, occurs when the initial mass ratio of the binary proceeding through a CE phase is close to unity, $q \sim 1$, and causes the ejection of the envelope of *both* stars instead of just

the giant. Due to this mass ratio, the mass transfer from the primary to the secondary may cause the secondary to expand and evolve into a giant as well, and to fill its own Roche lobe, creating a shared atmosphere made of material from both stars. After envelope ejection, this would leave the pre-CE cores exposed, and although it has not been confirmed at the time of writing, this would leave an interesting system to observe.

CE evolution is an exceedingly complex process, and recent reviews (e.g. Ivanova et al., 2013) indicate that in order to accurately model this relatively quick, violent phase, we must use hydrodynamic simulations. While these calculation-intensive scenarios may have proven impossible 40 years ago, recent advances in technology show an increase in computational power that may be used to solve many of the problems of CE evolution. As it is the most common case, many studies have focused on simulations in which at least one star is a giant; a list of the initial conditions of such systems, and their outcomes after the CE phase, can be found in Table 1 of Iaconi et al. (2017). Due to the overall complexity of the issue at hand, in this work we seek to focus only on the dynamical evolution of the system as the star's evolve through a CE. For example, any mass lost from the binary is assumed to be ejected isotropically (if it is not transferred directly to the companion star), thus removing any associated angular momentum, and this mass does not have the potential to fall back and form into a circumbinary disk around the binary. While we recognize that a circumbinary disk could affect orbiting planets, we leave these complications for implementation in a future hydrodynamical study.

The need for CE evolution studies was first presented by Paczynski (1976), and comprehensive calculations followed soon after. For example, Meyer & Meyer-Hofmeister (1979) calculated the results of a CE phase between a mass-transferring 5 $M_{\odot}$ giant and a 1 $M_{\odot}$ MS star, in which the inner cores rotate at a slower rate than that of the overlying envelope. This led to a relatively smooth evolution, in which the envelope was eventually ejected, with the main uncertainty being the previously mentioned problem of spherical symmetry. The advent of computational hydrodynamical simulations allowed this effect, among others too complicated to perform in simple calculations, to be included, and more accurate CE evolution has been modelled in recent years. Our dynamical simulations do not complete the problem, although they do form a strong basis for the outcome of the CE phase of the circumbinary planet (CBP)-harbouring *Kepler* candidates.

Stellar evolution theory, both for single and binary stars, is required to interpret the results of our simulations. While there is still much work to be done to successfully calculate and model the CE phase, our understanding will continue to increase in the near-future through observations and more complex simulations (e.g. Ivanova et al., 2013) with an increase in computing power.

1.4 Post-Common-Envelope Circumbinary Planets

It is clear from the preceding section that binary stars can survive the common-envelope phase of their evolution. It stands to reason, then, that planets orbiting close binaries – circumbinary planets (CBPs) – could potentially survive the CE phase as well, and even be affected by ejected stellar material (which could form into a disk around the binary). Such planets, known as post-common-envelope circumbinary planets (PCE CBPs) have been the subject of some recent studies: Portegies Zwart (2013) involving the CV system HU Aquarius and its two candidate CBPs, Mustill et al. (2013) involving NN Serpentis and its two candidate CBPs, and Völschow et al. (2014) regarding the possibilty of second-generation formation – that is, CBPs formed from the PCE circumbinary disk – within NN Serpentis. Zorotovic & Schreiber (2013) list six single-planet and six two-planet PCE CBP systems.

It is stunning to consider the possibility that a CBP could survive the violent evolution from the MS to, say, a compact CV, instead of forming in a circumbinary disk of ejected stellar material (a second-generation formation mechanism), or a small planet accreting material and becoming a much larger planet (a mixed-formation mechanism). Since the *Kepler* CBP systems studied by Kostov et al. (2016) and within this thesis consist of MS-MS binaries, their evolution through the CE phase may provide clues for the origin of these late-stage systems (including the energetic CVs) through comparison of our PCE configurations with those of the observed PCE CBP measurements.

1.5 Previous Work

CBPs are an active field of research, but their response to the evolution of their host stars has not been fully explored. Here, I outline some recent studies to underline the gap in our current knowledge, which will be more rigorously considered through the current study of *Kepler* CBP candidates.

Circumprimary planets are present in wide binary systems, and Kratter & Perets (2012) studied the possibility of such planets migrating and being captured in a stable orbit around the primary or the secondary star during mass transfer due to dynamical instabilities. This capture mechanism is supported by captured satellites around the gas giants within our own solar system (Heppenheimer & Porco, 1977; Astakhov et al., 2003), and provides a reasonable hypothesis for the potential discovery of planets in tight, habitable-zone orbits around white dwarfs (WDs) (Agol, 2011; Bear et al., 2011), positing that future observations could find planets around the primary or secondary in a WD-MS binary. Other outcomes include planet-star collisions and planetary ejection, the latter of which is also possible in our study's evolving circumbinary systems. As these collisions and ejections occur in wide binary systems, the authors did not investigate the CE stage, and used the Single Star Evolution code (SSE, Hurley et al., 2000), which serves as the basis for the Binary Star Evolution code (Hurley et al., 2002).

Mustill et al. (2013) studied NN Serpentis, a PCE system (the final outcome of close binary evolution) with two CBP candidates, which could provide evidence that CBPs can survive the violent CE evolution of a binary. The stability of the planets in this PCE system is debatable, and the authors reconstructed likely progenitor systems with both CBPs in stable orbits until the CE phase began; however, their survival appears unlikely for the entirety of the binary's lifetime. These CBPs could be survivors of the CE stage, but the authors suggest that the CBPs may be the result of second-generation planet formation from a circumbinary disk. The CE phase of close binary evolution strongly influences the CBP, and this evolution is likely the key to determining whether the planet is able to survive throughout the system's lifetime.

A separate study by Portegies Zwart (2013) focused on two PCE CBPs in HU Aquarii, a CV system containing a WD and a low-mass MS star. The CBPs can survive when the envelope is ejected due to their orbital distance, and thus a stable progenitor configuration can be reasonably reconstructed; Portegies Zwart (2013), the author of this paper, also attempted to constrain CE parameters, such as the efficiency of envelope ejection and the timescale of the mass-loss event. CE mass-loss rates as high as $\dot{M} = 2\ M_{\odot}\ yr^{-1}$ seem probable (Ricker & Taam, 2012); the author, for simplicity, used a constant mass-loss rate based on the envelope mass and the planetary period. Two constant mass-loss regimes are adopted within the study, fast and slow, as within our study (outlined in the next section), with the fast mass loss leading to significant effects on the CBP eccentricity, and slow mass loss resulting in adiabatic orbital expansion. Defining a constant mass loss simplifies the complexity of the CE evolution, allowing numerical integration of the CBP orbit, and allowing determination of the timescale of the CE phase. The planetary progenitor parameters described by Portegies Zwart (2013) are consistent with *Kepler* CBPs, which we use in our study.

The survival prospects of a planet around an evolving single star was explored by Veras et al. (2011). When the planet's orbital timescale is much shorter than the mass-loss timescale, the adiabatic approximation (that is, slow mass loss in which the semi-major axis increases while the eccentricity remains constant (Hadjidemetriou, 1963)) is valid; however, for orbits comparable or much greater than the mass-loss timescale, a different approach must be adopted. This study, along with a second study by Veras & Tout (2012), outlined three regimes: the adiabatic regime, the transition regime, and the runaway regime, respectively (these three regimes are detailed in Chapter 2 of this thesis). This second study extended the ejection probabilities to multiple star systems, and discovered that planets on wide orbits are likely to be ejected as the host stars evolve. As our *Kepler* CBPs exist in the transition regime for the typically-considered CE mass-loss timescales of a few years – i.e., the CBP orbits are comparable to the mass-loss timescale during the CE stage – we use the equations defining each regime outlined by Veras et al. (2011) and Veras & Tout (2012) to check the validity of our dynamical evolution model during the CE phase.

Our initial study of nine close binary systems (Kostov et al., 2016, hereafter KM16) determined that *Kepler* CBPs predominantly remain bound to their host binaries after the CE phase, except

in a few cases where the simulations end in a SN explosion. It appears that a planet in an evolving close binary system has better survival prospects than one in an evolving single-star system; the massive influence of the two stars on each other causes the envelope to be much smaller than that of an expanding giant, and thus a Mercury-distance CBP can survive the evolution of a 1-$M_{\odot}$ binary. The PCE orbital configurations of *Kepler* CBPs are qualitatively consistent with observed PCE CBPs (e.g. Zorotovic & Schreiber, 2013). It should be noted, however, that observed PCE CBPs are highly controversial; our study is qualitatively and quantitatively much different than the studies which reconstruct possible progenitor configurations, in that we begin with 100% confirmed planets with well-known parameters.

Chapter 2

Methods & Materials

Studying the dynamical evolution of a CBP orbiting a *Kepler* binary is a computationally-heavy process. The required codes for binary star evolution and resolution of the CE phase are open-source, with the binary star evolution code, BSE, being widely preferred in binary population synthesis studies, and the CE phase-resolving numerical integrator, REBOUND, continuously updated to better account for evolutionary effects in multi-body systems. This chapter will briefly detail some important equations first proposed by Veras et al. (2011) and Veras & Tout (2012), and used in the initial study (KM16), to properly interpret the results of the BSE/REBOUND pipeline, followed by an explanation of the two codes, and their applicabilities to this study.

2.1 Relevant Equations

Interpretation of our results requires a few equations of varying complexity. These important equations, and their relevance to our results, will be noted here for completeness.

The dynamical evolution of CBPs around an evolving binary, especially as it evolves through a CE phase, can be divided into two regimes: adiabatic and non-adiabatic. We can characterize these using a mass-loss index Ψ, detailed by Veras & Tout (2012) for the case of a planet orbiting a single star.

$$\Psi \equiv \frac{\alpha_M}{n\mu} = (2\pi)^{-1} \left(\frac{\alpha_M}{1\ M_\odot\ \mathrm{yr}^{-1}} \right) \left(\frac{a_{p,0}}{1\ \mathrm{AU}} \right)^{\frac{3}{2}} \left(\frac{\mu}{1\ M_\odot} \right)^{-\frac{3}{2}}. \tag{2.1}$$

Here, α_M is the mass-loss rate, $a_{p,0}$ is the planet's initial semi-major axis, and $\mu = M_{star} + M_p$ is the total mass of the system. A mass-loss index of $\Psi \ll 1$ indicates that the planet is in the adiabatic regime, and its orbit will expand while its eccentricity remains constant. A mass-loss index of $\Psi \gg 1$ indicates the non-adiabatic regime, in which the planet sees an instantaneous mass loss; its orbital evolution is then said to be in the "runaway" regime, and its survival is critically dependent on the mass ratio between the final and initial total mass of the system, $\beta = \mu_{final}/\mu_{init}$, as well as the orbital phase configuration of the system when mass-loss begins. A highly eccentric planet at

periastron would then likely be ejected, while a planet at apastron on a circular orbit is likely to remain bound.

If significant mass is lost from the system during the mass-loss event, the planet may be ejected. Veras et al. (2011) define a critical mass ratio for determining ejection during mass-loss as,

$$\beta_{eject} \equiv 0.5\,(1 + e_{p,0}) \tag{2.2}$$

where $e_{p,0}$ is the planet's initial eccentricity. Using the previous two factors, $\beta < \beta_{eject}$ determines that a planet on a circular orbit, or at pericenter in an eccentric orbit, will be ejected. An eccentric planet at apocenter at the onset of mass-loss will remain bound regardless, and its orbit will expand and either circularize or gain a slight eccentricity. A planet that remains bound in the runaway regime will achieve a semi-major axis which can be calculated to be,

$$a_{runaway} \equiv \frac{a_{p,0}\,(1 \mp e_{p,0})}{2 - \beta\,(1 \pm e_{p,0})} \tag{2.3}$$

where the signs correspond to either the pericenter or apocenter case, respectively.

The CE stage occurs very rapidly on an astronomical timescale, and our *Kepler* CBPs have orbits on timescales comparable to the length of CE evolution; the CE phase of the host binary can begin and finish within a few CBP orbits, or even a single orbit. Because of the comparable timescales, we cannot classify this evolution as either uniquely adiabatic or non-adiabatic. Rather, the CBPs' orbital evolution exists in a transition regime between these two extremes, for $\Psi \sim 0.1 - 1$. Since both a_{CBP} and e_{CBP} can either increase or decrease, we cannot conclude with certainty if the CBP is likely to remain bound or become unbound before detailed simulations. As noted by KM16, since the *Kepler* CBPs are within this transition regime, CE evolution is likely to have a dramatic effect on the orbital parameters of the CBP, which was confirmed by the simulations of the initial circular, coplanar simulations.

In this thesis, the same critical mass-loss rate as KM16, α_{crit}, corresponding to $\Psi = 1$, is adopted to better interpret our REBOUND results. Through comparison of this value and the chosen mass-loss rate α_M, the stability of the CBP can be determined, as well as the potential of its ejection from the system. A system in which $\alpha_M \gg \alpha_{crit}$ will see an instantaneous mass loss, while more smooth adiabatic orbital expansion will be experienced when $\alpha_M \ll \alpha_{crit}$. A secondary CE phase will have two values of α_{crit}, corresponding to the results of the primary CE for each of the two mass-loss rates.

With this in mind, it is clear that the evolution of the binary, and the entire binary-planet system, is a complex problem due to the orbital and evolutionary timescales involved. The binary must be evolved independently first using a code which can account for significant effects and the important CE stage. This stage, as it is very short, can be resolved using an n-body numerical integrator, and the dynamical evolution during this phase can be tested. The two codes which achieve this, BSE and REBOUND, are outlined in the following sections.

2.2 Binary Star Evolution Code

Some important processes and stages of binary evolution are reiterated here to keep the description of the code cohesive, even if some of the statements appear redundant at first, and any assumptions made by Hurley et al. (2002) are included when necessary. Our initial study (KM16), as well as the study conducted for this thesis, uses the established, open-source Binary Star Evolution code (Hurley et al., 2002), or BSE, to evolve our stars. As stated previously, binaries can be categorized as either wide binaries or close binaries; *Kepler* CBP systems are classified as the latter. Varying α_{CE} in our simulations was key to determining the outcome of the CE phase; in our simulations, mergers only occurred for $\alpha_{CE} \leq 1$, as one would expect.

Observations of the 13 *Kepler* targets used in our simulations provide more information than required to run BSE, although these additional parameters prove useful in our REBOUND dynamical simulations, explored in the next section. BSE is an improvement over previous binary stellar evolutionary codes, as it includes additional binary-specific features such as mass transfer, wind accretion, CE evolution, and collisions (Hurley et al., 2002, hereafter HTP2002), and is widely used to simulate binary evolution. The evolution algorithm used is thorough and detailed, allowing many processes to be turned on or off based on specific requirements. Our simulations take advantage of this by turning tidal circularization on and off; in keeping with the terminology of KM16, these are TCP (Tidal Circularization Path) and NTCP (No Tidal Circularization Path) respectively. Since the *Kepler*-observed CBP systems contain MS stars, all simulated stars begin on the ZAMS for simplicity. It is possible, however, to begin at any potential evolutionary state, such as in corotation with the orbit. Though the evolution timestep range is robust, there are limiting factors to prevent the primary mass and radius changing too much (not more than 1% and 10%, respectively), which helps identify the time if and when the star fills its Roche lobe.

While the binary is detached, each star is individually evolved using SSE (Hurley et al., 2000) (which was also used by Kratter & Perets (2012) to evolve wide binaries), while including the necessary tidal and braking mechanisms. Wind accretion is included through setting the wind velocity in the model as the escape velocity from the stellar surface; however, if both stars have a stellar wind at the same time, the code ignores the interaction between the winds. When the companion accretes material from the wind, a fraction of the primary's intrinsic spin is transferred to the companion's spin angular momentum at assumed perfect efficiency. Orbital circularization is partially achieved by accounting for more mass accretion at periastron than apastron of an eccentric orbit, but mainly through tidal interactions, which are integral to binary evolution and also allow the exchange of orbital angular momentum with the instrinic stellar spins. If, at any point in the simulation before either Roche lobe is filled, the periastron separation is less than the combined radii of the two stars, they collide, and the outcome is determined based on the parameters at that time.

RLOF in the binary can lead to two outcomes: either the stars come into contact and coalesce, or initiate a CE phase. Most frequently, as previously mentioned, CE evolution occurs with a giant star

transferring mass to an MS star on a dynamical timescale; when the giant overfills the Roche lobes of both stars, the giant core and MS star are contained within a common envelope. BSE also allows a CE to begin through the collision between a dense core and a star. The envelope rotates slower than the orbiting "cores" within due to expansion, and this friction causes in-spiral and energy transfer to the envelope, with an efficiency of α_{CE}, a parameter previously outlined. The outcome of this phase is either ejection of the envelope (assumed to be isotropic), leaving a close PCE WD-MS pair (assumed to be in corotation with the orbit), or coalescence of the cores, leaving a single giant star. The code determines the outcome of this phase based on the initial binding energy of the envelope and the initial orbital energy of the two cores, similar to the energy formalism outlined in Ivanova et al. (2013). It should also be noted that the code accounts for the potential avoidance of a CE, and the possibility of collisions leading to core-sinking depending on the stellar types, which may lead to rejuvenation (i.e., the star returns, age-wise, to an earlier stage in its evolution).

The initial parameters for each of the 4 systems (and 1 previous system from KM16) studied in this thesis can be seen in Table 2.1. The input file for BSE contains the masses of the primary and secondary stars ($0.1 - 100 M_{\odot}$), their stellar types (see Table 2.2), the binary orbital period (in days), the eccentricity ($0.0 - 1.0$ inclusive), the maximum evolution time (chosen as 15 Gyr, roughly the age of the Universe (Chaboyer, 1998) (see Planck Collaboration et al., 2016, for a recent measurement), although some simulations are shorter if the system settles down and stops evolving, or the stars coalesce), and the metallicity ($0.0001 - 0.03$, where 0.02 is solar metallicity). Note that, unless otherwise stated, every star is initiated as a MS (or low-mass MS) star in the input. All input parameters are known to high precision. The parameters for model A of HTP2002, described as the most favourable and effective, were used as the default for all systems. Model A specifically turns tides on and uses a higher $\alpha_{CE} = 3$, instead of the usually chosen $\alpha_{CE} = 1$. This model used many of the code's default input parameters, including, but not limited to, all wind-related parameters. The value for the wind velocity factor, which affects the wind mass-loss rate, was set to one-quarter of the default value, simply as a conservative lower limit, since the default value within the code causes slower mass loss, but leaves the final state of the system unchanged. The slight differences observed in the choice of this variable were only noticeable in the 0.001% change in separation in the 0.05 Myr before the CE phase.

Table 2.1: *Kepler* Binary-CBP Candidate Default Initial Parameters

Name	Kepler ID	M_1 [$M_\odot$]	M_2 [$M_\odot$]	T_{bin} [days]	e_{bin}	Metallicity Z	P_{CBP} [days]	e_{CBP}	i_{CBP} [degrees]	M_{CBP} [M_{Jup}]
Kepler-64	4862625	1.47	0.37	20	0.22	0.03†	138.5	0.054	0.0	
KIC 782	7821010	1.28	1.23	24.24	0.68	0.02	995	0.35	6.0	2.6
KIC 393	3938073	1.45	0.83	48.48	0.43	0.02	270	0.1	15.0‡	
KIC 861	8610483	0.96	0.96	31	0.5	0.02	400	0.0	10.0	
KIC 509	5095259	1.21	0.51	18.61	0.246	0.01/0.02	237.71	0.06	26.0	7.7

†: While the actual default metallicity is $Z = 0.031$, this value is the upper limit allowed by BSE.

‡: The inclination of the CBP is not well defined, so we test a range of $i_{CBP} = [0, 30, 60, 90, 120, 150, 180]$.

Table 2.2: BSE Stellar Types

Stellar Type	Description
0	Deeply or fully convective low-mass MS star
1	Main Sequence star
2	Hertzsprung Gap (HG)
3	First Giant Branch (GB)
4	Core Helium Burning (CHeB)
5	Early Asymptotic Giant Branch (EAGB)
6	Thermally Pulsing Asymptotic Giant Branch (TPAGB)
7	Main Sequence Naked Helium star (HeMS)
8	Hertzsprung Gap Naked Helium star (HeHG)
9	Giant Branch Naked Helium Star (HeGB)
10	Helium White Dwarf (HeWD)
11	Carbon/Oxygen White Dwarf (COWD)
12	Oxygen/Neon White Dwarf (ONeWD)
13	Neutron Star (NS)
14	Black Hole (BH)
15	Massless Supernova/Massless Remnant

Our previous study (KM16) tested a wide range of variables based on the 1-σ uncertainties in the primary and secondary masses, M_1 and M_2, and the metallicity Z. This parameter space exploration can be seen in Table 2.3. The four new systems simulated within this thesis are relatively recent discoveries, and thus their uncertainties, including those of the CBP eccentricities and inclinations, are not well constrained. As such, only the values for M_1, M_2, and Z are tested, significantly reducing the number of simulations. While not included until our REBOUND simulations, it is worth noting that, due to large uncertainty in measurements of the inclination of the CBP in KIC393, we test a

range of inclinations ($i_{CBP} = [0, 30, 60, 90, 120, 150, 180]^\circ$) to explore the impact of CBP inclination on the dynamical stability.

Table 2.3: BSE Parameter Space

Parameter	Values Tested (Kostov et al., 2016)	New Values Tested†
M_1	$\mathbf{M_1}, M_1 + 3\sigma, M_1 - 3\sigma$	$\mathbf{M_1}$
M_2	$\mathbf{M_2}, M_2 + 3\sigma, M_2 - 3\sigma$	$\mathbf{M_2}$
Metallicity Z	$\mathbf{Z}, Z + 1\sigma, Z + 2\sigma, Z + 3\sigma, Z - 1\sigma, Z - 2\sigma, Z - 3\sigma$	$\mathbf{Z}$
α_{CE}	$0.5, 1.0, \mathbf{3.0}, 5.0, 10.0$	$0.5, 1.0, \mathbf{3.0}, 5.0, 10.0$
Tides	OFF, **ON**	OFF, **ON**
de Kool CE Model	**OFF**, ON	Not tested
Force Corotation	**OFF**, ON	Not tested

Note: Values denoted in boldface represent the default parameters used in our simulations.

†: Uncertainties for most systems unpublished, so much smaller initial parameter space for this study.

The CE efficiency factor, α_{CE}, is an uncertain parameter, and so we test five values ($\alpha_{CE} = 0.5, 1.0, 3.0, 5.0, 10.0$), where higher values account for energy sources other than orbital energy. These can also be seen in Table 2.3. Tides are speculated to be a dominant source of uncertainty in binary evolution, and thus we simulate both tidal circularization on (Tidal Circularization Path, TCP) and off (No Tidal Circulation Path, NTCP).

As the stars evolve, the stellar types change, and each type is checked throughout the code to ensure the correct evolutionary tracks for both the individual stars as well as the entire system. These numerical values, as well as what they represent, can be seen in Table 2.2, and are also printed out at each major stage of the code (for example, when the type changes, or when Roche lobe overflow begins; see Table 2.5). The output printout of BSE over the allotted maximum time for each system includes the mass of each star, the aforementioned stellar types, the binary separation, the eccentricity, the log of the radius over the Roche lobe radius of each star, and the "Type" label. This label marks significant events relevant to the system at a given time; the beginning and end of RLOF and the CE phase, coalescence of the two stars, and stellar contact are just a few. These labels, along with their meaning, can be seen in Table 2.4. It is through these labels that the instantaneous timescale of CE evolution can be determined.

Table 2.4: BSE Output Evolution Stages

Evolutionary Stage Label	Description
INITIAL	Initial configuration
KW CHNGE	Stellar type change
BEG RCHE	Begin Roche lobe overflow
END RCHE	End Roche lobe overflow
CONTACT	Contact system
COELESCE	Coalescence of stars
COMENV	Common-envelope system
GNTAGE	New giant star from CE; appropriate age and initial mass set to match core-mass and stellar mass
NO REMNT	No remnant
MAX TIME	Max evolutionary time reached; end of program
DISRUPT	System is disrupted
BEG SYMB	Begin symbiotic system
END SYMB	End symbiotic system
BEG BSS	Begin blue stragglers

Table 2.5: BSE evolution of KIC393 for $\alpha_{CE} = 0.5$, NTCP (top) and $\alpha_{CE} = 1.0$, TCP (middle), and KIC861 for $\alpha_{CE} = 1.0$, NTCP (bottom). Note that in this table, Ty1 and Ty2 are Stellar Type 1 and Stellar Type 2, respectively.

Time [Gyr]	M_1 $[M_\odot]$	M_2 $[M_\odot]$	Ty1	Ty2	a_{bin} $[R_\odot]$	e_{bin}	$R_1/R_{RL,1}$	$R_2/R_{RL,2}$	Evol. Stage
KIC393									
0.00	1.450	0.830	1	1	73.616	0.43	0.045	0.031	INITIAL
3.027	1.450	0.830	2	1	73.616	0.43	0.080	0.031	KW CHNGE
3.126	1.450	0.830	3	1	73.625	0.43	0.104	0.031	KW CHNGE
3.308	1.440	0.831	3	1	73.785	0.43	1.00	0.031	BEG RCHE
3.308	0.322	0.831	10	1	1.828	0.00	1.00	0.031	COMENV
3.308	0.322	0.831	10	1	1.828	0.00	0.032	0.909	END RCHE
4.862	0.322	0.831	10	1	1.680	0.00	0.035	1.000	BEG RCHE
5.268	0.322	0.717	10	0	1.131	0.00	0.050	1.361	KW CHNGE
5.268	1.039	0.717	3	15	0.00	0.00	0.00	-1.00	COELESCE
5.273	1.036	0.00	4	15	0.00	-1.00	0.00	-1.00	KW CHNGE
5.428	0.955	0.00	5	15	0.00	-1.00	0.00	-1.00	KW CHNGE
5.432	0.874	0.00	6	15	0.00	-1.00	0.00	-1.00	KW CHNGE
5.433	0.608	0.00	11	15	0.00	-1.00	0.00	-1.00	KW CHNGE
15.00	0.608	0.00	11	15	0.00	-1.00	0.00	-1.00	MAX TIME
KIC393									
0.00	1.450	0.830	1	1	73.616	0.43	0.045	0.031	INITIAL
3.027	1.450	0.830	2	1	73.616	0.43	0.080	0.031	KW CHNGE
3.126	1.450	0.830	3	1	73.632	0.43	0.104	0.031	KW CHNGE
3.304	1.443	0.830	3	1	53.607	0.00	1.00	0.043	BEG RCHE
3.304	0.297	0.830	10	1	2.368	0.00	1.00	0.043	COMENV
3.304	0.297	0.830	10	1	2.368	0.00	0.026	0.690	END RCHE
3.341	0.297	0.830	10	1	1.636	0.00	0.038	1.00	BEG RCHE
3.468	0.327	0.717	10	0	0.911	0.00	0.061	1.672	KW CHNGE
3.468	1.044	0.717	3	15	0.00	0.00	0.00	-1.00	COELESCE
3.473	1.040	0.00	4	15	0.00	-1.00	0.00	-1.00	KW CHNGE
3.625	0.960	0.00	5	15	0.00	-1.00	0.00	-1.00	KW CHNGE
3.628	0.877	0.00	6	15	0.00	-1.00	0.00	-1.00	KW CHNGE
3.629	0.610	0.00	11	15	0.00	-1.00	0.00	-1.00	KW CHNGE
15.00	0.610	0.00	11	15	0.00	-1.00	0.00	-1.00	MAX TIME
KIC861									
0.00	0.960	0.960	1	1	51.597	0.50	0.043	0.043	INITIAL
12.888	0.960	0.960	2	2	51.597	0.50	0.079	0.079	KW CHNGE
13.567	0.959	0.959	3	3	51.624	0.50	0.109	0.109	KW CHNGE
14.308	0.952	0.952	3	3	51.805	0.50	0.661	0.661	CONTACT
14.308	0.249	0.249	10	10	0.378	0.00	0.661	0.661	COMENV
14.415	0.249	0.249	10	10	0.052	0.00	1.001	1.001	BEG RCHE
14.415	0.249	0.249	15	15	0.00	0.00	0.00	-1.00	COELESCE

The instantaneous timescale of the CE phase seen in the output (for some example outputs, see Table 2.5) are caused by the very short lifetime of the CE, which is not resolved within the code; BSE thus recognizes the process, beginning with RLOF, and forces the system through this phase instantaneously, allowing the evolution to proceed with calculated PCE parameters. Since drastic changes in the binary configuration will strongly affect the CBP, the initial and final state of the

system during this phase is used as the input for REBOUND, and the effects on the planet must be accounted for using numerical integration. While BSE provides a robust framework to deal with the binary stars in our system, the effects of the CE phase on the CBP must be handled by REBOUND, which will be detailed in the following section.

2.3 Dynamical Simulations

The dramatic mass loss during CE occurs on scales of tens to hundreds of years, much too small for BSE to adequately resolve. The open-source REBOUND (Rein & Liu, 2012) package contains a high-order n-body numerical integrator, IAS15 (Rein & Spiegel, 2015), that allows us to resolve the instantaneous CE phase from BSE, while also adding a third body, the CBP, and directly integrate the orbit of the CBP during the CE. REBOUNDx (`https://github.com/dtamayo/reboundx`) allows additional effects such as orbital migration and mass loss to be included in our simulations of point-mass objects, achieving clearer dynamical evolution with this extra toolbox. The REBOUNDx routine modify_orbits_forces adds a drag force opposite to the stars' motion, allowing modification of the orbits (in this case, shrinkage) (Papaloizou & Larwood, 2000). In our dynamical CE evolution, we choose a constant mass-loss rate, similar to the one used by Portegies Zwart (2013). Since our CBP orbits are on timescales comparable to the length of the CE, we test two mass-loss regimes, α_M, which determine the length of the CE in our simulations – fast ($1 M_\odot\ yr^{-1}$) and slow ($0.1 M_\odot\ yr^{-1}$, which guarantees adiabatic orbital expansion (Hadjidemetriou, 1963)). Another REBOUNDx routine, modify_mass, employs an exponential mass loss on an e-folding timescale τ_M.

Our BSE simulations provide the necessary REBOUND inputs for both stars, specifically their initial and final masses, M_0 and M_f, with which we can calculate the length of the CE phase using our mass-loss rate α_M as,

$$T_{CE} = \frac{M_f - M_0}{\alpha_M} \tag{2.4}$$

We adopt exponential decay for the semi-major axis to be consistent with CE hydrodynamical simulations. For simplicity, we adopt the same functional decay for the stellar mass loss. This mass-loss rate, in terms of τ_M, within our REBOUND simulations is then,

$$\dot{M} = -\frac{M}{\tau_M},\ \tau_M = \frac{\tau_{M,0}}{(1 - t/T_{CE})} \tag{2.5}$$

where

$$\tau_{M,0} = \frac{T_{CE}}{2\ln(M_0/M_f)} \tag{2.6}$$

This allows the preceding equation to be solved analytically.

$$M(t) = M_f \left(\frac{M_0}{M_f}\right)^{(1-t/T_{CE})^2} \tag{2.7}$$

REBOUND allows evolution of both the semi-major axis of the binary a_{bin} and the total mass of the binary M_{bin}, although through Kepler's 3rd Law, these two are intimately linked. While they are

changing independently (i.e. for a merger, the secondary mass M_2, and a_{bin} are trying to go to zero), the relation between them must still hold. We force the relation to hold at each timestep, however, using corrections, allowing the non-merger final binary semi-major axis a_{bin} to agree with the values output by BSE, and allow the merger of the two stars to be smooth and occur at the correct time ($t/T_{CE} = 1$), as truncating the merger is a problem within the code. In some simulations, we see e_{CBP} decrease or fluctuate – this is caused by solving equations of motion for orbits that are not closed, and it normalizes to the required circularization value of zero as the simulation runs. This accounts for orbital circularization.

When a perfect merger occurs (i.e., a merger without mass loss) there is no effect on the planet, as there is no noticeable effect on the system and no mass or angular momentum is lost – the resulting merged star (usually a giant) contains the exact sum of the pre-CE stars' masses, and the angular momentum is assumed to spin up the star, thus the planet sees no change. Perfect mergers can be seen in some of our simulations, e.g. KIC393, $\alpha_{CE} = 0.5$, NTCP, and $\alpha_{CE} = 1.0$, TCP (see Table 2.5). To maintain consistency with the previous study (KM16), the CBP ejection limit was set to $e_{CBP} = 0.95$, chosen to represent the uncertainties in the explored large parameter space, and allowing quantification of the survival probability of the *Kepler* CBPs. The CBP inclination, i_{CBP}, does not change in our REBOUND simulations from its initial input value due to the conservation of angular momentum within the system, and so we see, e.g., the CBP in KIC861 remaining at $i_{CBP} = 10^\circ$ for the duration of the CE phase, precessing at constant inclination. Any secondary CE begins with the mode values of a_{CBP} and e_{CBP} from the preceding CE simulations.

Another important parameter is the orbital phases of the bodies at the onset of the CE. For example, a CBP at periastron at the beginning of the short-lived CE phase is more likely to be ejected than a CBP at apastron. This phase offset ($\Delta\theta_0 \equiv \theta_{CBP,0} - \theta_{bin,0} - \omega_{bin}$, in which the θ values are the true anomalies, the angular position in the orbit, of the CBP and binary, respectively, and ω_{bin} is the angle from the binary's ascending node to its periapsis) is accounted for by testing 50 initial CBP phases between 0 and 1, sampled in steps of 0.02, and 4 initial binary phases (Eastern and Western Elongations, EE and WE, and Superior and Inferior Conjunctions, SC and IC, the four binary orbit turning points).

To summarize, the BSE simulations provide tests of $\alpha_{CE} = [0.5, 1.0, 3.0, 5.0, 10.0]$ and TCP/NTCP, while REBOUND allows the addition of two constant mass loss-rates $\alpha_M = 0.1 M_\odot\ yr^{-1}$ and $1 M_\odot\ yr^{-1}$ and the 200 initial orbital phase configurations to adequately fill the parameter space in which the system evolves through a CE. We note that the *Kepler* systems are dynamically stable prior to the CE stage.

It is with the combination of our BSE/REBOUND pipeline that we can determine the ultimate fate of the *Kepler* CBPs as their stars proceed through a CE stage. The large range of values tested cover many uncertainities, and may provide a reasonable origin for PCE CBPs seen in the literature (e.g. Mustill et al., 2013; Portegies Zwart, 2013; Zorotovic & Schreiber, 2013). The results of our

dynamical evolution simulations are detailed in the following chapter.

Chapter 3

Simulations & Results

Our initial study (KM16) forms the foundation of this thesis, serving as a strong background with which the additional four *Kepler* candidate CBPs can be compared. Nine systems were evolved, five of which experienced at least one CE phase (and three of which will be briefly detailed in this chapter), and the CBPs predominantly remained bound, with their orbits expanding while their host stars either became single stars or tight, late-evolution binaries. Other scenarios, which were also seen in the new results, included tests of the secondary CE (which indicated that ejections were much more likely during this stage), and the possibility of the binary exploding in a Supernova explosion at some point in its evolution, disrupting the entire system. The surviving binary-CBP systems, however, allowed comparisons with observed PCE CBPs, providing an origin for some of these highly-evolved CBP systems as the results appeared qualitatively consistent.

The nine *Kepler* CBP systems studied by Kostov et al. (2016) had CBP orbits which were both circular (or nearly circular) and coplanar with the orbit of their host binary. This thesis focuses on four new MS systems from *Kepler*, where the CBPs are on eccentric, inclined orbits relative to their host binaries. While there are still clearly limitations caused by the exclusion of hydrodynamics, the results for the four eccentric, non-coplanar systems – KIC782, KIC393, KIC861, and KIC509 – are fascinating, and form an interesting contrast with those of the study of KM16.

3.1 Select Highlights of Previous Results

The responses of the nine *Kepler* binaries studied by Kostov et al. (2016) to CE are quite diverse; the binary will exit this stage as a merged giant star, a tight PCE binary, or through a SN explosion. In the original study (KM16), Kepler-38 showed a simple dynamical outcome compared to some of the other systems. The stars spiral-in during their CE phase, from an orbital period of 18 days to 0.6 days, with the primary evolving from a RGB star to a C-O WD, and the secondary remains as a low-mass MS star. Other systems, such as Kepler-64, show the capabilities of BSE for systems

that do not remain as a binary. These stars survive the first CE after primary RLOF, and this first envelope is driven off from the system, leaving a helium WD primary and a low-mass MS secondary. After the secondary fills its Roche lobe, a second CE phase occurs, and the stars coalesce, leaving a single RGB star which continues to evolve into, eventually, a C-O WD. This possibility, among others such as destruction of both stars through a SN explosion, show the flexibility of the BSE framework, as all relevant processes are included.

Some of the original systems (KM16) displayed unique results, which are interesting to mention due to the similar evolution seen in the new binaries. A few examples will be outlined below, with details from the original study included.

1. Kepler-34, initially consisting of a 1.05 $M_{\odot}$ + 1.02 $M_{\odot}$ binary on a highly eccentric ($e_{bin,0}$ = 0.52), 28-day orbit, ends in a Supernova during its primary CE stage, disrupting the entire system.

2. Kepler-47 has 3 planets on initial orbits of 0.3 AU, 0.72 AU, and 0.99 AU, and masses of 2 $M_{\oplus}$, 19 $M_{\oplus}$, and 3 $M_{\oplus}$, leading to adiabatic/non-adiabatic orbital expansion being experienced (by different planets) during the same CE phase. This evolution can be seen in Fig. 3.1, which shows the results for the primary CE merger case, resulting from $\alpha_{CE} = 0.5/1.0$. The middle planet may be ejected during this phase for $\alpha_M = 1.0 M_{\odot}\ yr^{-1}$, while all 3 planets remain bound and exhibit adiabatic orbital expansion in other cases. The presence of multiple CBPs mean they will continue interacting after the CE phase has ended, leading to the 1-Myr planet-planet ejection probabilities which can also be seen in Fig. 3.1, after Kostov et al. (2016).

3. Kepler-1647 has both primary- and secondary-triggered CE phases; in the non-merger case, after the primary CE (in which the planet remains bound, even in the runaway regime), the close HeWD-MS eventually initiaties a second RLOF event in which ejections are likely. This second CE either leads to a merger into a single C-O WD, a non-merger leaving a tight WD-WD binary, or a third RLOF which ends in a SN explosion.

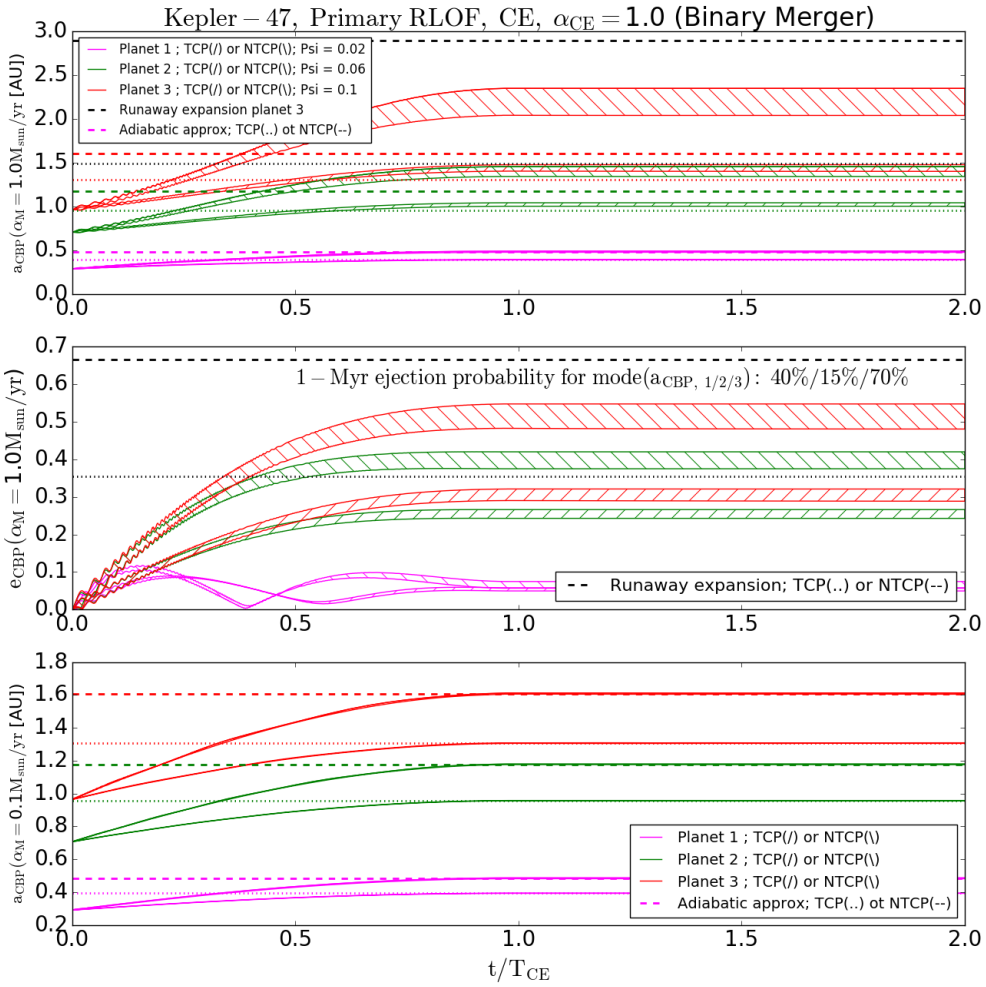

Figure 3.1: Kepler-47 Primary CE Merger plots, after Kostov et al. (2016), displaying the interesting evolution seen when 3 planets are present. The evolution of a_{CBP} and e_{CBP} is shown for fast mass-loss (top and middle panels, respectively), while the evolution of a_{CBP} for slow mass-loss is shown in the bottom panel. Both adiabatic and non-adiabatic orbital expansion may be experienced (by different planets) during the CE, based on the different CBP orbital timescales compared to the timescale of the CE mass-loss event, T_{CE}/P_{CBP}. As the planets continue to interact after the CE, the 1 Myr planet-planet ejection probabilities are shown in the second panel, which are 40%/15%/75% from inner to outer planet, respectively.

3.2 New Results

In addition to the nine systems studied by KM16, there are four additional *Kepler* CBP candidates. While three of these have not yet been published, they have been presented at numerous meetings and conferences. The fourth system was published very recently. The four new studied systems are KIC7821010, KIC3938073, KIC8610483 (Welsh et al., Towards Other Earths II Conference, 2014, Porto, Portugal), and KIC5095259 (Getley et al., 2017). These new systems expand the sample size by 44%, with a total of thirteen systems. The first nine systems' CBPs have negligible inclination and are in almost perfectly circular orbits, as previously mentioned; however, Kepler-64b, the confirmed CBP orbiting the binary Kepler-64, has a measured eccentricity. This system was tested as a precursor to the new systems to conceptualize the impact of eccentricity. Each of the new systems was simulated with its observed properties, including the measured e_{CBP} and i_{CBP}. Due to the uncertainties in their metallicities, all four new system candidates are simulated using solar metallicity ($Z = 0.02$; KIC509 also tests $Z = 0.01$), and a range of CBP inclinations from $0 - 180$ degrees is tested for KIC393.

As three of these CBPs are not published yet, there are currently no error bars on the measured values as of writing. The only published system, KIC509, also has no published uncertainties on either the binary or CBP parameters. Since a perfect merger (i.e. a merger without mass loss) of the binary has no effect on the orbiting CBP, it is not run through the REBOUND simulations as there will be no change to either a_{CBP} or e_{CBP}.

Many of our simulations lead to PCE CBP parameters with non-normal probability distribution functions; because of this, final outcomes of $a_{CBP,PCE}$ and $e_{CBP,PCE}$ are better represented by their mode values than their medians, like in KM16. Thus for secondary CE simulations, we use the modes of a_{CBP} and e_{CBP} from the prior CE as initial values. This is usually the case for TCP simulations, with probability distribution functions having a bimodal "peaked-at-edges" histogram, while NTCP simulations usually have a clear mode.

The simulations of the four new (and one previously studied) systems produce intriguing results, which will be outlined below, beginning with the previously evolved Kepler-64. The BSE outcomes for all α_{CE} and NTCP/TCP simulations are shown in Table A.1.

3.2.1 Kepler-64

One of the original systems (KM16) was first run through the pipeline with the actual values for these parameters. Although the evolution of the binary is the same as that in the original study, it will be outlined here for completeness, along with the new results including the CBP's eccentricity.

The Binary

The binary initially consists of a 1.53 $M_\odot$ primary and 0.41 $M_\odot$ secondary on a slightly eccentric ($e_{bin,0} = 0.22$), 20-day orbit. It should be noted that the metallicity tested in BSE was $Z = 0.03$, the maximum allowed value in the code, instead of the actual $Z = 0.031$. The primary CE begins at t$\sim$3.02 Gyr. For evolution in the fast mass-loss regime of $\alpha_M = 1 M_\odot\ yr^{-1}$, $\Psi \approx 0.03$ and $\alpha_{crit} \approx 32 M_\odot\ yr^{-1}$, much larger than both tested mass-loss regimes; however, the timescale of the CE event is comparable to the timescale of the CBP orbit, with $T_{CE}/P_{CBP} \sim 1.1-3.4$, depending on α_{CE}. This means that the CBP orbit will evolve non-adiabatically, although its evolution technically falls in the adiabatic regime.

The outcome of the CE depends on the value of α_{CE}. For $\alpha_{CE} = 0.5, 1.0$, the binary merges into a First Giant Branch star, losing $\sim$20 – 58% of its initial mass. The CBP may be ejected in a runaway regime for $\alpha_{CE} = 1.0$, NTCP, since $\beta < \beta_{eject}$; for $\alpha_{CE} = 0.5$ and $\alpha_{CE} = 1.0$, TCP, however, the CBP should remain bound, even if it is at pericenter at the onset of RLOF. The system continues evolving after the end of the CE, and by the end of our 15 Gyr BSE simulations, $a_{CBP,PCE}$ may expand adiabatically by up to a factor of 3 caused by slight mass loss, and the binary's final fate is a single C-O WD.

For $\alpha_{CE} = 3.0, 5.0, 10.0$, the binary does not merge, and the stars leave the CE as a helium WD/low-mass MS pair, its orbit shrinks by a factor of 5 – 25, and its mass decreases by $\sim$65%. In all cases, $\beta < \beta_{eject}$, and thus the CBP should be ejected in the runaway regime. A secondary RLOF occurs for $\alpha_{CE} = 3.0$, TCP, at t$\sim$6.2 Gyr, and the binary experiences a perfect merger (i.e., no effect on a_{CBP} or e_{CBP}) into a First Giant Branch star. For all other non-merger cases, however, the system remains identical to its PCE configuration until the end of our simulations.

The CBP

The CBP orbiting Kepler-64 is initially on a nearly circular ($e_{CBP,0} = 0.054$), coplanar (i.e. $i_{CBP} = 0°$), 138.5-day orbit around its host binary. The evolution of both a_{CBP} and e_{CBP} during the CE phase is shown in Fig. 3.2 for the merger case, $\alpha_{CE} = 0.5, 1.0$, while the evolution for the non-merger case, $\alpha_{CE} = 3.0, 5.0, 10.0$, is shown in Fig. 3.3. The colours of the curves correspond to the different values of α_M: green represents slow mass-loss $\alpha_M = 0.1 M_\odot\ yr^{-1}$, and red represents fast mass-loss $\alpha_M = 1.0 M_\odot\ yr^{-1}$. While a planet orbiting a single star would show only one curve, as stated previously, the evolution of the system is highly dependent on the initial binary/CBP phase configuration at the onset of RLOF; because of this, the hatched regions (\ hatching signifies TCP simulations while / hatching signifies NTCP) represent the evolution of a_{CBP} and e_{CBP} as a function of the initial phase.

The outcome of the CE phase is quite similar to when the CBP begins on a circular ($e_{CBP,0} = 0.0$) orbit (KM16); for example, beginning the CBP on a circular orbit, its dynamical response results in, depending on phase, $a_{CBP,PCE} = 1.6-1.9$ AU and $e_{CBP,PCE} = 0.2-0.3$ for the NTCP merger case

and fast mass-loss, while beginning the CBP with its real eccentricity gives $a_{CBP,PCE} = 1.58 - 1.83$ AU and $e_{CBP,PCE} = 0.16 - 0.35$. Thus, it seems the slight initial eccentricity does not significantly increase or decrease the CBP's survival prospects. Indeed, there were zero ejections in any of the Kepler-64 simulations, for both the circular and slightly eccentric initial configuration. This test of the addition of eccentricity provides a basis for testing the following four systems with different combinations of initial e_{CBP} and i_{CBP}, as no significant changes were seen with the slight increase in eccentricity.

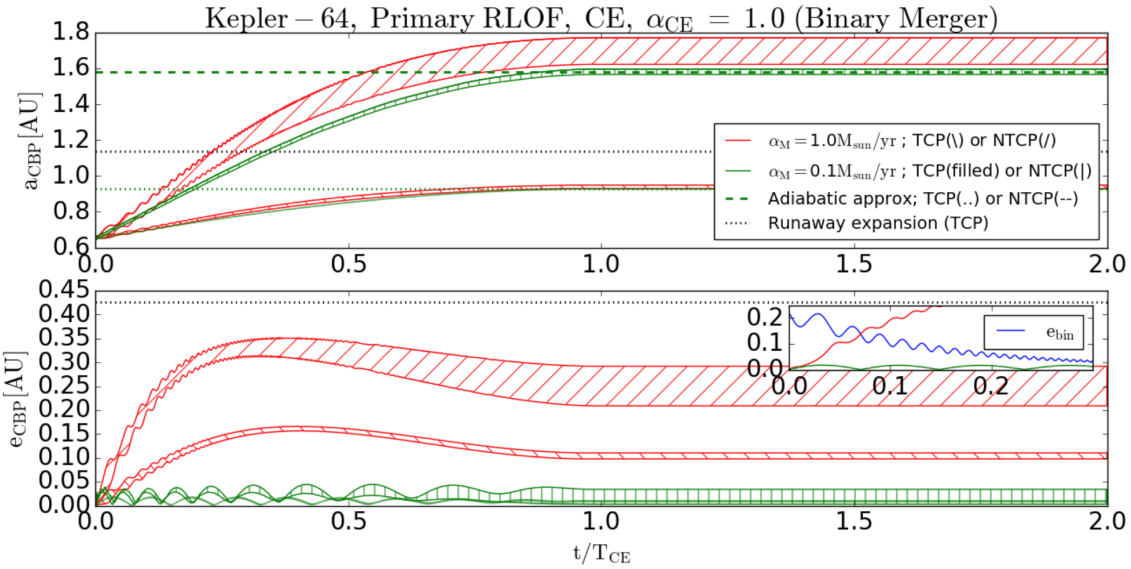

Figure 3.2: The evolution of the CBP for $\alpha_{CE} = 0.5/1$, in which Kepler-64 merges. The evolution of a_{CBP} and e_{CBP} can be seen in the top and bottom panels, respectively, with the red curves corresponding to fast mass loss $\alpha_M = 1.0 M_\odot\ yr^{-1}$ and the green curves corresponding to slow mass loss $\alpha_M = 0.1 M_\odot\ yr^{-1}$. The CBP remains bound in all cases, and the inclusion of $e_{CBP} = 0.054$ leads to similar results as the results of KM16, which simulated the planet as initially circular.

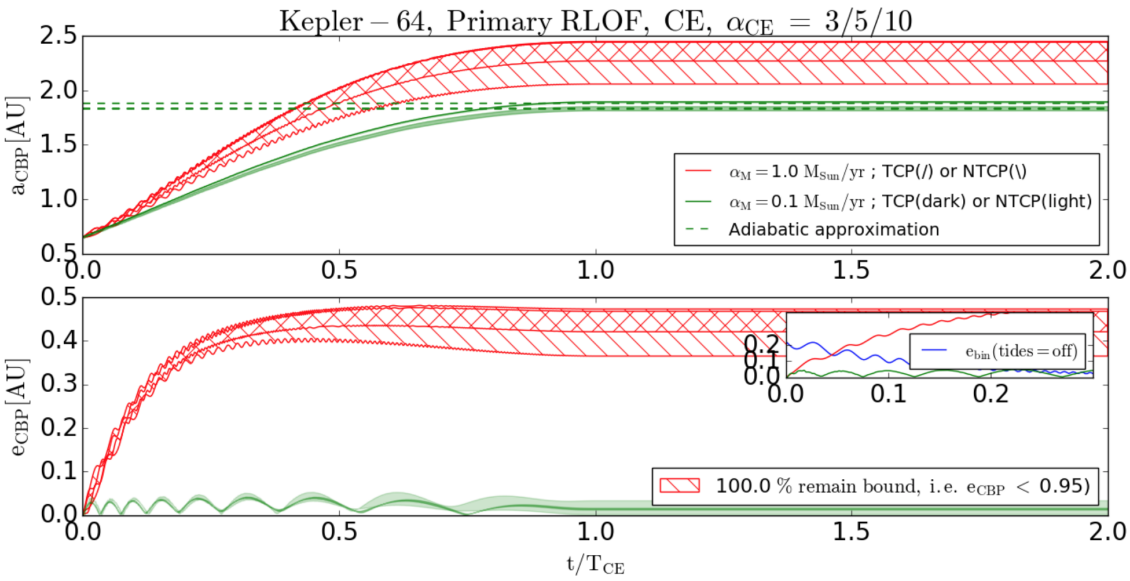

Figure 3.3: The evolution of the CBP for $\alpha_{CE} = 3/5/10$, in whch Kepler-64 does not merge but instead becomes a tight HeWD-MS binary. As with the previous figure, the evolution of a_{CBP} and e_{CBP} is shown in the upper and lower panels, respetively. The CBP remains bound for both mass-loss regimes with the addition of $e_{CBP} = 0.054$, the same as beginning the CBP on a circular orbit (KM16).

3.2.2 KIC7821010

The Binary

KIC7821010, or simply KIC782, initially consists of a 1.28 $M_{\odot}$ primary and 1.23 $M_{\odot}$ secondary, on a highly eccentric ($e_{bin,0} = 0.68$), 24.24-day orbit. Primary RLOF begins at t∼5.0 Gyr, and the system enters a CE. For evolution in the fast-mass loss regime, $\Psi \sim 0.03$ and $\alpha_{crit} = 5.8 M_{\odot}\ yr^{-1}$, significantly larger than the tested mass-loss regimes. In this case, $T_{CE}/P_{CBP} \sim 0.37$ for slow-mass loss and $T_{CE}/P_{CBP} \sim 3.7$ for fast-mass loss; again, these comparable timescales will lead to non-adiabatic orbital evolution.

For $\alpha_{CE} = 0.5, 1.0$, the binary merges into a First Giant Branch star, and loses $\sim 8 - 28\%$ of its initial mass. The CBP will remain bound, even in the runaway regime, since $\beta > \beta_{eject}$ in all cases. The system loses 66 – 68 % of its PCE mass by the end of the 15 Gyr simulation, and the system ends as a single CO-WD; in response, $a_{CBP,PCE}$ expands adiabatically by a factor of ∼3.0 – 3.6. The binary does not merge for $\alpha_{CE} = 3.0, 5.0, 10.0$, and instead the stars exit the CE as a HeWD-MS pair, losing ∼59% of its initial mass. The CBP is likely to be ejected in the runaway regime since $\beta < \beta_{eject}$ for all non-merger cases.

A secondary CE is experienced when the binary does not merge, and for $\alpha_{CE} = 3.0$, NTCP and

$\alpha_{CE} = 5.0$, TCP, this second CE leads to a Supernova, which disrupts the entire system and leaves no remnant of the binary, at t$\sim$5.5 Gyr/5.2 Gyr, respectively. For $\alpha_{CE} = 3.0$, TCP, the secondary CE leads to a perfect merger, and since there is no mass-loss, a_{CBP} and e_{CBP} remain unchanged. This system continues to evolve, however, and by the end of the simulation, a single C-O WD remains. In this evolution, the star loses $\sim$ 59% of its mass, and $a_{CBP,PCE}$ expands adiabatically by a factor of $\sim$2.4.

For $\alpha_{CE} = 5.0$, NTCP and $\alpha_{CE} = 10.0$, however, the secondary overfills its Roche lobe at t$\sim$5.4 – 5.7 Gyr and evolves from a First Giant Branch star into a HeWD, losing $\sim$ 84 – 86% of its mass; its orbit shrinks by 84 – 93%, leaving a very tight HeWD-HeWD pair with a separation of 0.468 – 2.358 $R_{\odot}$. In all cases, $\beta < \beta_{eject}$, and the CBP is likely to be ejected; indeed, we see 3370 ejections out of 3920 runs (86%).

The system remains as a tight HeWD-HeWD pair by the end of the simulation for $\alpha_{CE} = 10.0$, NTCP; interestingly, both $\alpha_{CE} = 5.0$, NTCP and $\alpha_{CE} = 10.0$, TCP experience a third RLOF at t$\sim$7.3 Gyr/6.0 Gyr, respectively, leading to a SN which disrupts the entire system, leaving no remnant of the binary.

The CBP

The CBP in KIC782 is initially on an eccentric ($e_{CBP,0} = 0.35$), 995-day orbit around its host stars, with an inclination of $i_{CBP} = 6°$ relative to the plane of the binary orbit. While the CBP has a measured mass of $M_{CBP} = 2.6 M_{Jup}$, it is both far enough away and small enough, relative to the mass of the binary, that we do not see any effects when including it in our simulations; instead, we simply treat it as a point mass, the same as all other simulations (with the exception of KIC509, which will be detailed later).

Fig. 3.4 shows the orbital reconfiguration of the binary (left) and the entire system (right) during the CE phase; the green orbit represents the adiabatic orbital expansion experienced for $\alpha_M = 0.1 M_{\odot}\ yr^{-1}$. The red orbit represents $\alpha_M = 1.0 M_{\odot}\ yr^{-1}$, beginning at two different initial phase configurations, and these result in the ejection of the CBP from the system. As the orbit expands during the CE phase, it does not represent a closed ellipse due to the comparable timescales of the CBP orbit and CE phase, and thus the orbital motion is not strictly Keplerian, as first noted by KM16. This is not a problem, however, as the orbital parameters settle at the end of the mass-loss phase (except when the CBP is ejected).

Fig. 3.5 shows the evolution of a_{CBP} and e_{CBP} during the CE phase when the binary merges, while Fig. 3.6 shows the same parameters but for the non-merger case. For slow mass-loss, the CBP orbit evolves adiabatically (i.e., it is consistent with the adiabatic approximation – see the green-dashed line). For fast mass-loss, the CBP orbit evolves in the transition regime, due to the comparable T_{CE} and P_{CBP}, and the evolution of e_{CBP} (bottom panel of both figures) shows an interesting symmetric plot, tending to either become circular by approaching zero or approach unity,

towards ejection . The CBP remains bound for all slow mass-loss simulations, and there are nearly no ejections for the merger (only 0.2% of the simulations), whereas 36% of our non-merger simulations result in ejection of the CBP for fast mass-loss, reaching $e_{CBP} > 0.95$. Orbital expansion may be relatively small ($\alpha_{CE} = 0.5/1$, TCP expands from 2.65 AU to a maximum of only 5.2 AU), or much larger, up to a factor of ∼15.4 (for $\alpha_{CE} = 3/5/10$, NTCP), reaching $a_{CBP,PCE} \sim 35$ AU.

The phase dependence of the CE evolution ($a_{CBP,PCE}$ and $e_{CBP,PCE}$) are shown in Figs. 3.7 and 3.8; phases that are not included in these two figures correspond to ejections of the CBP. The probability distribution functions, or PDFs, corresponding to this phase dependence, can be seen in Figs. 3.9 and 3.10 for the primary CE. Many of these PDFs are non-normal and bimodal; this is due to the alignment of some initial simulated phase configurations, in which 8 phases lead to the binary and planet being perfectly aligned at the onset of the CE, while for all other phases, the binary and planet are at least slightly offset. Thus, it is better to instead represent $a_{CBP,PCE}$ and $e_{CBP,PCE}$ using their modes instead of their medians. As such, any stated values of $a_{CBP,PCE}$ and $e_{CBP,PCE}$ are the mode of such distributions.

Fig. 3.11 shows the aforementioned secondary CE evolution of the CBP. The simulations begin with the corresponding values of $a_{bin,PCE}$ and $e_{bin,PCE}$ from the primary CE simulations, while the modes of $a_{CBP,PCE}$ and $e_{CBP,PCE}$ are used to initiate the CBP. The timescales of T_{CE} and P_{CBP} are much closer for this second CE, and for both mass-loss regimes are close to 1. The CBP only evolves adiabatically for $\alpha_M = 0.1 M_\odot\ yr^{-1}$, NTCP simulations, while evolving in the transition regime for slow mass-loss, TCP and fast mass-loss. This violent evolution leads to many more ejections (91% and 79% for fast and slow mass-loss, respectively), and very high values of both $a_{CBP,PCE}$ and $e_{CBP,PCE}$ when the planet remains bound. For example, for fast mass-loss, eccentricities of up to 0.94 may be reached, just below our ejection threshold. The PDFs for the secondary CE phase are shown in Fig. 3.12, showing the strong bimodality of some of the distributions more clearly.

As the evolution of the system after the second CE leads to a third RLOF for $\alpha_{CE} = 5.0$, NTCP and $\alpha_{CE} = 10.0$, TCP, and eventually a SN explosion, the CBP can only survive until 15 Gyr after the secondary CE for $\alpha_{CE} = 10.0$, NTCP.

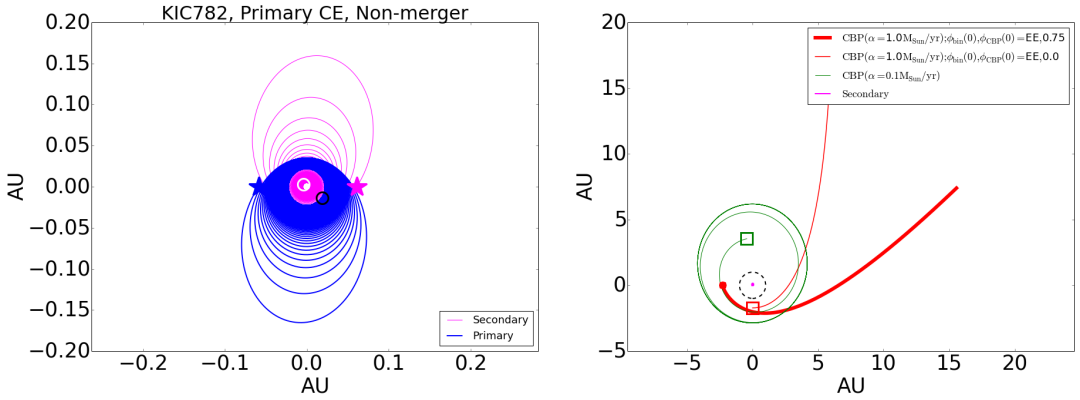

Figure 3.4: The orbital reconfiguration of the KIC782 binary (left panel) and CBP (right panel), in the non-merger case of $\alpha_{CE} = 3/5/10$. The initially eccentric binary, where the primary is in blue, and the secondary is in magenta, evolve into a much tighter orbit during the CE phase, with the final separation seen between the primary HeWD (black) and secondary MS star (white). The evolution of the CBP orbit shows the adiabatic expansion for slow mass-loss (green), and the ejection of the CBP for fast mass-loss at two initial phase configurations. The black dashed circle in the right panel is a 1-AU orbit, for reference.

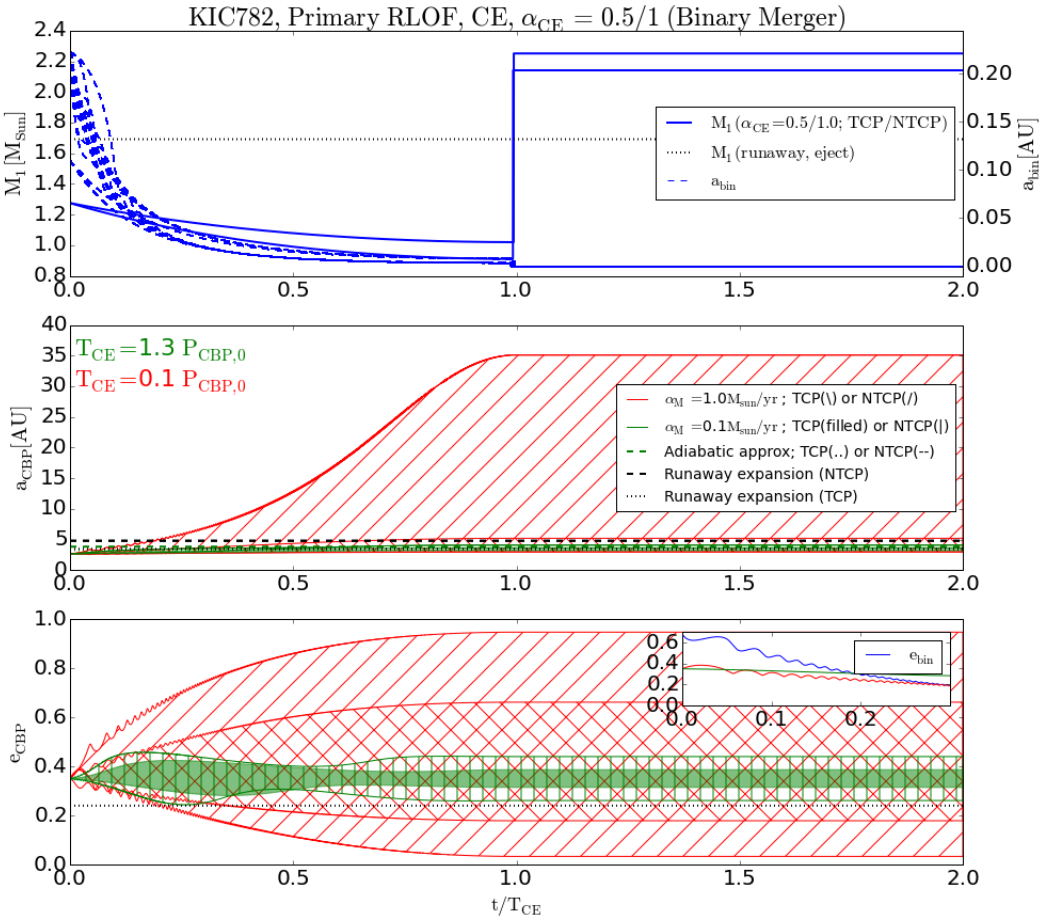

Figure 3.5: The evolution of the KIC782 binary (top) and CBP's a_{CBP} and e_{CBP} (middle and bottom), for $\alpha_{CE} = 0.5/1$. The binary's primary star mass (M_1) and separation (a_{bin}) decrease until the binary merges at the end of the CE phase, $t/T_{CE} = 1.0$. The CBP's orbit expands adiabatically, and remains bound for $\sim 99.8\%$ of all simulations. Interestingly, for fast mass-loss (red), e_{CBP} either drastically increases towards unity (and thus ejection), or its orbit circularizes during the CE phase.

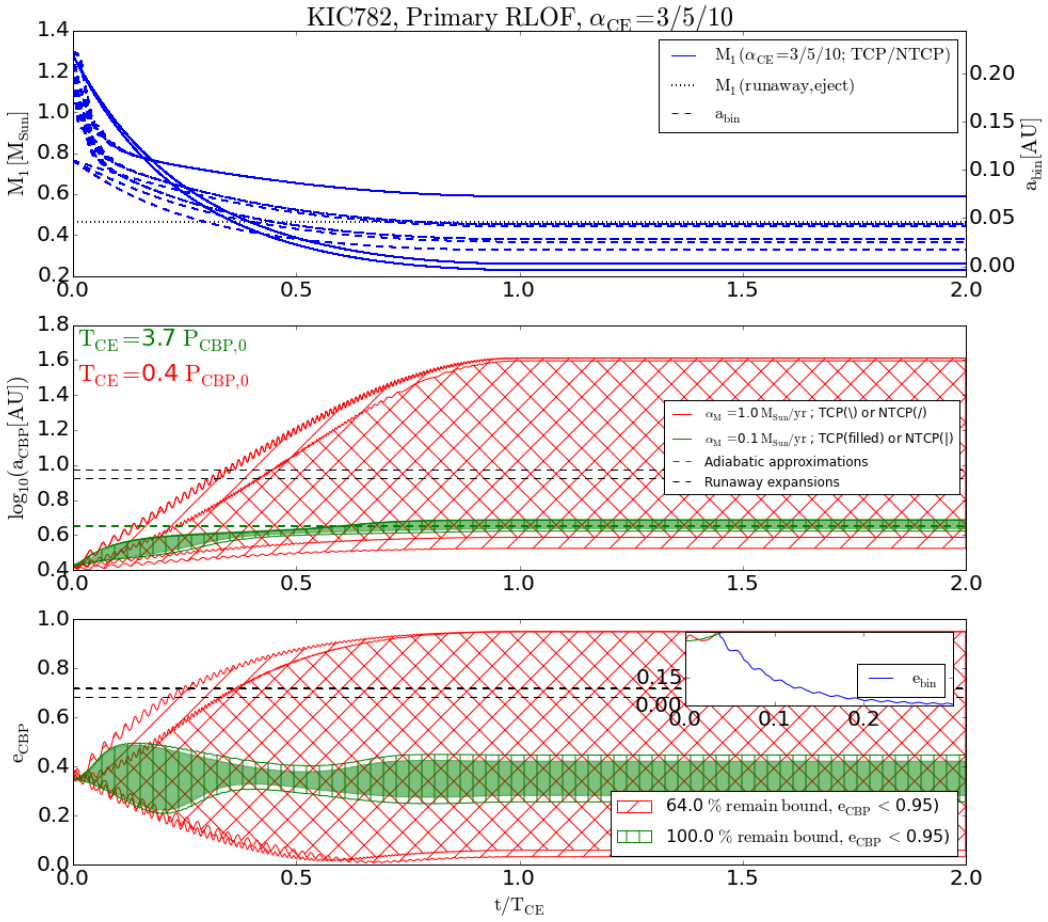

Figure 3.6: Same as Fig. 3.5, but for $\alpha_{CE} = 3/5/10$, for the case in which the binary does not merge at the end of the CE. The separation between the stars decreases rapidly and the primary star loses mass throughout the CE phase. The CBP remains bound for slow mass-loss, but is ejected in $\sim$ 36% of the simulations for fast mass-loss. The symmetric behaviour of the evolution of e_{CBP} is once again present.

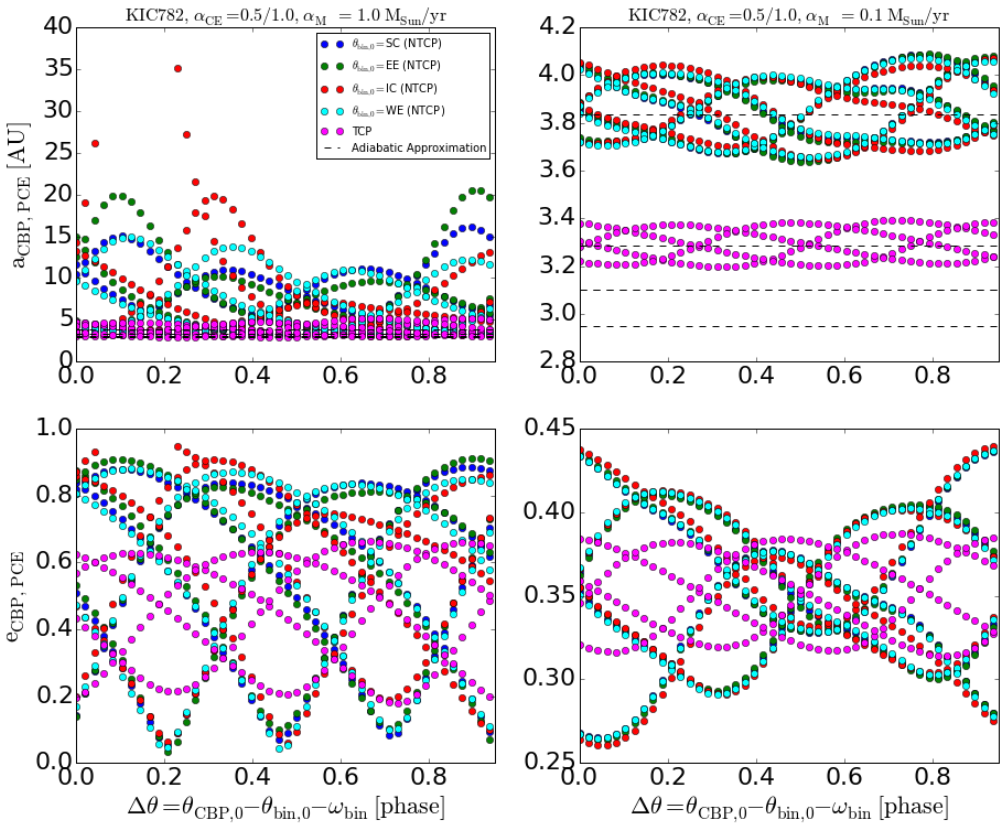

Figure 3.7: The dependence of $a_{CBP,PCE}$ (top) and $e_{CBP,PCE}$ (bottom) on initial phase of the system for fast mass-loss (left panels) and slow mass-loss (right panels) for $\alpha_{CE} = 0.5/1$. The outcome is highly dependent on the initial binary phase for NTCP (shown in four different colours for the four initial binary phases) due to the eccentricity of the binary at the onset of RLOF; TCP simulations begin on circular orbits, shown by the magenta points. The modes for slow mass-loss are $a_{CBP,PCE} = 3.7/3.2$ AU for NTCP/TCP, and $e_{CBP,PCE} = 0.26/0.31$, with maximum values of 4.09 AU and 0.4, respectively. The modes for fast mass-loss are $a_{CBP,PCE} = 4.6/3.1$ AU for NTCP/TCP, and $e_{CBP,PCE} = 0.8/0.6$, while the maximum values are 35.1 AU and 0.95 (our ejection limit).

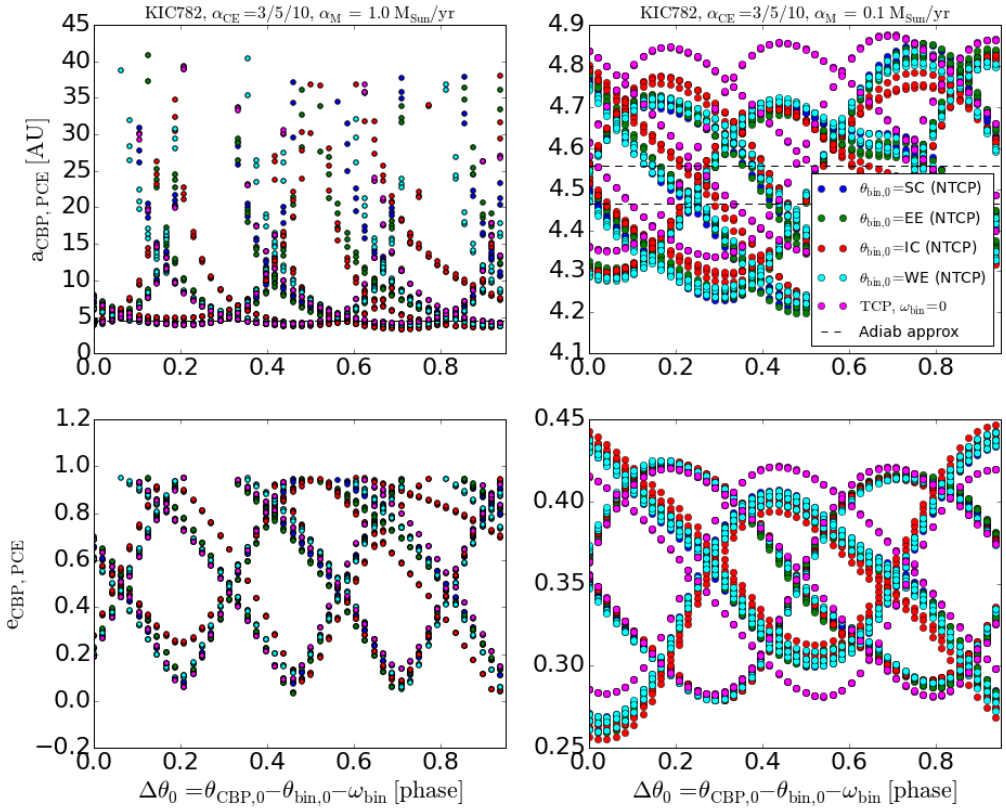

Figure 3.8: Same as Fig. 3.7, but for $\alpha_{CE} = 3/5/10$, the non-merger cases. The modes for slow mass-loss are $a_{CBP,PCE} = 4.3/4.4$ AU for NTCP/TCP, and $e_{CBP,PCE} = 0.4/0.41$, with maximum values of 4.88 AU AU and 0.45, respectively. The modes for fast mass-loss are $a_{CBP,PCE} = 5.2/4.8$ AU for NTCP/TCP, and $e_{CBP,PCE} = 0.9/0.9$, while the maximum values are 30.8 AU and 0.95 (our ejection limit).

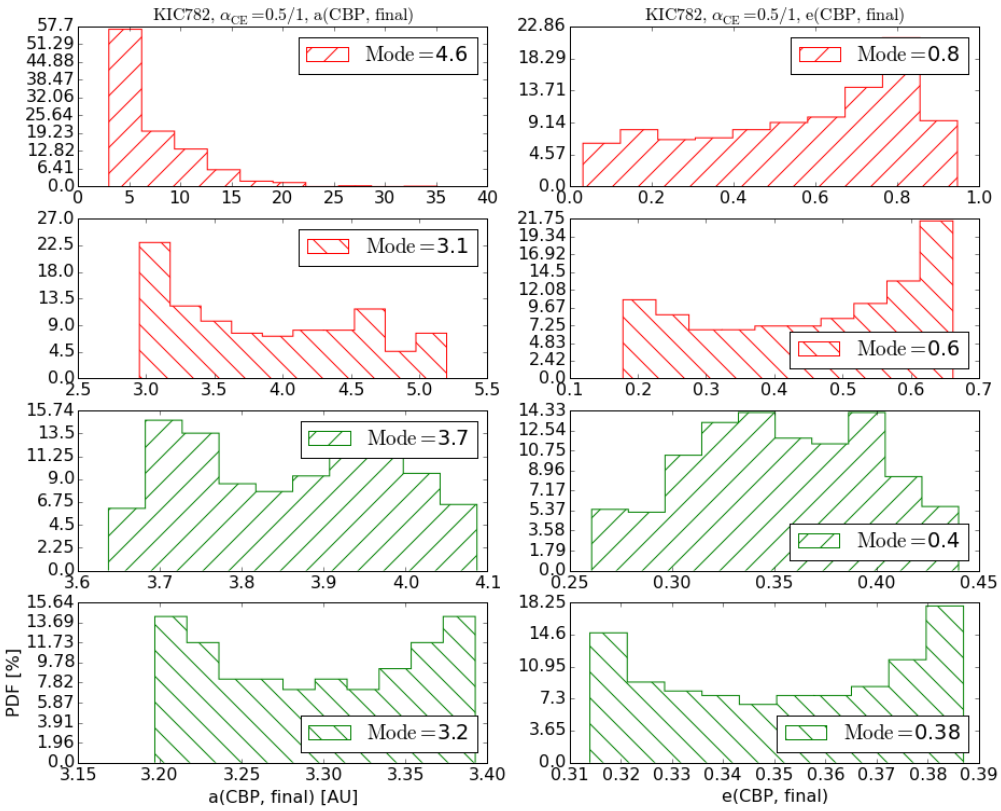

Figure 3.9: Probability Distribution Functions for the primary CE of KIC782 for the merger case, $\alpha_{CE} = 0.5/1$, showing $a_{CBP,PCE}$ (left) and $e_{CBP,PCE}$ (right). Red histograms indicate fast mass-loss $\alpha_M = 1.0 M_\odot\ yr^{-1}$, while green histograms indicate slow mass-loss $\alpha_M = 0.1 M_\odot\ yr^{-1}$. (Note also that / hatching represents NTCP, and \ represents TCP.) These mode values are used as the initial values for the KIC782 secondary CE simulations.

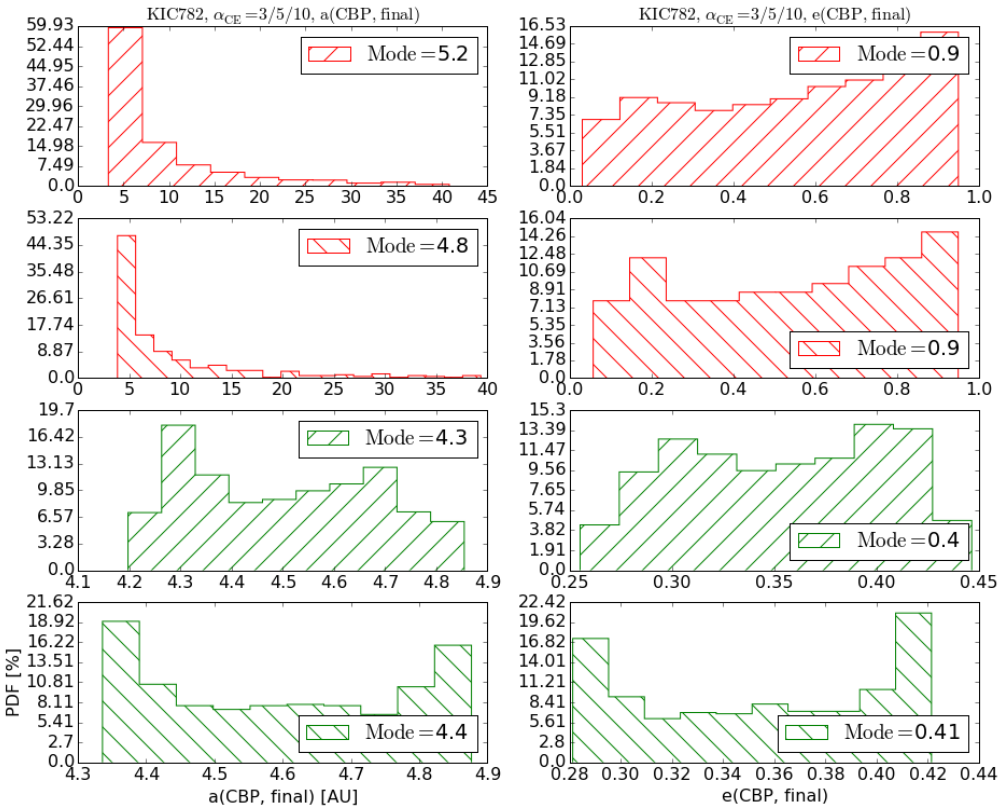

Figure 3.10: Same as Fig. 3.9, but for the non-merger primary CE of KIC782, $\alpha_{CE} = 3/5/10$.

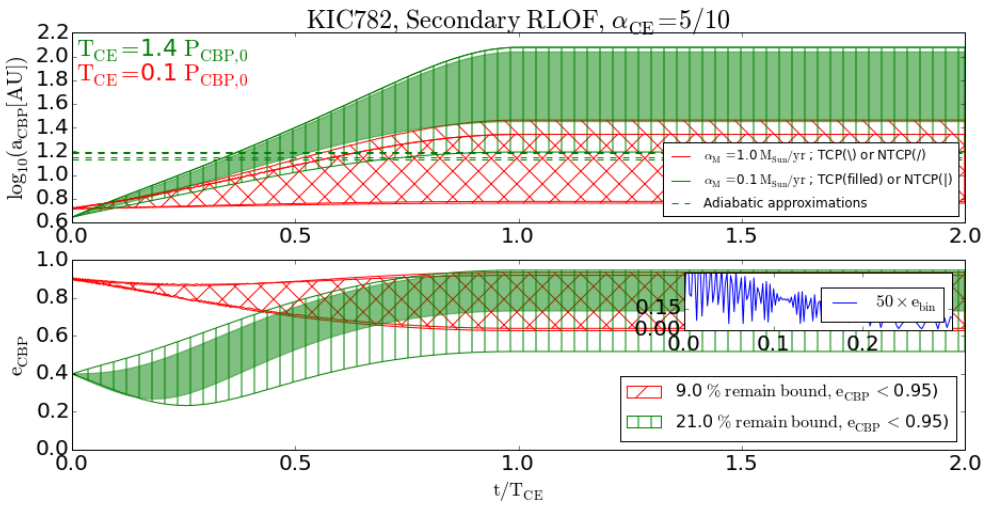

Figure 3.11: Evolution of KIC782's CBP during the secondary CE, following the non-merger primary CE case, for $\alpha_{CE} = 5/10$. The inset box in the lower panel shows the evolution of e_{bin} during the secondary CE. The evolution of a_{CBP} and e_{CBP} is shown in the top and bottom panels, and the wide range of final orbital distances can be seen clearly. The CBP is very likely to be ejected (91% of the simulations for fast mass-loss, and 79% for slow mass-loss), but gains significant eccentricity ($e_{CBP,PCE} > 0.5$) in the cases in which the CBP remains bound. Interestingly, $a_{CBP,PCE}$ becomes much larger for slow mass-loss than fast mass-loss, the opposite of what is seen in the primary CE simulations for all systems.

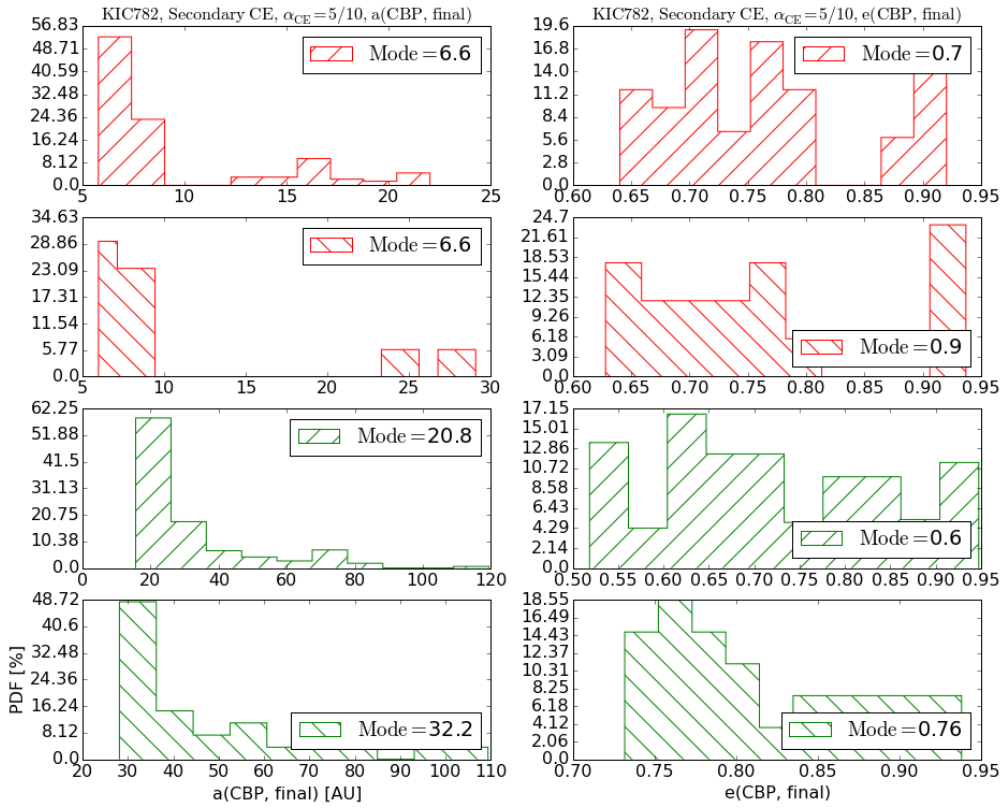

Figure 3.12: Same as Fig. 3.9, but for the secondary CE of KIC782 for $\alpha_{CE} = 5/10$.

3.2.3 KIC3938073

The Binary

KIC3938073, or simply KIC393, initially consists of 1.45 $M_\odot$ + 0.41 $M_\odot$ stars on an eccentric ($e_{bin,0} = 0.43$), 48.48-day orbit. The binary enters its primary CE stage at t$\sim$3.3 Gyr, during which $\Psi \approx 0.05$ and $\alpha_{crit} \approx 19.3 M_\odot\ yr^{-1}$ for both mass-loss regimes. As the timescales of the CE mass-loss event and the CBP orbital period are comparable for $\alpha_M = 1.0 M_\odot\ yr^{-1}$ ($T_{CE}/P_{CBP} \sim 1.52$), then the planet may experience non-adiabatic orbital expansion. However, for the slow mass-loss regime of $\alpha_M = 0.1 M_\odot\ yr^{-1}$, $T_{CE}/P_{CBP} \sim 15$, which is clearly non-adiabatic, and the CBP will experience instantaneous mass loss in the runaway regime.

For $\alpha_{CE} = 0.5$, TCP, the binary merges into a First Giant Branch Star during the primary CE, losing $\sim$40% of its initial mass; here, $\beta > \beta_{eject}$, and the CBP will remain bound even in a runaway regime. The remaining single star continues evolving until 15 Gyr, losing an additional $\sim$58% of its PCE mass (thus $a_{CBP,PCE}$ expands adiabatically by a factor of $\sim$2.4), and finally becoming a C-O WD.

The binary does not merge for $\alpha_{CE} = 0.5$, NTCP and $\alpha_{CE} = 1.0, 3.0, 5.0, 10.0$ during the primary CE stage, losing $\sim$86 – 87% of its initial mass depending on whether the simulations are NTCP/TCP. The binary separation decreases by a factor of $\sim$3 – 7.5 for NTCP, and by a factor of $\sim$3.1 – 8.2 for TCP, depending on the value of α_{CE}. The primary evolves from a First Giant Branch star to a HeWD, leaving a HeWD-MS pair after the primary CE. Again, $\beta > \beta_{eject}$, and the CBP remains bound in all inclination tests.

A secondary CE is experienced at t$\sim$4.8 Gyr / 3.4 Gyr for $\alpha_{CE} = 0.5$, NTCP and $\alpha_{CE} = 1.0$, TCP, respectively. However, as both lead to a perfect merger (i.e., coalescence without mass loss), there is no effect on the CBP orbital parameters. Additional mass is lost by the end of 15 Gyr, however, as the star eventually becomes a single C-O WD, losing $\sim$41% of its PCE mass in both cases; in response, $a_{CBP,PCE}$ expands adiabatically by a factor of $\sim$1.7. All other non-merger cases which do not experience a secondary CE see no additional mass loss by the end of our 15 Gyr simulations, and thus the CBP retains its PCE orbital parameters around the tight HeWD-MS binary.

The CBP

The CBP orbiting KIC393 is initially on a slightly eccentric ($e_{CBP,0} = 0.1$), 270-day orbit around its host binary. As measurement of i_{CBP} is highly uncertain for this system (estimated to be around 15°, but it could be much higher), this system is instead used as a test for the effects of i_{CBP} on the dynamical evolution of the planet. Thus, the range we explore is $i_{CBP} = [0, 30, 60, 90, 120, 150, 180]°$, giving 7 initial inclinations to test for both the merger and non-merger cases.

The evolution for the single merger case can be seen in Fig. 3.13 for an initial inclination of

$i_{CBP} = 0°$, while the non-merger response can be seen in Fig. 3.14. As with the primary CE evolution of KIC782, the CBP evolves adiabatically for slow mass-loss (green curves), while fast mass-loss leads to non-adiabatic orbital expansion due to the comparable $T_{CE}/P_{CBP,0} \sim 1$, which can be seen in the upper panels of both figures. The CBP remains bound in both cases, although the planet's eccentricity may become quite high for fast mass-loss in Fig. 3.14, up to a mode value of $e_{CBP} = 0.84$. The phase dependence for KIC393 are shown in Figs. 3.15 and 3.16.

The noticeable changes in a_{CBP} and e_{CBP} are clear as i_{CBP} is increased, and thus four additional plots are included: for $i_{CBP} = 90°$, the merger and non-merger evolution of the CBP can be seen in Fig. 3.17, while the maximum tested inclination of $i_{CBP} = 180°$ can be seen in Fig. 3.18. While e_{CBP} can reach a maximum value of 0.84 for $i_{CBP} = 0°$, in the same scenario ($\alpha_{CE} = 0.5/1/3/5/10$, NTCP) for $i_{CBP} = 90°$, a maximum mode value of only 0.72 is achieved. Thus, the inclination clearly affects the outcome of the CBP's evolution, although the mode values for both $a_{CBP,PCE}$ and $e_{CBP,PCE}$ are very similar for all three inclinations, and is difficult to properly quantify without tests of differently evolving systems at varied initial i_{CBP}.

Overall, for both merger and non-merger, the CBP remains bound to the system throughout the CE phase, and for the entire 15 Gyr of the simulations, for all tested values of i_{CBP}. The CBP orbits either a single C-O WD or a HeWD-MS binary, with an orbit $\sim$2 – 3 times larger than its initial orbit.

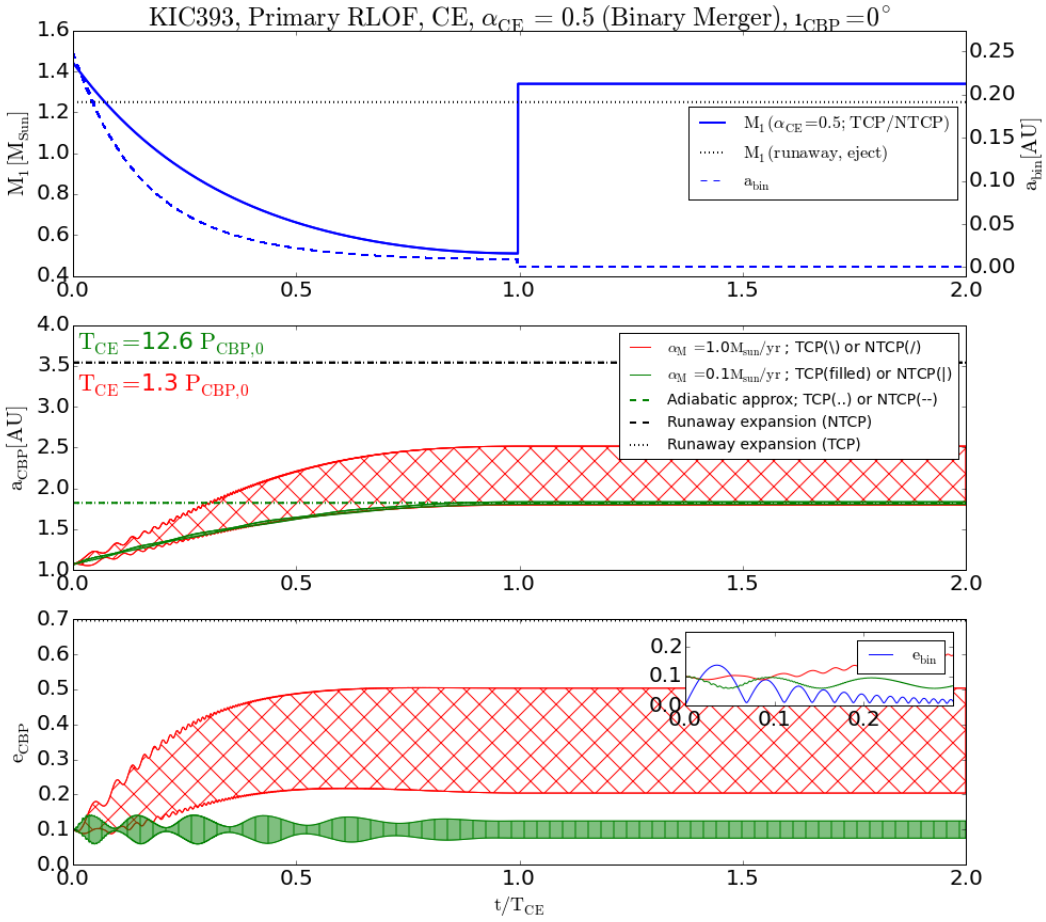

Figure 3.13: Evolution of the CBP orbiting KIC393, with initial inclination of $i_{CBP} = 0°$, for $\alpha_{CE} = 0.5$, TCP. The binary merger can be seen at $t/T_{CE} = 1.0$ in the top panel, while the evolution of a_{CBP} and e_{CBP} can be seen in the middle and bottom panels, respectively. As with previous plots, red indicates fast mass-loss and green indicates slow mass-loss. The CBP remains bound in all simulations.

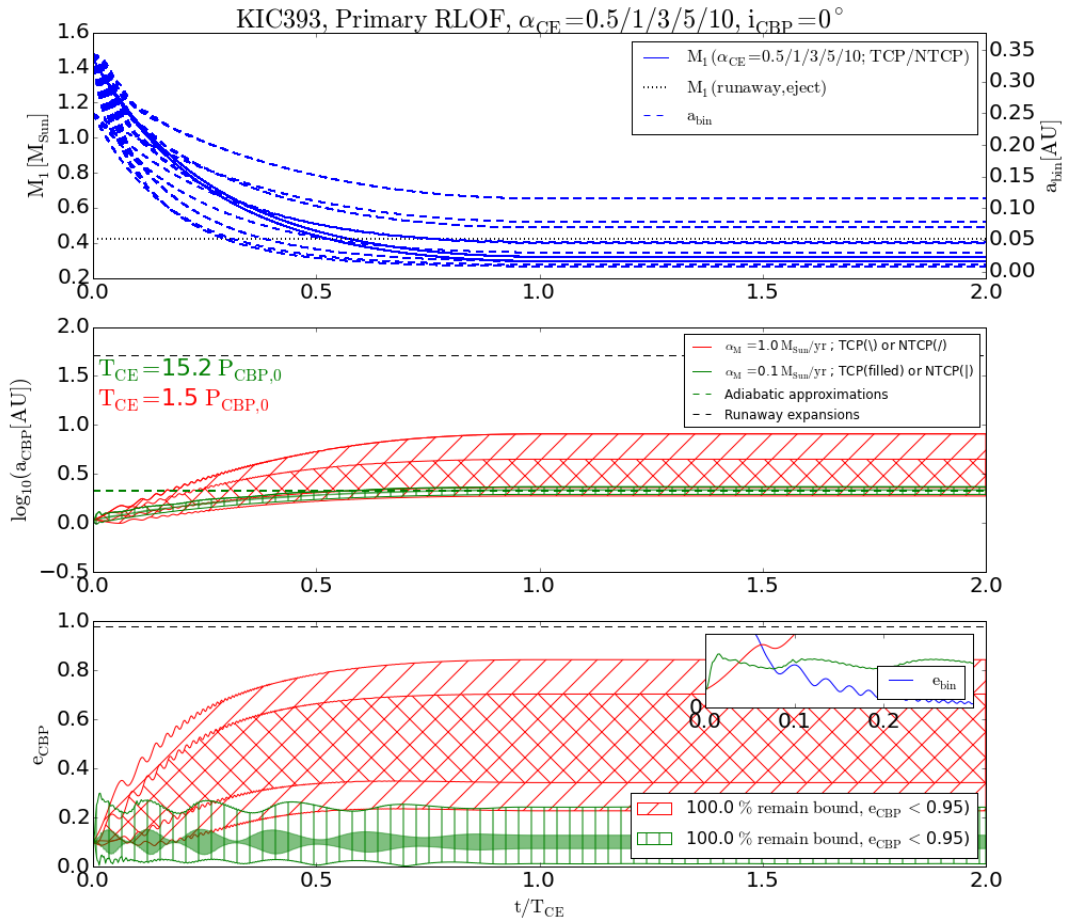

Figure 3.14: Same as Fig. 3.13 but for $\alpha_{CE} = 0.5$, NTCP and $\alpha_{CE} = 1/3/5/10$. The shrinking of the binary orbit can be seen in the non-merging top panel for each value of α_{CE}. Like the merger case, the CBP remains bound in all simulations.

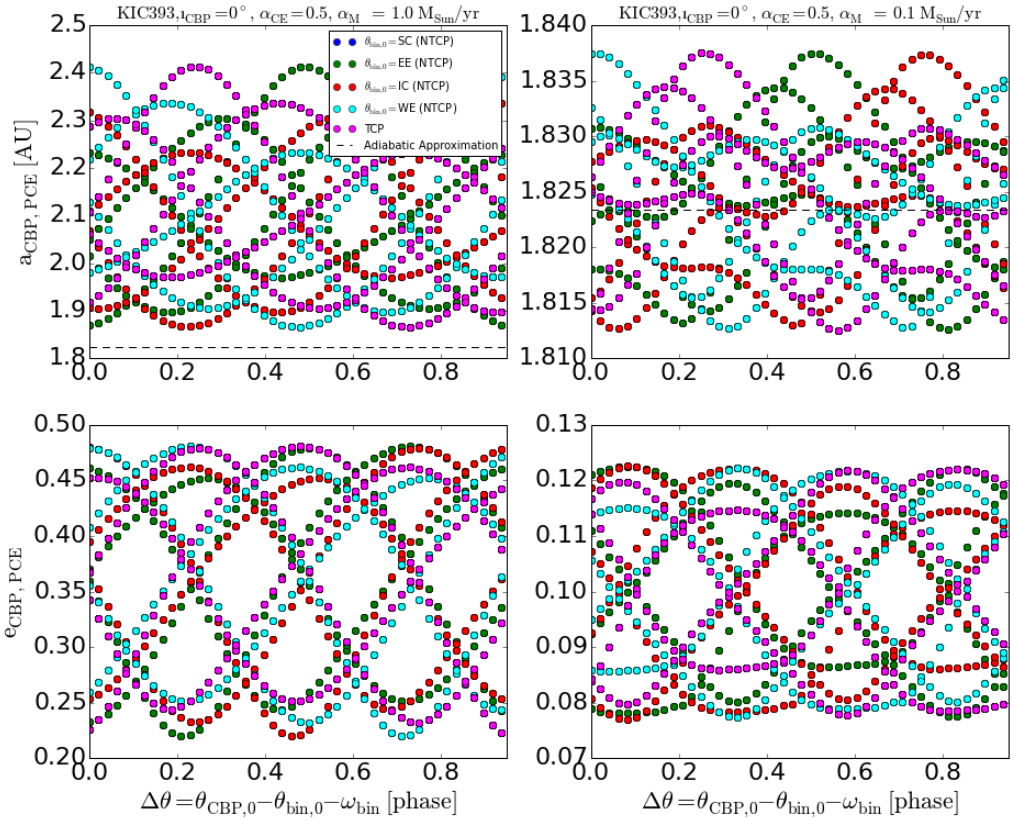

Figure 3.15: Same as Fig. 3.7, but for KIC393, $i_{CBP} = 0°$, $\alpha_{CE} = 0.5$, TCP, the merger case. The modes for fast mass-loss are $a_{CBP,PCE} = 2.1$ AU and $e_{CBP,PCE} = 0.4$ for both, with maximum values of 2.52 AU and 0.48, respectively. The modes for slow mass-loss are $a_{CBP,PCE} = 1.8$ AU and $e_{CBP,PCE} = 0.1$, while the maximum values are 1.84 AU and 0.116. Phase plots are not included for the other values of i_{CBP}, as they are almost identical and do not convey any additional information.

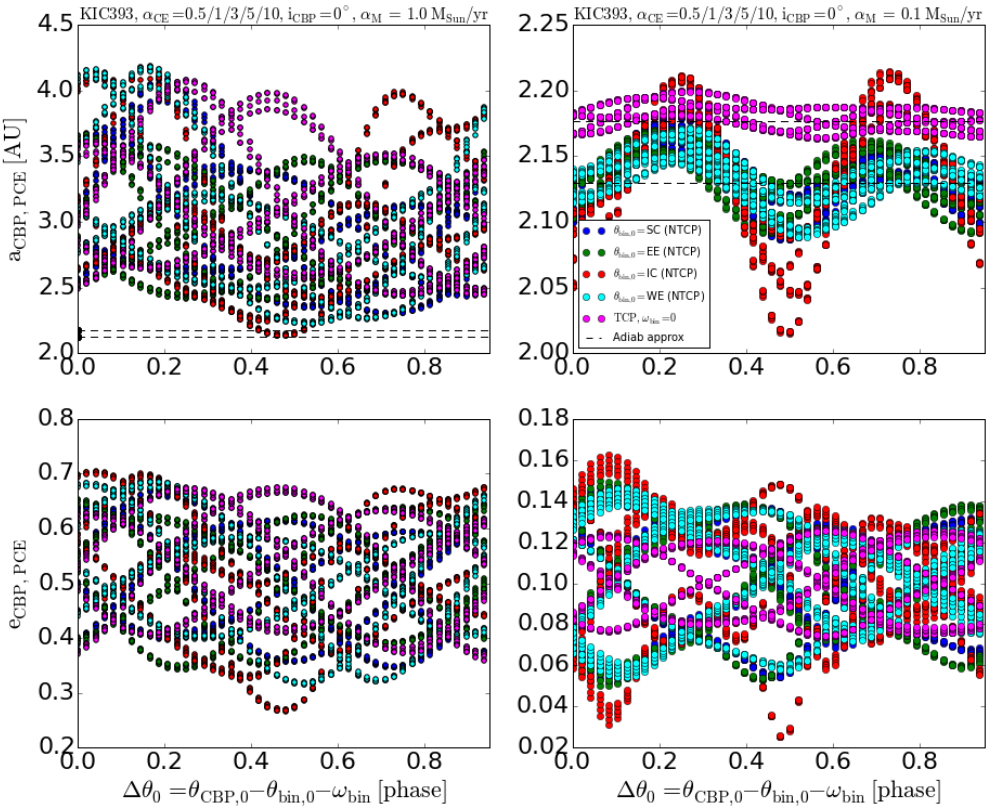

Figure 3.16: Same as Fig. 3.15, but for $\alpha_{CE} = 0.5$, NTCP and $\alpha_{CE} = 1/3/5/10$, the non-merger case. The modes for fast mass-loss are $a_{CBP,PCE} = 2.8/3.2$ AU for NTCP/TCP, and $e_{CBP,PCE} = 0.6$ for both, with maximum values of 8.12 AU and 0.84, respectively. The modes for slow mass-loss are $a_{CBP,PCE} = 2.1/2.2$ AU for NTCP/TCP, and $e_{CBP,PCE} = 0.1/0.08$, while the maximum values are 2.35 AU and 0.242.

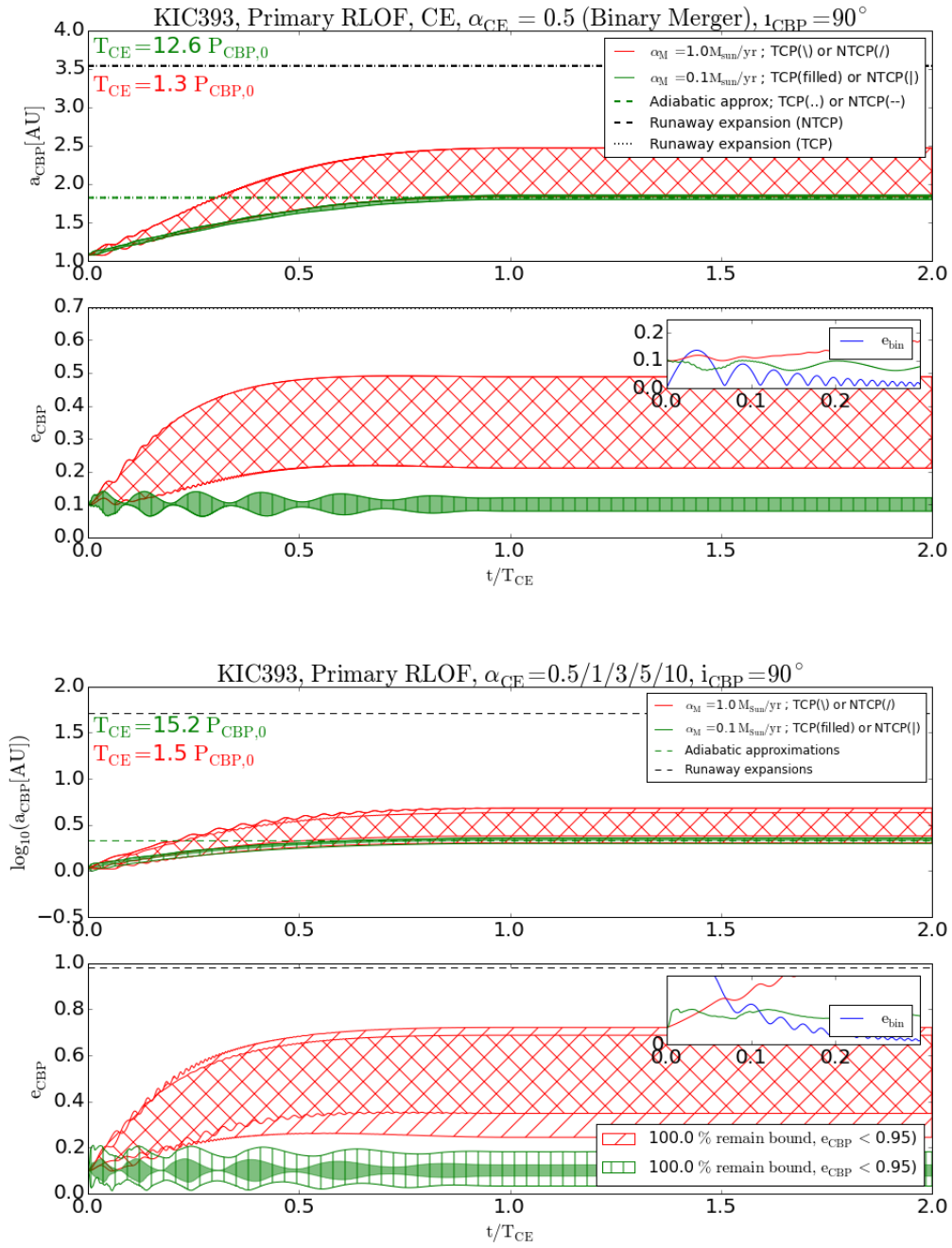

Figure 3.17: Same as Figs. 3.13 and 3.14, but for an initial inclination of $i_{CBP} = 90°$. As the stellar evolution is the same, it is not shown in either the merger (top two panels) or non-merger (bottom two panels) plots. The CBP remains bound in all simulations, even with the initially inclined orbit, although the evolution is qualitatively different when compared with the plots of $i_{CBP} = 0°$.

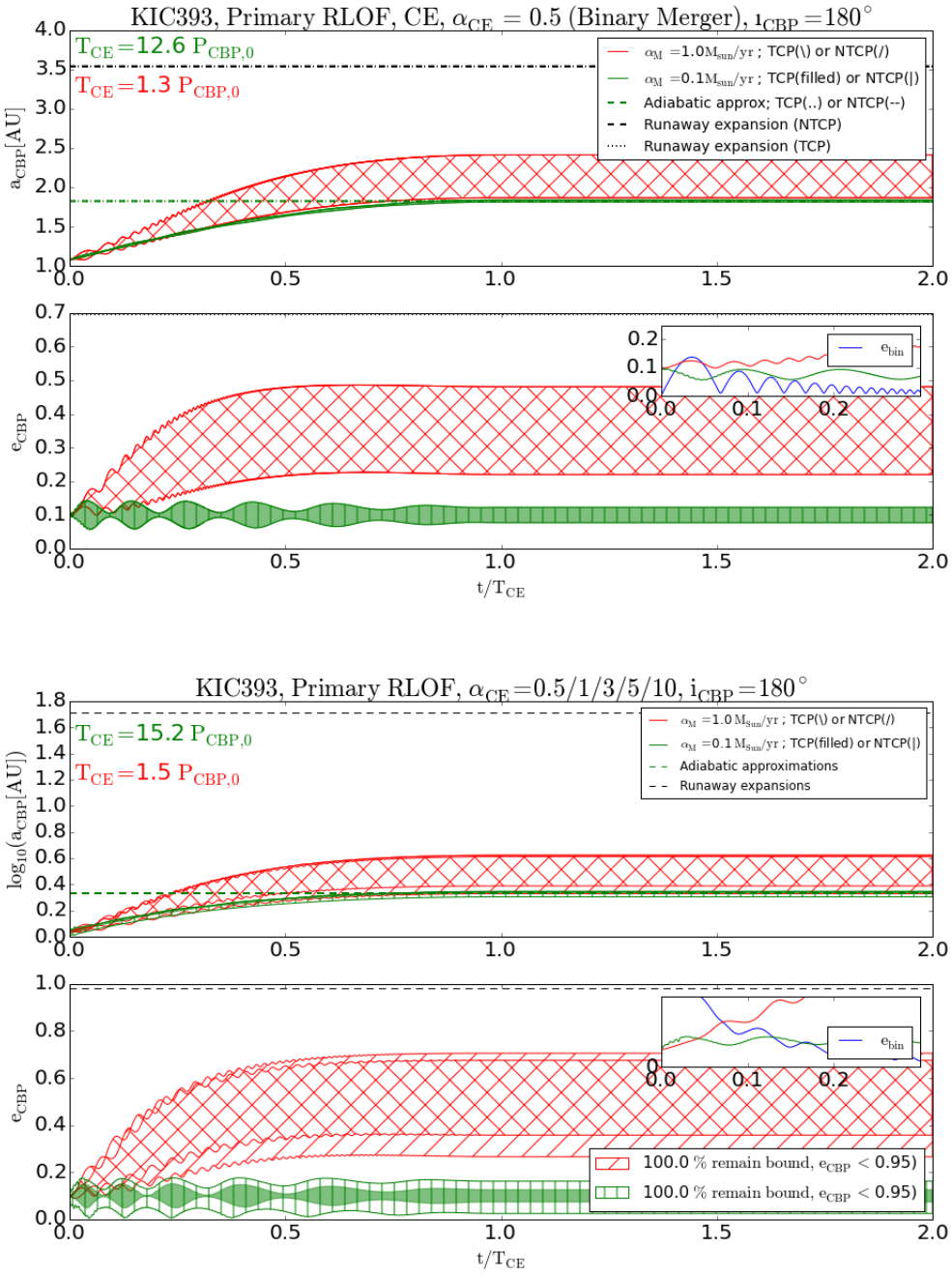

Figure 3.18: Same as Fig. 3.17, but for an initial inclination of $i_{CBP} = 180°$. The CBP again remains bound in all simulations, but the evolution of both a_{CBP} and e_{CBP} is qualitatively different than both $i_{CBP} = 0°$ and 90°.

3.2.4 KIC8610483

The Binary

KIC8610483, or simply KIC861, is initially a 0.96 $M_\odot$ + 0.96 $M_\odot$ binary on an eccentric ($e_{bin,0}$ = 0.5), 31-day orbit. The primary first fills its Roche lobe at t∼14.3 Gyr, depending on α_{CE}, initiating the CE phase. Here, $\Psi \approx 0.09$ and $\alpha_{crit} \approx 10.9 M_\odot\ yr^{-1}$, which is much larger than both the fast and slow mass-loss regimes tested. $T_{CE}/P_{CBP} \sim 6.4/0.64$ for slow and fast mass-loss respectively, and thus we may see non-adiabatic orbital expansion in both cases.

For $\alpha_{CE} = 0.5$, the binary either comes into contact (for NTCP) or the primary RLOF begins (for TCP), leading to a SN explosion which disrupts the entire system, leaving no remnant. For $\alpha_{CE} = 1.0, 3.0, 5.0, 10.0$, the same initial step happens at the onset of RLOF, with the NTCP simulations leading to a contact binary and TCP simulations leading to the primary overfilling its Roche lobe, at which point the stars share a CE. Both of these stars enter this stage as First Giant Branch Stars, and due to their similar mass ratio ($q \sim 1$), experience double-core evolution; the stars exit the CE as a HeWD-HeWD pair, losing ∼74% of their initial mass. The separation decreases by a factor of $\sim 28/19$ for NTCP/TCP respectively, and remain at a separation of ∼1.8 $R_\odot$, without further mass loss, until the end of our 15 Gyr simulations, for $\alpha_{CE} = 3.0, 5.0, 10.0$.

Interestingly, at t∼14.4 Gyr, a secondary RLOF is experienced for $\alpha_{CE} = 1.0$, in which the binary coalesces, resulting in a SN explosion which leaves no remnant. During the CE phase, $\beta > \beta_{eject}$, and thus the CBP will remain bound, even in the runaway regime.

The CBP

KIC861 has a CBP initially on a circular ($e_{CBP,0} = 0.0$), 400-day orbit, inclined at $i_{CBP} = 10°$ relative to the orbit of its host binary. When the binary evolution ends in a SN (the primary CE for $\alpha_{CE} = 0.5$ and the secondary CE for $\alpha_{CE} = 1.0$), there is no remnant left behind, and the system is disrupted; the CBP may either be destroyed in this explosion, or ejected and continue existence as a rogue planet. However, as we are only concerned with bound systems, we do not follow this case after disruption of the system.

The reconfiguration of the system is shown in Fig. 3.19: the binary evolution is shown in the left panel, while the evolution of the CBP orbit is shown in the right panel, with the red curves indicating the fast mass-loss regime (beginning at two initial phase configurations), and the green curve indicating the slow mass-loss, adiabatic regime. While slow mass-loss leads to adiabatic expansion in a few orbits, fast mass-loss leads to a rapid expansion of the orbit and an increase in e_{CBP}, which can be seen in the two red ellipses.

The distinct behaviour between the two mass-loss regimes is evident in the evolution of a_{CBP} and e_{CBP}, which can be seen in Fig. 3.20. While for $\alpha_M = 0.1 M_\odot\ yr^{-1}$, the (green) evolution is clearly consistent with the adiabatic approximation in the second panel and its orbit remains nearly

circular, for $\alpha_M = 1.0 M_\odot\ yr^{-1}$, the rapid change of the CBP orbit is caused by the comparable timescales, $T_{CE} = 0.6 P_{CBP,0}$. It is clear from Fig. 3.20 that the planet remains bound, as even for fast mass-loss, $e_{CBP} \leq 0.63$. The phase dependence is shown in Fig. 3.21.

Overall, when the system is not disrupted, the CBP remains bound. The CBP orbit adiabatically expands for slow mass-loss, gaining slight eccentricity, and non-adiabatically for fast mass-loss, becoming fairly eccentric, during the primary CE, and remains in its PCE orbit around a tight HeWD-HeWD binary, for both mass-loss regimes, for the remainder of the 15 Gyr simulations.

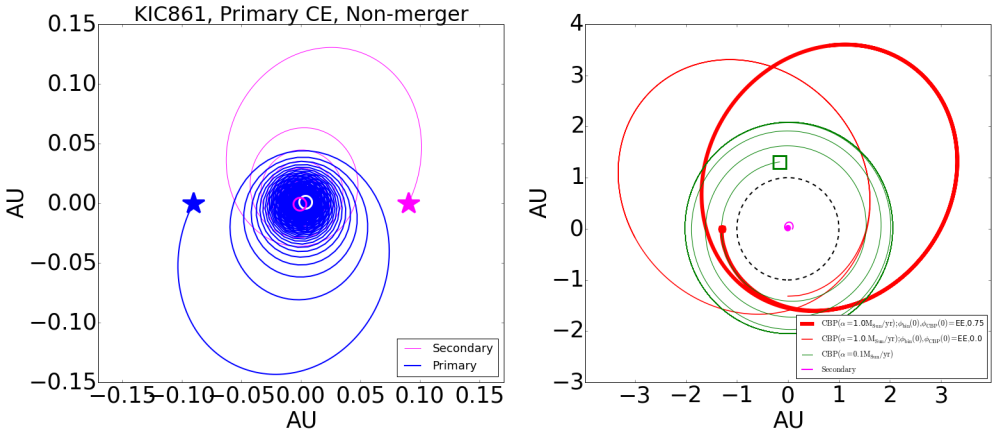

Figure 3.19: The orbital reconfiguration of KIC861 for $\alpha_{CE} = 1/3/5/10$. The left panel shows the shrinkage of the binary orbit, as the MS-MS pair evolves into a tight HeWD-HeWD pair, with blue and magenta representing the primary and secondary stars, respectively. The right panel shows the evolution of the CBP orbit; green is slow mass-loss, and the orbit expands adiabatically. The red curves indicate fast mass-loss (for two initial phase configurations), showing the expansion of the orbit and the increase in e_{CBP}. The black circle is once again a 1-AU reference orbit.

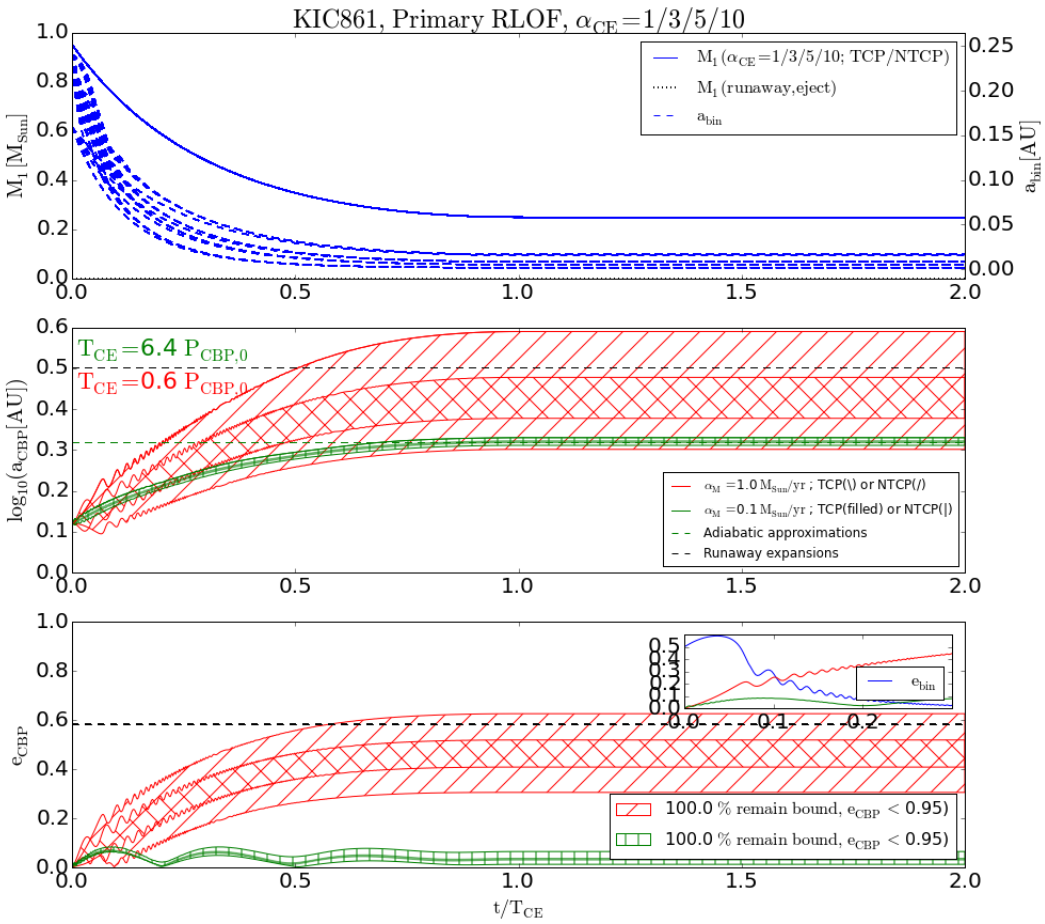

Figure 3.20: The primary CE non-merger evolution of KIC861 (top) and CBP (middle and bottom), for $\alpha_{CE} = 1/3/5/10$. The green curves represent slow mass-loss $\alpha_M = 0.1 M_\odot\ yr^{-1}$, and are consistent with the adiabatic approximation. The red curves represent fast mass-loss $\alpha_M = 1.0 M_\odot\ yr^{-1}$, also showing adiabatic orbital expansion in this case. While the CBP may experience runaway evolution, it remains bound in all simulations.

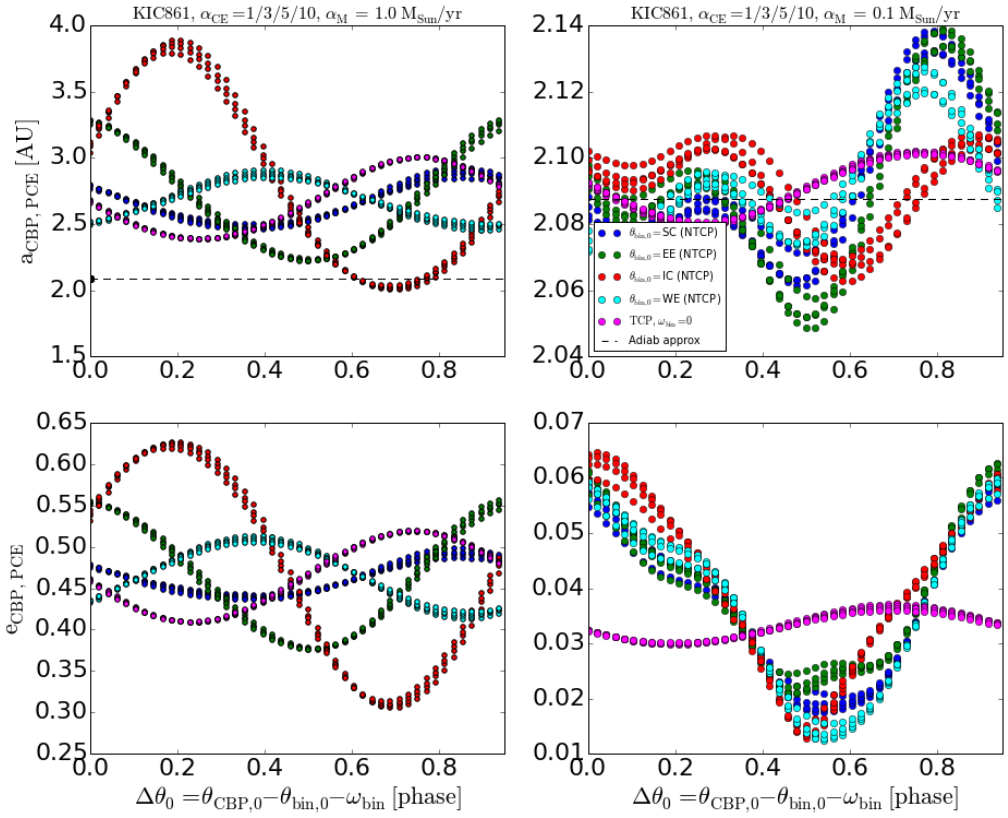

Figure 3.21: Same as Fig. 3.16, but for KIC861, $\alpha_{CE} = 1/3/5/10$. The modes for fast mass-loss are $a_{CBP,PCE} = 2.5/2.4$ AU for NTCP/TCP, and $e_{CBP,PCE} = 0.4/0.5$, with maximum values of 3.89 AU and 0.52, respectively. The modes for slow mass-loss are $a_{CBP,PCE} = 2.1/2.1$ AU for NTCP/TCP, and $e_{CBP,PCE} = 0.05/0.03$, while the maximum values are 2.14 AU and 0.065.

3.2.5 KIC5095259

KIC5095259, or simply KIC509, is a recent discovery (Getley et al., 2017). Due to the uncertainties involved in measuring metallicity, two values are tested – $Z = 0.01$ and $Z = 0.02$, solar metallicity – to constrain the potential outcome of the evolution of the system. Since the evolution of the binary using both initial metallicites was almost identical, only the differing times of each event will be mentioned, or any distinct differences if important.

The Binary

KIC509 initially consists of a 1.21 $M_\odot$ primary and a 0.51 $M_\odot$ secondary on a slightly eccentric ($e_{bin,0} = 0.246$), 18.61-day orbit, which first encounters primary RLOF at t∼5.2 Gyr – 6.2 Gyr,

depending on the initial metallicity tested ($Z = 0.01/0.02$, respectively). For both metallicities, $\Psi \approx 0.06$ and $\alpha_{crit} \approx 16.5 M_\odot\ yr^{-1}$ during the CE stage, a value which is once again much greater than our tested mass-loss regimes. The mass-loss timescale is comparable to the CE timescale for $\alpha_M = 0.1 M_\odot\ yr^{-1}$, with $T_{CE}/P_{CBP} \sim 1.4$, which falls within the adiabatic regime, but will likely display a non-adiabatic dynamical response; for $\alpha_M = 1.0 M_\odot\ yr^{-1}$, $T_{CE}/P_{CBP} \sim 14.3$, and thus the orbital expansion will be strictly non-adiabatic.

The binary merges for $\alpha_{CE} = 0.5$ and $\alpha_{CE} = 1.0$, TCP into a single First Giant Branch (FGB) star, losing $\sim$29 – 40% of its initial mass. $\beta < \beta_{eject}$ for slow mass-loss and TCP, and the CBP will be lost in the runaway regime; otherwise, $\beta > \beta_{eject}$, and the planet will remain bound. The system continues evolving to 15 Gyr, eventually becoming a C-O WD and losing $\sim$38 – 59% of its PCE mass, leading to the adiabatic expansion of $a_{CBP,PCE}$ by a factor of ~ 1.6 – 2.4.

The binary does not merge for $\alpha_{CE} = 1.0$, NTCP and $\alpha_{CE} = 3.0, 5.0, 10.0$; instead, the FGB primary evolves into a HeWD, losing $\sim$76 – 78% of its initial mass, while the separation with its low-mass MS companion decreases by a factor of $\sim$3.5 – 26, depending on α_{CE}. In all non-merger cases, $\beta < \beta_{eject}$, and the CBP will likely be ejected in the runaway regime. Due to our upper ejection limit of $e_{CBP} = 0.95$, however, we do not see any ejections, for either Z, for both merger and non-merger simulations.

For $\alpha_{CE} = 3.0, 5.0, 10.0$, this PCE configuration remains without mass loss until 15 Gyr, leading to no additional effects on the CBP. A secondary CE is experienced at t$\sim$7.8 Gyr / 8.3 Gyr (for $Z = 0.01/0.02$), leading to coalescence without mass loss of the binary, which again has no effect on a_{CBP} and e_{CBP}, and thus the CBP retains its post-primary CE values. This single FGB star eventually evolves into a C-O WD and loses an additional $\sim$26 – 33% of its post-merger mass. By 15 Gyr, then, $a_{CBP,PCE}$ expands adiabatically by an additional factor of $\sim$1.3 – 1.5.

The CBP

The CBP orbiting KIC509 is initially on a nearly circular ($e_{CBP} = 0.06$), 237.71 day orbit, at an inclination of $i_{CBP} = 26°$. Since this planet is massive ($M_{CBP} = 7.7 M_{Jup}$) and orbits relatively close to the binary, its mass is expected to have a noticeable effect on the system's evolution, and thus we include this mass in our REBOUND simulations for accuracy.

The evolution of a_{CBP} and e_{CBP} for $Z = 0.01$ can be seen in Figs. 3.22 and 3.23 for the merger and non-merger cases respectively. As with the previous three systems, the (green) slow mass-loss is consistent with the adiabatic approximation, as expected, and the orbit expands while remaining relatively circular. Interestingly, there is a clear gap between the NTCP and TCP simulations for fast mass-loss (red): when $\alpha_{CE} = 0.5/1$, NTCP, $e_{CBP,PCE} = 0.21 - 0.39$ while for TCP, $e_{CBP,PCE} = 0.56 - 0.79$. KIC509 is the only system that shows this behaviour (for both Z), whereas all other plots show an overlap between NTCP/TCP outcomes. The phase dependence of KIC509, $Z = 0.01$ is shown in Figs. 3.24 and 3.25.

For $Z = 0.02$, the evolution is shown in Figs. 3.26 and 3.27. While the evolution is very similar and the planet experiences adiabatic orbital expansion for both values of Z, the slightly different evolution of the binary leads to slight differences in the overall outcome of a_{CBP} and e_{CBP}, and thus both metallicities are included. The mass-loss timescale is slightly different ($T_{CE} = 8.5P_{CBP,0}$ for $Z = 0.01$ merger while $T_{CE} = 8.0P_{CBP,0}$ for $Z = 0.02$), but this difference does not significantly change the evolution: the CBP orbit expands adiabatically for slow mass-loss, and in the transition regime for fast mass-loss.

The CBP remains bound in all simulations, for both tested values of Z, for all α_{CE} and NTCP/TCP, even with the additon of M_{CBP}.

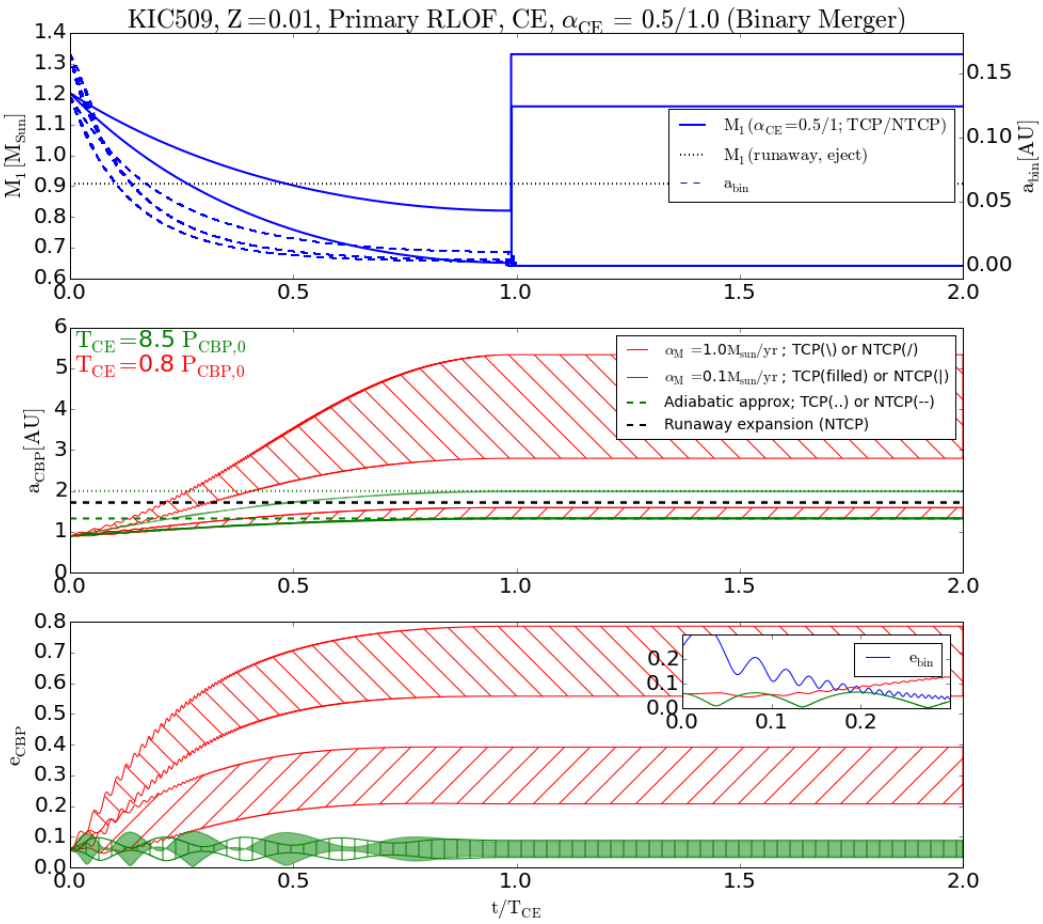

Figure 3.22: The evolution of KIC509 for $\alpha_{CE} = 0.5/1$, with an initial metallicity of $Z = 0.01$. The binary merger can be seen in the top panel, while the evolution of a_{CBP} and e_{CBP} are shown in the middle and bottom panels. The green, slow mass-loss is consistent with the adiabatic approximation, and the red, fast mass-loss also shows adiabatic expansion. Note the gap between NTCP (/) and TCP (\) evolution of e_{CBP}, reaching a maximum of 0.39/0.79, respectively.

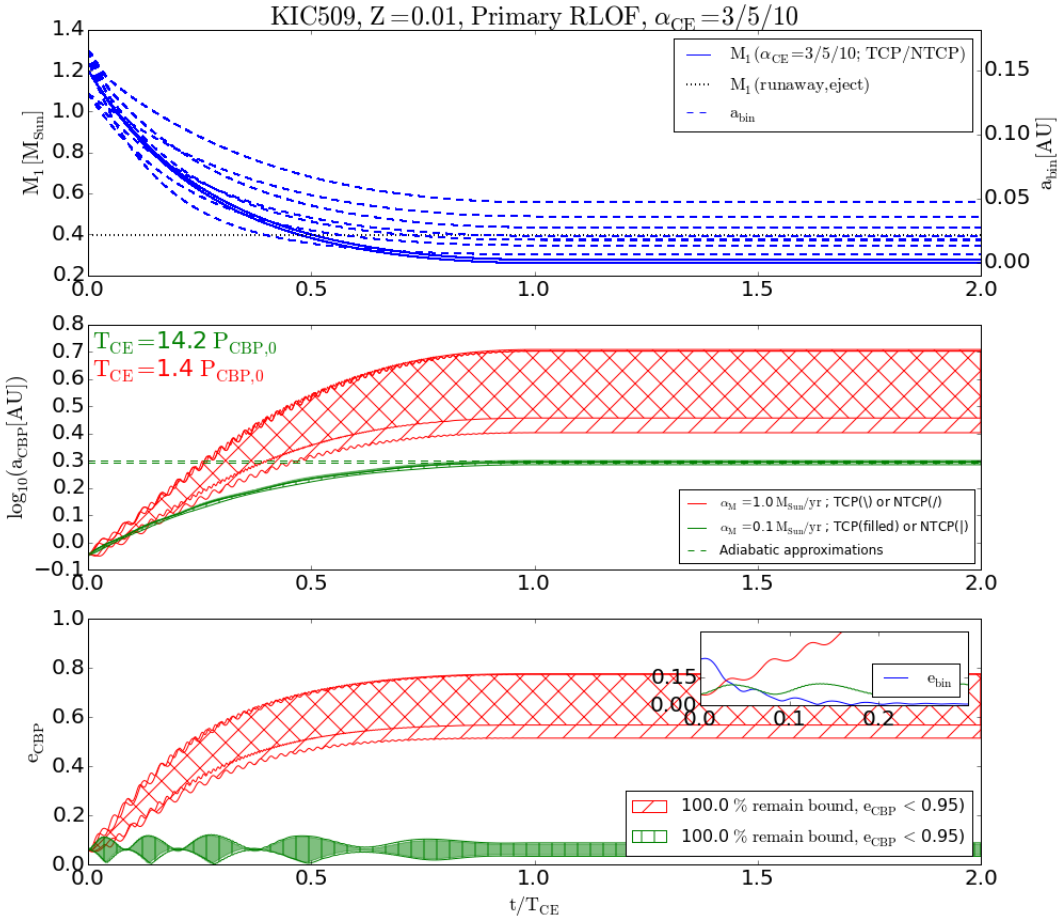

Figure 3.23: Same as Fig. 3.22, but for $\alpha_{CE} = 3/5/10$. The green curve is consistent with the adiabatic approximation for a_{CBP}, while the red curves reach much larger values and are thus plotted on a log scale. Regardless of the intense evolution, the CBP remains bound, for both mass-loss regimes, in all simulations.

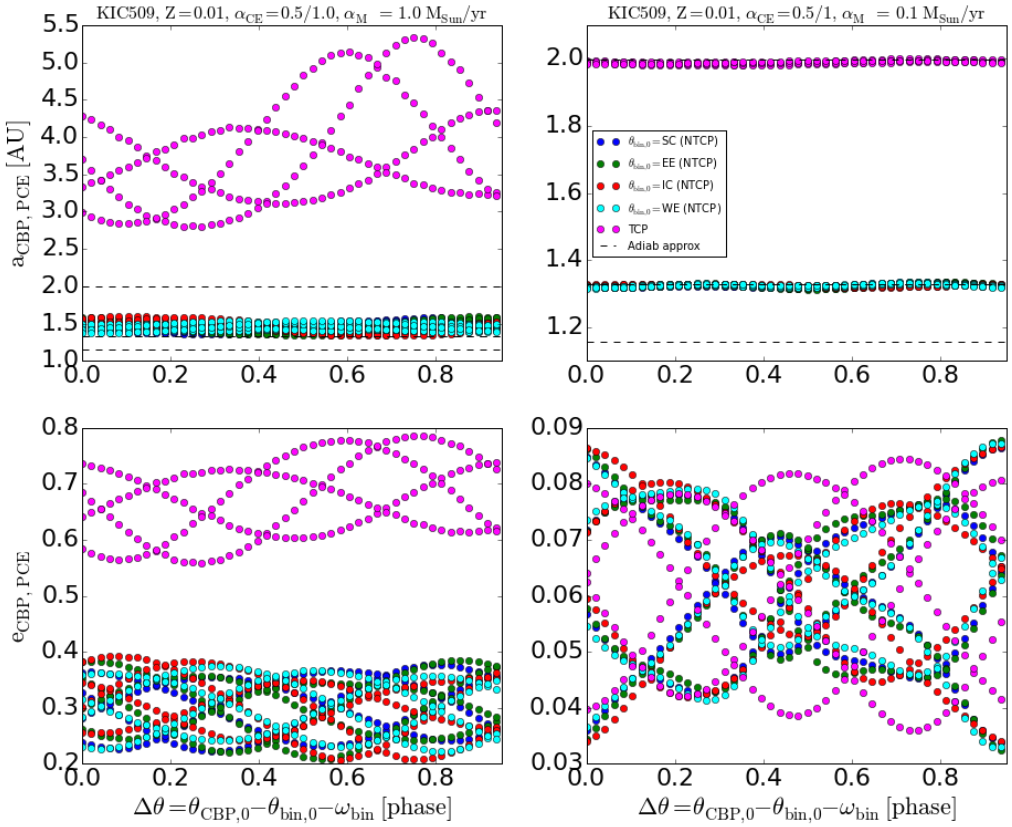

Figure 3.24: Same as Fig. 3.15, but for KIC509, $Z = 0.01$, $\alpha_{CE} = 0.5/1$. The modes for fast mass-loss are $a_{CBP,PCE} = 1.4/3.2$ AU for NTCP/TCP, and $e_{CBP,PCE} = 0.3/0.7$, with maximum values of 5.33 AU and 0.79, respectively. The modes for slow mass-loss are $a_{CBP,PCE} = 1.3/2.0$ AU for NTCP/TCP, and $e_{CBP,PCE} = 0.03/0.03$, while the maximum values are 1.99 AU and 0.082. Since there is no notable differences in the phase plots for $Z = 0.02$, they are excluded from this thesis.

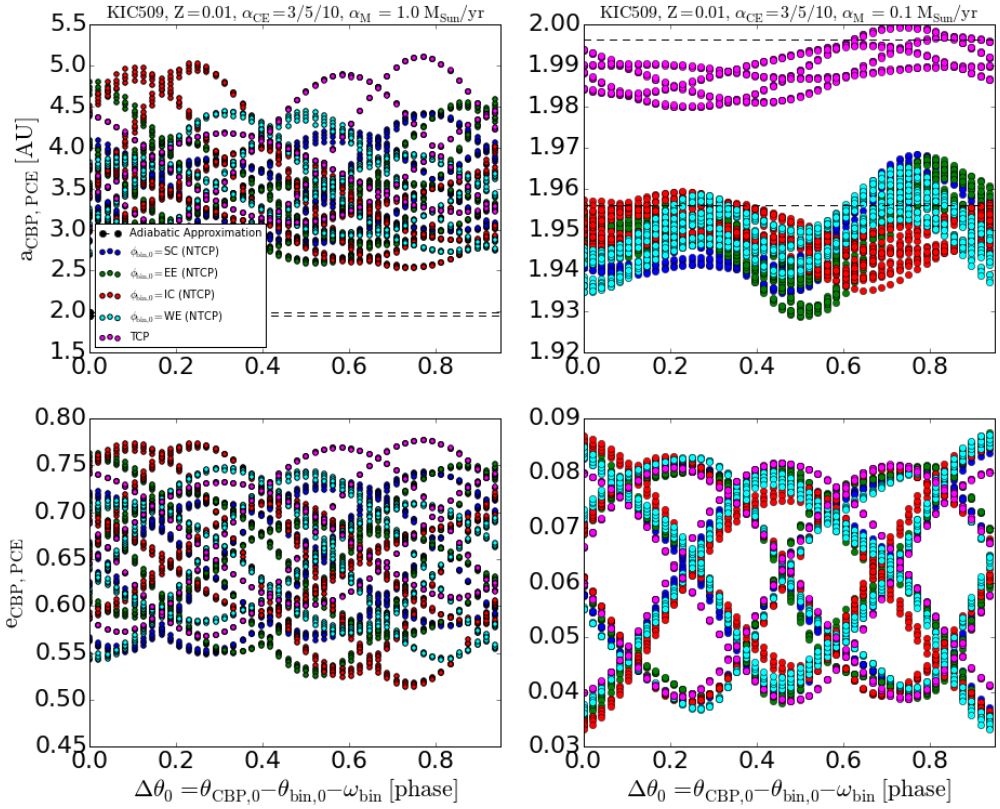

Figure 3.25: Same as Fig. 3.24, but for $\alpha_{CE} = 3/5/10$. The modes for fast mass-loss are $a_{CBP,PCE} = 2.9/3.3$ AU for NTCP/TCP, and $e_{CBP,PCE} = 0.7/0.7$, with maximum values of 5.1 AU and 0.78, respectively. The modes for slow mass-loss are $a_{CBP,PCE} = 1.9/2.0$ AU for NTCP/TCP, and $e_{CBP,PCE} = 0.09/0.08$, while the maximum values are 2.0 AU and 0.088.

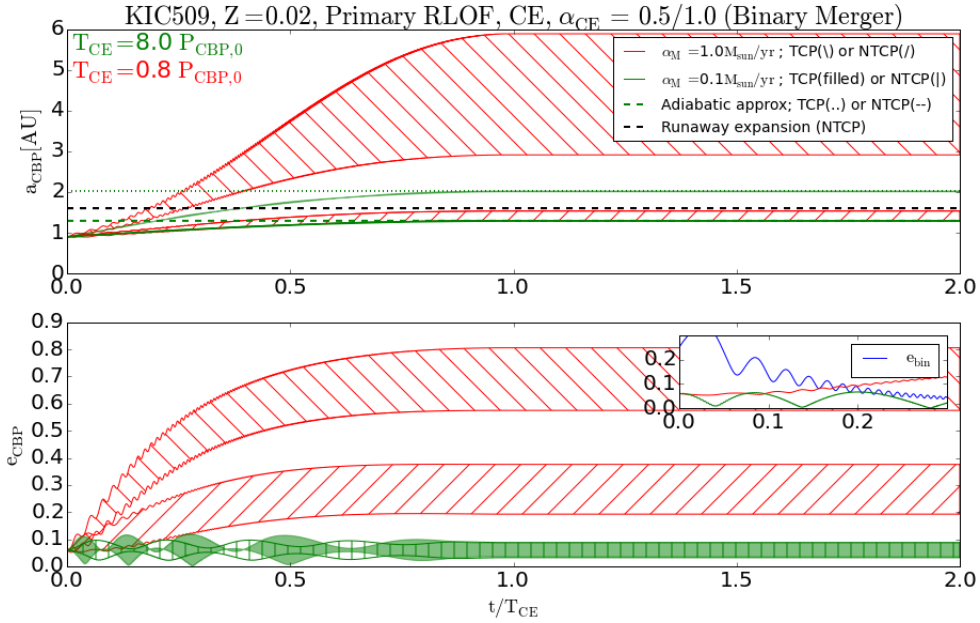

Figure 3.26: Same as Fig. 3.22 but for $Z = 0.02$. While the evolution is very similar, a_{CBP} reaches a maximum of 5.89 AU instead of 5.33 AU, and e_{CBP} reaches a maximum of 0.81.

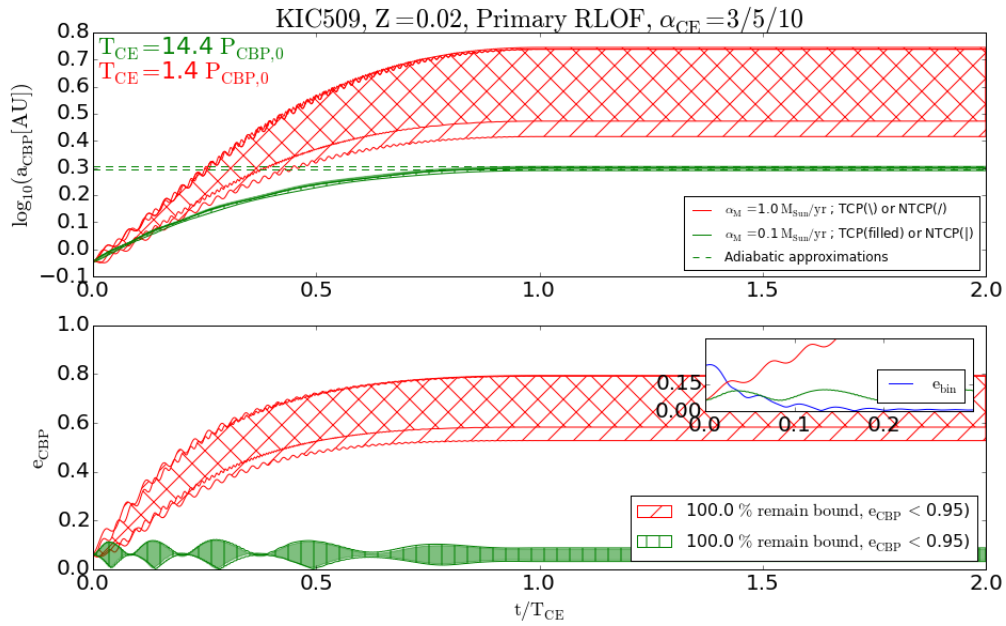

Figure 3.27: Same as Fig. 3.23, but for $Z = 0.02$. The maximum $a_{CBP} = 5.55$ AU instead of 5.1 AU (for $Z = 0.01$), while the maximum e_{CBP} is identical, within a few percent.

3.3 Summary of the Results

The outcomes of the CE (both primary and secondary for KIC782) for each CBP are summarized in Table 3.1 for fast mass-loss and Table 3.2 for slow mass-loss, displaying the mode, median, and mode range of $a_{CBP,PCE}$ and $e_{CBP,PCE}$. Overall, the CBP remains bound, with the exception of KIC782, which experiences ejections for both mass-loss regimes in its primary and secondary CE phases.

Table 3.1: PCE CBP semi-major axis and eccentricity for fast mass-loss, $\alpha_M = 1.0 M_\odot\ yr^{-1}$, and the primary CE. The modes of each include 1-σ uncertainties, even when the distributions are clearly non-Gaussian. Any secondary CE evolution is clearly indicated.

α_{CE}	Tides	$a_{CBP,PCE}$ [AU]			$e_{CBP,PCE}$			Notes
		Mode	Median	Range	Mode	Median	Range	
Kepler-64								[$a_{CBP,0} = 0.65$]
0.5/1	NTCP	$1.7^{+0.02}_{-0.06}$	1.68	1.58 – 1.83	$0.3^{+0.0}_{-0.08}$	0.25	0.16 – 0.35	
0.5/1	TCP	$0.9^{+0.05}_{-0.0}$	0.94	0.92 – 0.96	$0.16^{+0.0}_{-0.11}$	0.12	0.04 – 0.16	
3/5/10	NTCP	$2.2^{+0.09}_{-0.12}$	2.22	1.97 – 2.67	$0.4^{+0.06}_{-0.04}$	0.41	0.3 – 0.54	
3/5/10	TCP	$2.3^{+0.26}_{-0.12}$	2.37	2.15 – 2.68	$0.5^{+0.1}_{-0.12}$	0.45	0.35 – 0.54	
KIC782†								[$a_{CBP,0} = 2.65$]
0.5/1	NTCP	$4.6^{+0.03}_{-0.03}$	5.53	3.03 – 35.08	$0.8^{+0.11}_{-0.26}$	0.63	0.03 – 0.95	0.2% ejected
0.5/1	TCP	$3.1^{+1.54}_{-0.04}$	3.78	2.95 – 5.2	$0.6^{+0.03}_{-0.4}$	0.49	0.18 – 0.66	
3/5/10	NTCP	$5.22^{+0.0}_{-0.0}$	5.92	3.35 – 40.8	$0.9^{+0.01}_{-0.73}$	0.58	0.03 – 0.95	36% ejected
3/5/10	TCP	$4.8^{+1.73}_{-0.04}$	5.9	3.87 – 39.35	$0.9^{+0.0}_{-0.71}$	0.57	0.06 – 0.95	
KIC782‡								
5/10	NTCP	$6.59^{+0.0}_{-0.0}$	7.15	5.78 – 22.01	$0.71^{+0.19}_{-0.0}$	0.76	0.64 – 0.92	91% ejected
10	TCP	$6.6^{+2.27}_{-0.04}$	7.39	5.98 – 29.06	$0.9^{+0.03}_{-0.25}$	0.73	0.63 – 0.94	
KIC393	$i_{CBP} = 0^\circ$							[$a_{CBP,0} = 1.07$]
0.5	TCP	$2.1^{+0.1}_{-0.19}$	2.1	1.8 – 2.52	$0.4^{+0.08}_{-0.13}$	0.37	0.2 – 0.5	
0.5/1/3/5/10	NTCP	$2.82^{+0.0}_{-0.0}$	2.9	1.89 – 8.12	$0.6^{+0.03}_{-0.16}$	0.52	0.23 – 0.84	
1/3/5/10	TCP	$3.2^{+0.03}_{-0.73}$	3.06	2.31 – 4.48	$0.6^{+0.05}_{0.17}$	0.54	0.34 – 0.7	
KIC393	$i_{CBP} = 90^\circ$							[$a_{CBP,0} = 1.07$]
0.5	TCP	$1.9^{+0.28}_{-0.03}$	2.08	1.84 – 2.47	$0.4^{+0.07}_{-0.15}$	0.36	0.21 – 0.49	
0.5/1/3/5/10	NTCP	$2.44^{+0.55}_{-0.0}$	2.84	2.02 – 4.79	$0.55^{+0.0}_{-0.14}$	0.5	0.24 – 0.72	
1/3/5/10	TCP	$2.7^{+0.69}_{-0.25}$	2.97	2.4 – 4.29	$0.6^{+0.04}_{-0.16}$	0.53	0.35 – 0.69	
KIC393	$i_{CBP} = 180^\circ$							[$a_{CBP,0} = 1.07$]
0.5	TCP	$1.9^{+0.32}_{-0.0}$	2.1	1.87 – 2.41	$0.46^{+0.0}_{-0.2}$	0.37	0.22 – 0.48	
0.5/1/3/5/10	NTCP	$2.6^{+0.45}_{-0.16}$	2.88	2.13 – 4.19	$0.59^{+0.0}_{-0.17}$	0.52	0.27 – 0.71	
1/3/5/10	TCP	$2.6^{+0.86}_{-0.12}$	3.02	2.44 – 4.08	$0.6^{+0.06}_{-0.19}$	0.54	0.36 – 0.68	
KIC861								[$a_{CBP,0} = 1.32$]
1/3/5/10	NTCP	$2.5^{+0.35}_{-0.03}$	2.67	2.0 – 3.89	$0.42^{+0.10}_{-0.0}$	0.46	0.31 – 0.63	
1/3/5/10	TCP	$2.4^{+0.54}_{-0.0}$	2.66	2.39 – 3.0	$0.5^{+0.02}_{-0.08}$	0.46	0.41 – 0.52	
KIC509	$Z = 0.01$							[$a_{CBP,0} = 0.9$]
0.5	NTCP	$1.4^{+0.1}_{-0.0}$	1.46	1.34 – 1.59	$0.3^{+0.06}_{-0.06}$	0.31	0.21 – 0.39	
0.5/1	TCP	$3.2^{+0.24}_{-0.27}$	3.67	2.8 – 5.33	$0.7^{+0.03}_{-0.09}$	0.68	0.56 – 0.79	
1/3/5/10	NTCP	$2.9^{+0.76}_{-0.0}$	3.37	2.53 – 5.03	$0.7^{+0.01}_{-0.12}$	0.65	0.51 – 0.77	
3/5/10	TCP	$3.3^{+0.85}_{-0.38}$	3.66	2.86 – 5.1	$0.7^{+0.02}_{-0.08}$	0.68	0.57 – 0.78	
KIC509	$Z = 0.02$							[$a_{CBP,0} = 0.9$]
0.5	NTCP	$1.4^{+0.03}_{-0.05}$	1.4	1.3 – 1.53	$0.3^{+0.05}_{-0.08}$	0.29	0.19 – 0.38	
0.5/1	TCP	$3.4^{+0.56}_{-0.34}$	3.9	2.91 – 5.89	$0.7^{+0.05}_{-0.07}$	0.7	0.58 – 0.81	
1/3/5/10	NTCP	$3.03^{+0.86}_{-0.0}$	3.54	2.6 – 5.46	$0.7^{+0.02}_{-0.11}$	0.67	0.53 – 0.79	
3/5/10	TCP	$3.4^{+1.31}_{-0.37}$	3.85	2.97 – 5.55	$0.7^{+0.08}_{-0.07}$	0.69	0.58 – 0.79	

†: Primary RLOF and CE.

‡: Secondary RLOF and CE.

Table 3.2: Same as Table 3.1, but for slow-mass loss, $\alpha_M = 0.1 M_\odot\ yr^{-1}$.

α_{CE}	Tides	$a_{CBP,PCE}$ [AU] Mode	Median	Range	$e_{CBP,PCE}$ Mode	Median	Range	Notes
Kepler-64								$[a_{CBP,0} = 0.65]$
0.5/1	NTCP	$1.58^{+0.01}_{-0.0}$	1.59	1.56 – 1.6	$0.07^{+0.0}_{-0.027}$	0.056	0.019 – 0.087	
0.5/1	TCP	$0.93^{+0.0}_{-0.0}$	0.93	0.93 – 0.93	$0.05^{+0.014}_{-0.004}$	0.054	0.042 – 0.066	
3/5/10	NTCP	$1.83^{+0.02}_{-0.0}$	1.84	1.81 – 1.86	$0.074^{+0.0}_{-0.03}$	0.056	0.017 – 0.09	
3/5/10	TCP	$1.89^{+0.01}_{-0.0}$	1.89	1.89 – 1.9	$0.062^{+0.0}_{-0.02}$	0.055	0.037 – 0.071	
KIC782†								$[a_{CBP,0} = 2.65]$
0.5/1	NTCP	$3.7^{+0.27}_{-0.0}$	3.86	3.64 – 4.09	$0.395^{+0.0}_{-0.071}$	0.353	0.261 – 0.44	
0.5/1	TCP	$3.21^{+0.17}_{-0.0}$	3.3	3.2 – 3.39	$0.38^{+0.004}_{-0.62}$	0.354	0.314 – 0.387	
3/5/10	NTCP	$4.29^{+0.4}_{-0.0}$	4.5	4.2 – 4.85	$0.4^{+0.02}_{-0.1}$	0.356	0.255 – 0.446	
3/5/10	TCP	$4.4^{+0.45}_{-0.03}$	4.59	4.34 – 4.88	$0.41^{+0.007}_{-0.123}$	0.358	0.281 – 0.421	
KIC782‡								
5/10	NTCP	$20.81^{+0.0}_{-0.0}$	23.24	15.62 – 119.38	$0.6^{+0.321}_{-0.059}$	0.698	0.519 – 0.947	
10	TCP	$32.2^{+8.12}_{-0.0}$	38.03	28.14 – 109.35	$0.76^{+0.04}_{-0.02}$	0.807	0.732 – 0.938	79% ejected
KIC393	$i_{CBP} = 0^\circ$							$[a_{CBP,0} = 1.07]$
0.5	TCP	$1.82^{+0.01}_{-0.0}$	1.82	1.81 – 1.84	$0.1^{+0.016}_{-0.018}$	0.101	0.075 – 0.124	
0.5/1/3/5/10	NTCP	$2.1^{+0.07}_{-0.0}$	2.14	1.96 – 2.35	$0.1^{+0.042}_{-0.008}$	0.109	0.011 – 0.242	
1/3/5/10	TCP	$2.18^{+0.0}_{-0.01}$	2.18	2.15 – 2.2	$0.083^{+0.04}_{-0.0}$	0.101	0.073 – 0.128	
KIC393	$i_{CBP} = 90^\circ$							$[a_{CBP,0} = 1.07]$
0.5	TCP	$1.81^{+0.02}_{-0.0}$	1.82	1.8 – 1.85	$0.1^{+0.019}_{-0.014}$	0.102	0.08 – 0.121	
0.5/1/3/5/10	NTCP	$2.1^{+0.07}_{-0.02}$	2.13	1.99 – 2.27	$0.1^{+0.027}_{-0.013}$	0.105	0.033 – 0.182	
1/3/5/10	TCP	$2.2^{+0.0}_{-0.04}$	2.18	2.15 – 2.22	$0.11^{+0.012}_{-0.028}$	0.103	0.076 – 0.125	
KIC393	$i_{CBP} = 180^\circ$							$[a_{CBP,0} = 1.07]$
0.5	TCP	$1.82^{+0.01}_{-0.0}$	1.82	1.81 – 1.84	$0.1^{+0.02}_{-0.021}$	0.1	0.77 – 0.123	
0.5/1/3/5/10	NTCP	$2.12^{+0.02}_{-0.0}$	2.13	2.02 – 2.21	$0.1^{+0.027}_{-0.023}$	0.103	0.025 – 0.162	
1/3/5/10	TCP	$2.19^{+0.0}_{-0.02}$	2.18	2.16 – 2.2	$0.12^{+0.003}_{-0.047}$	0.101	0.074 – 0.126	
KIC861								$[a_{CBP,0} = 1.32]$
1/3/5/10	NTCP	$2.09^{+0.0}_{-0.02}$	2.09	2.05 – 2.14	$0.053^{+0.0}_{-0.03}$	0.041	0.012 – 0.065	
1/3/5/10	TCP	$2.1^{+0.0}_{-0.02}$	2.09	2.08 – 2.1	$0.03^{+0.01}_{-0.0}$	0.033	0.03 – 0.037	
KIC509	$Z = 0.01$							$[a_{CBP,0} = 0.9]$
0.5	NTCP	$1.32^{+0.01}_{-0.0}$	1.32	1.31 – 1.34	$0.074^{+0.0}_{-0.028}$	0.062	0.032 – 0.088	
0.5/1	TCP	$1.99^{+0.0}_{-0.0}$	1.99	1.98 – 2.0	$0.08^{+0.002}_{-0.042}$	0.063	0.036 – 0.084	
1/3/5/10	NTCP	$1.94^{+0.01}_{-0.0}$	1.95	1.93 – 1.97	$0.083^{+0.0}_{-0.04}$	0.063	0.033 – 0.088	
3/5/10	TCP	$1.99^{+0.0}_{-0.0}$	1.99	1.98 – 2.0	$0.08^{+0.002}_{-0.038}$	0.063	0.038 – 0.082	
KIC509	$Z = 0.02$							$[a_{CBP,0} = 0.9]$
0.5	NTCP	$1.29^{+0.0}_{-0.0}$	1.29	1.28 – 1.3	$0.046^{+0.028}_{-0.0}$	0.062	0.032 – 0.088	
0.5/1	TCP	$2.01^{+0.01}_{-0.0}$	2.02	2.01 – 2.03	$0.08^{+0.002}_{-0.043}$	0.063	0.035 – 0.085	
1/3/5/10	NTCP	$1.97^{+0.0}_{-0.0}$	1.97	1.95 – 1.99	$0.083^{+0.0}_{-0.04}$	0.063	0.032 – 0.088	
3/5/10	TCP	$2.0^{+0.02}_{-0.0}$	2.01	2.0 – 2.02	$0.08^{+0.002}_{-0.038}$	0.063	0.038 – 0.082	

†: Primary RLOF and CE.

‡: Secondary RLOF and CE.

Chapter 4

Discussions & Conclusions

4.1 Discussion & Contribution

Half of all stars in the Universe are members of binary or higher-order multiple systems, and roughly 25% of all binaries are close enough to interact through a CE phase when the primary evolves into a giant (Willems & Kolb, 2004). Millions of CBPs are expected to orbit such main sequence close binaries (Welsh et al., 2012), highlighting the importance of understanding the evolution of close binary stars, and the effects on their circumbinary planets as they evolve through a common envelope phase, before extending these results to triple or higher-order star systems with planets. Previous studies have taken PCE CBPs and reconstructed their progenitor systems to test the stability of the system, mainly focusing on the pre-CE stabilility to determine CBP survivability through the CE phase, or as evidence supporting second-generation or mixed formation mechanisms. This inverse method suffers from uncertainties in both the PCE CBPs (with major uncertainties in their measurements), and in the CE process itself. We tackle the opposite situation, i.e. we remove the former issue by starting with well-characterized MS CBPs and evolve them through the CE stage. The importance of studying the stability of CBPs throughout the CE phase has recently been reinforced (e.g. Veras et al., 2017; Shevchenko, 2017), and the addition of e_{CBP} and i_{CBP} expands upon the results of KM16, leading to the following conclusions.

All tested systems (Kepler-64 + KIC782, 393, 861, 509) experience at least one CE phase for the initial observational parameters within the 15 Gyr NTCP/TCP BSE simulations. KIC509 experiences a CE for both tested $Z = 0.01$ and $Z = 0.02$, albeit at slightly different times. $\alpha_{CE} = 0.5/1.0$ usually led to binary mergers during the primary CE, while $\alpha_{CE} = 1/3/5/10$ allowed the stars to survive the CE as a binary, the outcome of which was strongly dependent on both $e_{bin,0}$ and $a_{bin,0}$. Merged binaries continued to evolve after the CE until 15 Gyr, usually becoming C-O WDs.

Binaries which did not merge exited the CE as either a tight WD-MS pair or a WD-WD pair

(KIC861), and sometimes saw a second onset of RLOF leading to a secondary CE. Kepler-64 experienced a secondary CE for $\alpha_{CE} = 3.0$, TCP, merging into a giant, while KIC393 experienced a secondary CE for $\alpha_{CE} = 0.5$, NTCP and $\alpha_{CE} = 1$, TCP, merging without mass loss into a giant as well; both of these systems evolve into C-O WDs by 15 Gyr. A secondary CE which resulted in a short period WD-WD binary was experienced by KIC782 for $\alpha_{CE} = 5.0/10.0$, NTCP and $\alpha_{CE} = 10.0$, TCP. Double-degenerate Supernova (DD SN) explosions were seen in two systems – KIC782 (during secondary RLOF for $\alpha_{CE} = 3.0$, NTCP and $\alpha_{CE} = 5.0$, TCP and during third RLOF for $\alpha_{CE} = 5.0$, NTCP and $\alpha_{CE} = 10.0$, TCP), and KIC861 (during primary RLOF for $\alpha_{CE} = 0.5$ and during secondary RLOF for $\alpha_{CE} = 1.0$).

Consistent with the study conducted by KM16, the immense mass-loss experienced by some systems is stunning – for example, KIC861 may lose up to ∼74% of its initial mass during primary CE, while KIC782 loses ∼42% during primary CE and another 73% of this PCE mass during secondary CE. The drastic in-spiral of the binary separations are present, with ∼tens of $R_{\odot}$(0.5 – 2 months) orbits shrinking to within 1 – 10 $R_{\odot}$(∼several hours – days), and sometimes shrinking to sub-$R_{\odot}$separations (e.g. KIC782, with $a_{bin,0} = 47.9R_{\odot}$, shrinks to $a_{bin,PCE} = 0.47R_{\odot}$) after a secondary CE phase. It is these very short orbit binaries which are likely to end in DD SNe.

For both fast and slow mass-loss regimes, the CBPs remain bound and dynamically survive the CE phase in the vast majority of our simulations. The CBPs experience adiabatic orbital expansion during the primary CE in all scenarios for $\alpha_M = 0.1M_{\odot}\ yr^{-1}$, while the quicker evolution involving $\alpha_M = 1.0M_{\odot}\ yr^{-1}$ is in the transition regime and, for the most part, strictly non-adiabatic. The only system in which ejections occur (for our limiting factor of $e_{CBP} = 0.95$) is KIC782, which has some ejections for fast mass-loss during primary CE, depending on the initial phase configuration, and many ejections for both mass-loss regimes during its secondary CE. It is during this secondary CE that non-adiabatic orbital expansion is seen for the slow mass-loss regime as well, likely leading to many of the ejections seen with the steep increase in e_{CBP}. In the aforementioned SNe, the CBP has no chance of remaining bound, and thus it is in these scenarios that it is certain that the CBP will be ejected.

KIC782 has an initially eccentric CBP ($e_{CBP,0} = 0.35$) orbiting an eccentric binary ($e_{bin,0} = 0.68$), and there are distinct ejection probabilities during both the primary and secondary CE phases. The effect of CBP inclination i_{CBP} on the PCE orbital configuration of the CBP in the new systems is difficult to quantify. The most inclined planet, KIC509, at $i_{CBP} = 26°$, remains bound in all simulations around its eccentric host binary ($e_{bin,0} = 0.25$), as does the less inclined CBP in KIC861 with $i_{CBP} = 10°$. While KIC393, with its highly uncertain inclination, provided a test of seven inclinations from $0 - 180°$ in 30° increments, there were no ejections in any of these test simulations, although the values of $a_{CBP,PCE}$ and $e_{CBP,PCE}$ varied slightly. Based on these results, inclination of the CBP, i_{CBP}, does not affect ejection prospects. We note that the inclination does not change, i.e., the CBP orbit precesses at constant inclination as the system evolves.

A comparison of the current configurations of the *Kepler* systems tested within this thesis and eclipse-timing variation (ETV) candidate PCE CBPs is shown in Fig. 4.1. These include the previously mentioned planets NN Ser-c, NN Ser-d (Mustill et al., 2013), and HU Aqr-c (Portegies Zwart, 2013), along with 14 others. The parameter space occupied by each is clearly different, likely due to their significantly different evolutionary stages: while the observed *Kepler* CBPs tend to have relatively low a_{CBP} and e_{CBP}, the PCE CBPs have higher a_{CBP} (due to expansion of the initial orbit, second-generation formation, or some mixed-formation mechanism) and a large range of e_{CBP}, from relatively circular to extremely eccentric. If the *Kepler* CBPs survive the violent evolution of their host stars, their orbits may evolve to values similar to those seen in PCE CBPs, providing a plausible origin for some of these PCE CBP systems.

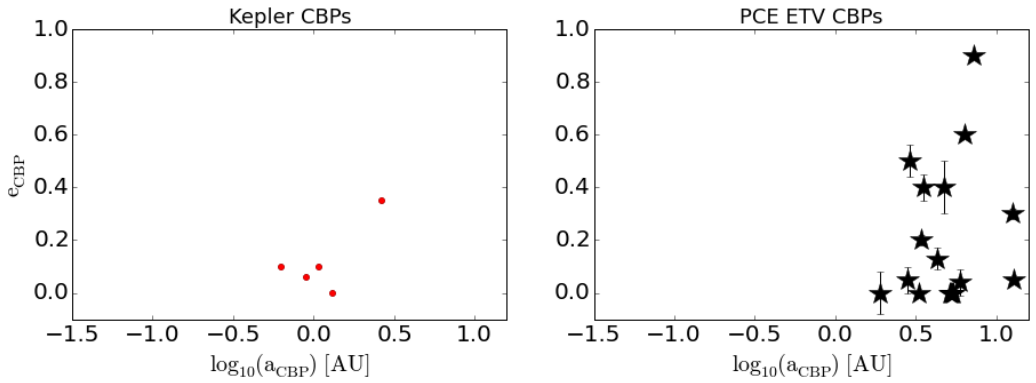

Figure 4.1: The pre-CE configurations of the current *Kepler* candidates (Kepler-64 + the four new systems, shown on the left) compared with observational data of PCE CBP candidates (right). Note the larger orbits of the PCE CBPs; this expansion is expected to occur due to mass-loss during the CE phase, and this behaviour is reproduced through our REBOUND evolution of the binary-CBP systems.

One of the most exciting aspects of studying exoplanets is the prospect of discovering life elsewhere in the Universe. However, until observational instruments advance significantly, we may only be able to fantasize about this popular aspect of science-fiction through possible signs of biological processes found through spectroscopic measurements. The Earth falls within the habitable zone (HZ) of the Sun, a region in which the conditions are just right for liquid water and by extension, life as we know it, to exist. While it is difficult to determine the HZ of the new systems presented within this thesis (for example, using the equations presented within Kopparapu et al. (2014)) due to uncertainties in the measurements of the properties of the system (i.e. the stellar types of the host binary stars and their energy output are not well constrained), it should be clear that throughout the evolution of these systems, the HZ will move. A CBP which orbits farther in than the HZ could potentially expand into an orbit within the HZ zone during the CE phase, however the HZ zone will also move based on the evolution of the binary. The opposite is also true – a CBP currently

within the HZ around its binary may expand to a larger orbit while the HZ moves inwards. With more information on the four new CBPs, it would be possible to determine when, and if, any of the planets exist within the HZ for a significant enough amount of time for life (as we know it) to evolve.

Fig. 4.2 shows the comparison between $a_{CBP,PCE}$ and $e_{CBP,PCE}$, a major result of this work that helps connect *Kepler* CBPs to PCE CBPs. The upper six panels display $e_{CBP,PCE}$ vs. $a_{CBP,PCE}$ for Kepler-64, KIC782, KIC861, KIC509[1], and KIC393 for two inclinations ($i_{CBP} = 0°$ and $180°$). Red and blue points indicate fast mass-loss for NTCP and TCP respectively, while green points indicate slow mass-loss; squares (in the plot of KIC782) are results from the secondary CE. These results are collected in the bottom two plots, and compared with the PCE ETV CBPs immediately following the respective CE phases (left), and at the end of our 15 Gyr simulations (right). From these results, it is clear that the simulation results are qualitatively consistent with the observed PCE CBP candidates, within the given uncertainties. As with the original study (KM16), this is not a direct comparison, as the ages of our five systems and the PCE CBP candidates do not directly correlate; instead, this displays a potential spread of CBP populations possible through various channels of binary evolution. However, these additional results should help guide future observations through recognition of the possible configurations late in a system's evolution.

[1]Only the results for $Z = 0.02$, as the plots looked almost identical for both tested metallicities.

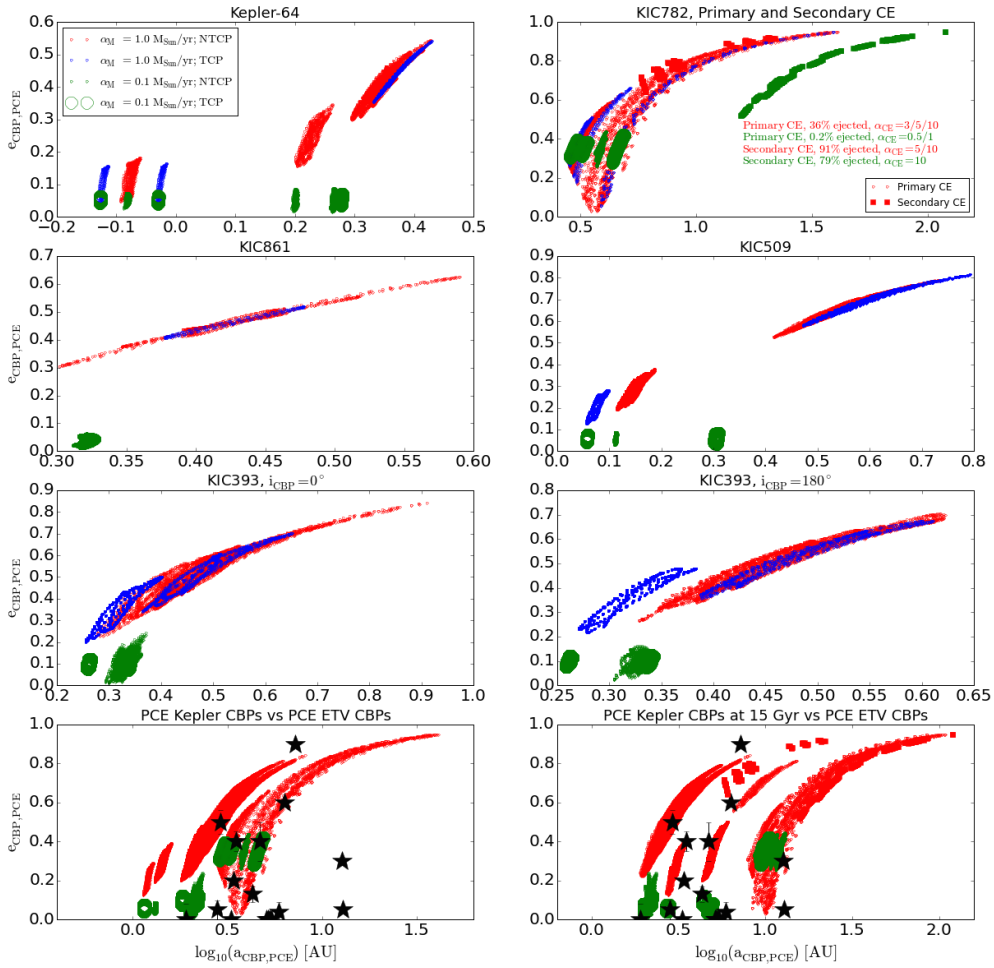

Figure 4.2: The final REBOUND outcomes for all α_{CE}, initial phase configurations, and NTCP/TCP simulations, displaying $e_{CBP,PCE}$ vs. $a_{CBP,PCE}$ for (from top left): Kepler-64, KIC782, KIC861, KIC509, KIC393 $i_{CBP} = 0°$, and KIC393 $i_{CBP} = 180°$. The bottom two panels show the same PCE configurations of all 5 systems immediately after the CE (left), and at the end of the 15 Gyr simulations (right), vs. observed PCE eclipse-timing variation (ETV) CBPs. As with the original nine circular, coplanar systems (Kostov et al., 2016), these four new eccentric, inclined *Kepler* CBP candidates are qualitatively consistent with observed PCE CBPs, when taking into account inherent uncertainties in their observations and intrinsic uncertainties within our code pipeline.

4.2 Future Directions

The results presented within this thesis improve the determination of the survivability of planets around close binary hosts. This thesis adds a layer of complexity to previous work by including CBP eccentricity and inclination. As stated above, our results have implications for future studies of MS and PCE CBP discoveries, as these simulations give an idea of the parameter space in which these planets could be observed around binaries (see Fig. 4.2), with both the *Kepler*/*K2* mission, and future exoplanetary observations using both spaceborne and ground-based telescopes. PCE CBP systems that appear to have no stable progenitor configurations could provide some evidence of second-generation formation, while PCE CBPs currently in configurations similar to our results may support the first-generation formation mechanism.

The binary-CBP models involving the BSE/REBOUND pipeline could be extended to simulate a triple star system, such as a close binary with a distant third companion, or a classical triple system in which a binary orbits a primary star, such as HD 188753 (which also contains a planet around the primary). This would be achieved in the same manner as within this study: the binary star would be evolved using BSE, and the third body added using REBOUND. However, REBOUND treats CBPs as point masses, since they are much smaller than the masses of the host stars; by substituting our point-mass CBP with a massive third body, complexity could arise between the three massive bodies if orbiting close enough to one another. Simple dynamical evolution, similar to that presented within this thesis, would be the easiest to simulate without heavy modification of the codes involved.

BSE/REBOUND could also be combined with and compared to, for example, a hydrodynamical code, allowing for the formation of a circumbinary disk due to mass loss caused by stellar evolution, or the CE phase in close binaries. As noted by Ivanova et al. (2013), the CE phase is so complex that it cannot be treated with a single code, since it is likely that the evolution leading up to the CE, and immediately following its expulsion, may occur on longer timescales than current computational power can achieve. This limitation indicates that our strict dynamical evolution of the system, including the results of BSE, are far from realistic, but a great starting point in treating the overwhelming problem of CE. The importance of the inclusion of a CB disk arises from the fact that up to 10% of the ejected material may fall back into a disk (Kashi & Soker, 2011), while up to 80% of the ejected material can remain gravitationally bound to the system after CE (Passy et al., 2012); since our current code neglects this (i.e. any ejected material is assumed to be completely lost from the system), its inclusion would drastically improve the realism of the results. Aside from the CB disk, hydrodynamical simulations would account for mass falling onto the third body (either a massive star or a comparitively small planet), or accretion as the third body travels through the disk. The addition of hydrodynamics could offer a test of the aforementioned second-generation formation mechanism by having one (or many) planets form out of this disk, and provide a basis for simulations of these multi-planet binary systems as the host stars evolves through a CE phase.

A mixed-formation scenario is also possible, in which a CBP "seed" accretes enough material from the disk to become a planet itself, clearing its orbit in the process.

BSE simulations in this thesis, for both NTCP and TCP, result in tidal circularization of the binary orbit either before the onset of CE, or during the CE phase itself. Ivanova et al. (2013) noted that the many instances of circular WD-MS binaries – a result we see in our simulations from the primary CE for $\alpha_{CE} = 3/5/10$ – is a limitation on observations of eccentric systems, causing them to be tremendously rare. More advanced codes may allow the simulation of PNe which, instead of guaranteed circularization like BSE, contain eccentric binaries at the centre of their ejected envelope. There are very few observations of eccentric PCE binaries, but it appears they do exist (e.g., a WD-MS pair with $e_{bin} = 0.068 \pm 0.004$ (Delfosse et al., 1999)). Observations of more eccentric binaries will be guided by increases in computational power, and should give a better overview of the outcomes of CE evolution.

4.3 Conclusion

Each of the five systems tested within this thesis experiences at least one CE phase, and their orbiting CBPs respond accordingly. Kepler-64, KIC861, and KIC509 each experience only one CE, while KIC393 evolves through both a primary and secondary CE phase. KIC782 survives two CE phases, and can experience a third onset of RLOF leading to a Double-Degnerate Supernova explosion; a DD SN is also experienced for KIC782 in one case during the secondary CE. Binaries which survive the CE phase either coalesce (usually into a First Giant Branch star), or spiral-in becoming tight WD-MS or WD-WD pairs. The results indicate that eccentric, inclined CBPs predominantly survive the quick and dramatic CE phase of their host stars for both mass-loss regimes. For fast mass-loss of $1 M_{\odot}\ yr^{-1}$, the orbital expansion is non-adiabatic, and the orbit becomes highly eccentric which sometimes leads to ejection of the CBP, strongly dependent on the initial phase configuration of the binary-CBP system at the onset of RLOF. Slow mass-loss of $0.1 M_{\odot}\ yr^{-1}$ led to adiabatic orbital expansion, as expected, and already eccentric CBPs became slightly more eccentric in their outward spiral. Inclined planets seem to have no advantage over their coplanar counterparts; their final orbits differ very slightly as inclination is increased (as evidenced by the tests of KIC393), and there is no apparent effect on the ejection probability. The outcomes produced are consistent with those of observed PCE CBP candidates, providing a possible origin for these late-stage binary-planet systems, while guiding future observations of similar populations as the PCE configurations of the original nine + four new systems. Based on the evolution of KIC782 and its CBP, eccentric planets around eccentric binaries appear to have much lower survival prospects than systems in which either the binary orbit or CBP orbit are circular (or close to circular). CBPs which proceed through multiple CE stages may experience smooth, adiabatic orbital expansion during the first CE while responding non-adiabatically during the second, attributed to the dramatic reconfiguration of

not only the binary, but also the planet itself, during the complex CE phase. There is still much work to be done to better understand the CE phase and the response of CBPs through advances in computational methods.

Bibliography

Agol, E. 2011, Astrophys. J. Lett., 731, L31

Astakhov, S. A., Burbanks, A. D., Wiggins, S., & Farrelly, D. 2003, Nature, 423, 264

Bear, E., Soker, N., & Harpaz, A. 2011, Astrophys. J. Lett., 733, L44

Boehm-Vitense, E. 1989, Introduction to stellar astrophysics. Volume 1 - Basic stellar observations and data. Volume 2 - Stellar atmospheres. Volume 3 - Stellar structure and evolution.

Brown, G. E. 1995, Astrophys. J., 440, 270

Carroll, B. W. & Ostlie, D. A. 1996, An Introduction to Modern Astrophysics

Chaboyer, B. 1998, Phys. Rep., 307, 23

Darwin, G. H. 1879, Proceedings of the Royal Society of London, 29, 168

Delfosse, X., Forveille, T., Beuzit, J.-L., Udry, S., Mayor, M., & Perrier, C. 1999, Astron. Astrophys., 344, 897

Doyle, L. R., Carter, J. A., Fabrycky, D. C., Slawson, R. W., Howell, S. B., Winn, J. N., Orosz, J. A., Prsa, A., Welsh, W. F., Quinn, S. N., Latham, D., Torres, G., Buchhave, L. A., Marcy, G. W., Fortney, J. J., Shporer, A., Ford, E. B., Lissauer, J. J., Ragozzine, D., Rucker, M., Batalha, N., Jenkins, J. M., Borucki, W. J., Koch, D., Middour, C. K., Hall, J. R., McCauliff, S., Fanelli, M. N., Quintana, E. V., Holman, M. J., Caldwell, D. A., Still, M., Stefanik, R. P., Brown, W. R., Esquerdo, G. A., Tang, S., Furesz, G., Geary, J. C., Berlind, P., Calkins, M. L., Short, D. R., Steffen, J. H., Sasselov, D., Dunham, E. W., Cochran, W. D., Boss, A., Haas, M. R., Buzasi, D., & Fischer, D. 2011, Science, 333, 1602

Getley, A. K., Carter, B., King, R., & O'Toole, S. 2017, ArXiv e-prints

Hadjidemetriou, J. D. 1963, Icarus, 2, 440

Hayashi, C. 1961, Publ. Astron. Soc. Jpn., 13

Hayashi, C. & Cameron, R. C. 1962, Astrophys. J., 136, 166

Heppenheimer, T. A. & Porco, C. 1977, Icarus, 30, 385

Hilditch, R. W. 2001, An Introduction to Close Binary Stars, 392

Hurley, J. R., Pols, O. R., & Tout, C. A. 2000, Mon. Not. R. Astron. Soc., 315, 543

Hurley, J. R., Tout, C. A., & Pols, O. R. 2002, Mon. Not. R. Astron. Soc., 329, 897

Iaconi, R., Reichardt, T., Staff, J., De Marco, O., Passy, J.-C., Price, D., Wurster, J., & Herwig, F. 2017, Mon. Not. R. Astron. Soc., 464, 4028

Iben, Jr., I. & Livio, M. 1993, Publ. Astron. Soc. Pac., 105, 1373

Iben, Jr., I. & Tutukov, A. V. 1984, Astrophys. J., 284, 719

Ivanova, N., Justham, S., Chen, X., De Marco, O., Fryer, C. L., Gaburov, E., Ge, H., Glebbeek, E., Han, Z., Li, X.-D., Lu, G., Marsh, T., Podsiadlowski, P., Potter, A., Soker, N., Taam, R., Tauris, T. M., van den Heuvel, E. P. J., & Webbink, R. F. 2013, Astron. Astrophys. Rev., 21, 59

Izzard, R. G., Hall, P. D., Tauris, T. M., & Tout, C. A. 2012, in IAU Symposium, Vol. 283, IAU Symposium, 95–102

Jones, D. & Boffin, H. M. J. 2017, Nature Astronomy, 1, 0117

Kashi, A. & Soker, N. 2011, Mon. Not. R. Astron. Soc., 417, 1466

Kippenhahn, R. & Weigert, A. 1990, Stellar Structure and Evolution, 192

Kopparapu, R. K., Ramirez, R. M., SchottelKotte, J., Kasting, J. F., Domagal-Goldman, S., & Eymet, V. 2014, Astrophys. J. Lett., 787, L29

Kostov, V. B., Moore, K., Tamayo, D., Jayawardhana, R., & Rinehart, S. A. 2016, Astrophys. J., 832, 183

Kratter, K. M. & Perets, H. B. 2012, Astrophys. J., 753, 91

Livio, M. & Soker, N. 1988, Astrophys. J., 329, 764

Melia, F. & Falcke, H. 2001, Annu. Rev. Astron. Astrophys., 39, 309

Meyer, F. & Meyer-Hofmeister, E. 1979, Astron. Astrophys., 78, 167

Mustill, A. J., Marshall, J. P., Villaver, E., Veras, D., Davis, P. J., Horner, J., & Wittenmyer, R. A. 2013, Mon. Not. R. Astron. Soc., 436, 2515

Ostriker, J. 1976, in Bull. Am. Astron. Soc., Vol. 8, Bulletin of the American Astronomical Society, 438

Paczynski, B. 1976, in Bull. Am. Astron. Soc., Vol. 8, Bulletin of the American Astronomical Society, 442

Papaloizou, J. C. B. & Larwood, J. D. 2000, Mon. Not. R. Astron. Soc., 315, 823

Passy, J.-C., De Marco, O., Fryer, C. L., Herwig, F., Diehl, S., Oishi, J. S., Mac Low, M.-M., Bryan, G. L., & Rockefeller, G. 2012, Astrophys. J., 744, 52

Planck Collaboration, Ade, P. A. R., Aghanim, N., Arnaud, M., Ashdown, M., Aumont, J., Baccigalupi, C., Banday, A. J., Barreiro, R. B., Bartlett, J. G., & et al. 2016, Astron. Astrophys., 594, A13

Portegies Zwart, S. 2013, Mon. Not. R. Astron. Soc., 429, L45

Portegies Zwart, S. F. & Meinen, A. T. 1993, Astron. Astrophys., 280, 174

Raghavan, D., McAlister, H. A., Henry, T. J., Latham, D. W., Marcy, G. W., Mason, B. D., Gies, D. R., White, R. J., & ten Brummelaar, T. A. 2010, Astrophys. J. Suppl. Ser., 190, 1

Rein, H. & Liu, S.-F. 2012, Astron. Astrophys., 537, A128

Rein, H. & Spiegel, D. S. 2015, Mon. Not. R. Astron. Soc., 446, 1424

Ricker, P. M. & Taam, R. E. 2012, Astrophys. J., 746, 74

Schröder, K.-P. & Connon Smith, R. 2008, Mon. Not. R. Astron. Soc., 386, 155

Shevchenko, I. I. 2017, The Astronomical Journal, 153, 273

Silvotti, R., Schuh, S., Janulis, R., Solheim, J.-E., Bernabei, S., Østensen, R., Oswalt, T. D., Bruni, I., Gualandi, R., Bonanno, A., Vauclair, G., Reed, M., Chen, C.-W., Leibowitz, E., Paparo, M., Baran, A., Charpinet, S., Dolez, N., Kawaler, S., Kurtz, D., Moskalik, P., Riddle, R., & Zola, S. 2007, Nature, 449, 189

van den Heuvel, E. P. J. 1969, Astron. J., 74, 1095

van den Heuvel, E. P. J. 1976, in IAU Symposium, Vol. 73, Structure and Evolution of Close Binary Systems, ed. P. Eggleton, S. Mitton, & J. Whelan, 35

Veras, D. 2016, Royal Society Open Science, 3, 150571

Veras, D., Georgakarakos, N., Dobbs-Dixon, I., & Gänsicke, B. T. 2017, Mon. Not. R. Astron. Soc., 465, 2053

Veras, D. & Tout, C. A. 2012, Mon. Not. R. Astron. Soc., 422, 1648

Veras, D., Wyatt, M. C., Mustill, A. J., Bonsor, A., & Eldridge, J. J. 2011, Mon. Not. R. Astron. Soc., 417, 2104

Vink, J. S. 2013, in Massive Stars: From alpha to Omega, 135

Völschow, M., Banerjee, R., & Hessman, F. V. 2014, Astron. Astrophys., 562, A19

Welsh, W. F., Orosz, J. A., Carter, J. A., Fabrycky, D. C., Ford, E. B., Lissauer, J. J., Prša, A., Quinn, S. N., Ragozzine, D., Short, D. R., Torres, G., Winn, J. N., Doyle, L. R., Barclay, T., Batalha, N., Bloemen, S., Brugamyer, E., Buchhave, L. A., Caldwell, C., Caldwell, D. A., Christiansen, J. L., Ciardi, D. R., Cochran, W. D., Endl, M., Fortney, J. J., Gautier, III, T. N., Gilliland, R. L., Haas, M. R., Hall, J. R., Holman, M. J., Howard, A. W., Howell, S. B., Isaacson, H., Jenkins, J. M., Klaus, T. C., Latham, D. W., Li, J., Marcy, G. W., Mazeh, T., Quintana, E. V., Robertson, P., Shporer, A., Steffen, J. H., Windmiller, G., Koch, D. G., & Borucki, W. J. 2012, Nature, 481, 475

Willems, B. & Kolb, U. 2004, Astron. Astrophys., 419, 1057

Zorotovic, M. & Schreiber, M. R. 2013, Astron. Astrophys., 549, A95

Appendix A

Appendix

A.1 Abbreviations & Parameters

CBP – CircumBinary Planet
CE – Common Envelope
PCE – Post-Common Envelope
ZAMS – Zero-Age Main Sequence
MS – Main Sequence
GB – Giant Branch
RGB – Red Giant Branch
FGB – First Giant Branch
WD – White Dwarf
C-O WD – Carbon-Oxygen White Dwarf
HeWD – Helium White Dwarf
NS – Neutron Star
BH – Black Hole
SN – Supernova
PN – Planetary Nebula
RLOF – Roche Lobe Overflow
SSE – Single Star Evolution code
BSE – Binary Star Evolution code
NTCP – No Tidal Circularization Path (BSE Tides OFF)
TCP – Tidal Circularization Path (BSE Tides ON)

α_M – Common Envelope mass-loss rate
α_{crit} – Critical Common Envelope mass-loss rate

α_{CE} – Common Envelope efficiency parameter

$a_{bin,0}$ – Initial binary separation

$a_{bin,PCE}$ – Post-Common Envelope binary separation

$e_{bin,0}$ – Initial binary eccentricity

$e_{bin,PCE}$ – Post-Common Envelope binary eccentricity

$a_{CBP,0}$ – Initial semi-major axis of orbiting circumbinary planet

$a_{CBP,PCE}$ – Post-Common Envelope semi-major axis of orbiting circumbinary planet

$e_{CBP,0}$ – Initial eccentricity of orbiting circumbinary planet

$e_{CBP,PCE}$ – Post-Common Envelope eccentricity of orbiting circumbinary planet

i_{CBP} – Inclination of orbiting circumbinary planet

β – Ratio between initial and final mass of the system

β_{eject} – Runaway ejection ratio between initial and final mass of the system

Ψ – Common Envelope mass-loss index

P_{CBP} – Period of orbiting circumbinary planet

T_{CE} – Common Envelope mass-loss timescale

$M_{\odot}$– One Solar mass, i.e. the mass of the Sun

$M_{\oplus}$– One Earth mass, i.e. the mass of the Earth

A.2 Additional Tables

Table A.1: BSE Binary Evolution Results.

α_{CE}	Tides	M_1 $[M_\odot]$	M_2 $[M_\odot]$	a_{bin} $[R_\odot]$	e_{bin}	Time RLOF [Gyr]	Notes
Kepler-64							
–	–	1.53	0.41	38.7	0.22	0	
0.5	NTCP	1.53	–	–	–	3.02	CE + Merger
0.5	TCP	1.68	–	–	–	3.02	CE + Merger
1.0	NTCP	0.8	–	–	–	3.02	CE + Merger
1.0	TCP	1.35	–	–	–	3.02	CE + Merger
3/5/10	NTCP	0.28	0.41	2.4/3.9/7.0	0	3.02	CE
3/5/10	TCP	0.26	0.41	1.6/2.6/4.7	0	3.02	CE
3	TCP	0.67	–	–	–	6.20	CE‡ + Merger
KIC782							
–	–	1.28	1.23	47.9	0.68	0	
0.5	NTCP	2.19	–	–	–	5.04	CE + Merger
0.5	TCP	2.31	–	–	–	5.02	CE + Merger
1.0	NTCP	1.81	–	–	–	5.04	CE + Merger
1.0	TCP	2.08	–	–	–	5.02	CE + Merger
3/5/10	NTCP	0.26	1.23	6.1/9.3/15.6	0	5.04	CE
3/5/10	TCP	0.23	1.23	3.6/5.5/8.9	0	5.02	CE
3	NTCP	–	–	–	–	5.52	DD SN†
3	TCP	1.44	–	–	–	5.02	CE‡ + Merger
5	NTCP	0.26	0.19	0.69	0	5.67	CE‡
		–	–	–	–	7.30	DD SN
5	TCP	–	–	–	–	5.25	DD SN
10	NTCP	0.26	0.22	2.4	0	5.76	CE‡
10	TCP	0.23	0.16	0.47	0	5.44	CE‡
		–	–	–	–	5.97	DD SN
KIC393							
–	–	1.45	0.83	73.6	0.43	0	
0.5	NTCP	0.32	0.83	1.8	0	3.31	CE
		1.04	–	–	–	5.27	CE‡ + Merger
0.5	TCP	1.34	–	–	–	3.30	CE + Merger
1.0	NTCP	0.32	0.83	3.6	0	3.31	CE
1.0	TCP	0.30	0.83	2.4	0	3.30	CE
		1.04	–	–	–	3.47	CE‡ + Merger
3/5/10	NTCP	0.32	0.83	9.8/14.9/24.9	0	3.31	CE
3/5/10	TCP	0.30	0.83	6.5/10.1/16.9	0	3.30	CE
KIC861							
–	–	0.96	0.96	51.6	0.50	0	
0.5	NTCP	–	–	–	–	14.31	DD SN
0.5	TCP	–	–	–	–	14.31	DD SN
1.0	NTCP	0.25	0.25	0.38	0	14.31	CE
		–	–	–	–	14.41	DD SN
1.0	TCP	0.25	0.25	0.38	0	14.31	CE
		–	–	–	–	14.41	DD SN
3/5/10	NTCP	0.25	0.25	1.1/1.8/3.5	0	14.31	CE
3/5/10	TCP	0.25	0.25	1.1/1.8/3.4	0	14.31	CE
KIC509	$Z = 0.01$						
–	–	1.21	0.51	35.4	0.25	0	
0.5	NTCP	1.16	–	–	–	5.19	CE + Merger
0.5	TCP	1.33	–	–	–	5.18	CE + Merger
1.0	NTCP	0.28	0.51	1.4	0	5.19	CE
		0.79	–	–	–	7.85	CE + Merger
1.0	TCP	0.77	–	–	–	5.18	CE + Merger
3/5/10	NTCP	0.28	0.51	3.8/5.9/10.1	0	5.19	CE
3/5/10	TCP	0.26	0.51	2.9/4.5/7.7	0	5.18	CE
KIC509	$Z = 0.02$						
–	–	1.21	0.51	35.4	0.25	0	
0.5	NTCP	1.19	–	–	–	6.16	CE + Merger
0.5	TCP	1.35	–	–	–	6.15	CE + Merger
1.0	NTCP	0.27	0.51	1.3	0	6.16	CE
		0.78	–	–	–	8.33	CE + Merger
1.0	TCP	0.76	–	–	–	6.15	CE + Merger
3/5/10	NTCP	0.27	0.51	3.7/5.7/9.8	0	6.16	CE
3/5/10	TCP	0.25	0.51	2.8/4.3/7.5	0	6.15	CE

†: Double-degenerate Supernova.
‡: Secondary CE.